

Technische Universität München
TUM School of Engineering and Design

Uncertainty Quantification in the Modeling of Spray Combustion Dynamics

Sagar Ravindra Kulkarni

Vollständiger Abdruck der von der TUM School of Engineering and Design
der Technischen Universität München zur Erlangung eines
DOKTORS DER INGENIEURWISSENSCHAFTEN (DR.-ING.)
genehmigten Dissertation.

Vorsitz:

Prof. Dr. Sonja Berensmeier

Prüfer der Dissertation:

1. Prof. Wolfgang Polifke, Ph.D.
2. Prof. Dr. Antonio Andreini

Die Dissertation wurde am 13.05.2024 bei der Technischen Universität München eingereicht
und durch die TUM School of Engineering and Design am 26.08.2024 angenommen.

Abstract

This thesis focuses on understanding the response of various spray sub-processes such as droplet motion and evaporation to acoustic oscillations and then leverage this knowledge in analyzing the response of a spray flame produced by an aero-engine injector to acoustic excitation using Large Eddy Simulation and System Identification (LES/SI) procedure. The latter part of this dissertation is dedicated to creating a methodology for uncertainty quantification that can quantify both epistemic and aleatoric uncertainties in the dynamic flame response model. This approach aims to consider how the sensitivity of operating conditions affects predictions of flame model using the LES/SI method, and thereby thermoacoustic modal instability calculations.

To understand the response of spray processes to acoustics, an analytical formulation has been developed. This formulation evaluates how the motion and evaporation of droplets react with fluctuations in the upstream acoustic velocity. The proposed analytical model provides explicit expressions to describe how the motion of the population of evaporating droplets responds to velocity oscillations through the modulation of number density wave and spray evaporation rate. The source term for the modulation of the spray evaporation rate is then incorporated into a one-dimensional convective-diffusive transport equation to analyze how fluctuations in the equivalence ratio evolve over time. The dynamics of evaporation is described using a transfer function that depends on the frequency of the perturbations. The comparison between the frequency response obtained from the analytical transfer function and that from a one-dimensional computational fluid dynamics simulation demonstrates a close agreement. Additionally, the analysis reveals the system's low-pass characteristics and the inherent time delay, which are crucial factors to consider in the stability analysis of thermoacoustic systems.

In the following section of the thesis, an attempt is made to quantify the correlation of the unsteady heat release to upstream acoustic perturbation through a Flame Transfer Function obtained from the LES and System Identification of a turbulent spray flame generated by the GE Avio PERM (Partially Evaporating and Rapid Mixing) injector for aero-engines. The estimated flame transfer function from the combination of LES and system identification agrees qualitatively well with experimental trends with appropriate low-frequency behavior.

The dynamic flame response model obtained from LES/SI procedure is uncertain due to aleatoric uncertainties caused by data corrupted by noise and epistemic uncertainties caused by lack of knowledge of boundary conditions such as spray or wall thermal boundary condition in a CFD simulation. To quantify both types of uncertainties in the flame model a novel data-driven univariate Gaussian Process (GP) surrogate model is proposed. The univariate GP model trains on the Finite Impulse Response (FIR) models obtained from LES/SI at various wall thermal boundary conditions. Subsequently, a bootstrapping procedure is used to quantify

the variability of the FIR coefficients. The trained GP model applied to the FIR dataset obtained with varying wall thermal boundary condition, predicts an FIR with wider confidence interval as it takes into account both aleatoric and epistemic uncertainties. The Gaussian process model effectively predicts the FIR coefficients at new parameter values that were not part of the initial range studied, demonstrating the GP model's ability to successfully capture the underlying LES flame response to change in wall boundary conditions.

Kurzfassung

Diese Arbeit befasst sich mit dem Verständnis der Antwort verschiedener Sprühteilprozesse wie Tröpfchenbewegung und Verdampfung auf akustische Schwingungen und nutzt dieses Wissen, um die Antwort einer Sprühflamme, die von einem Flugzeugtriebwerksinjektor erzeugt wird, auf eine akustische Anregung mittels eines kombinierten Ansatzes aus Grobstruktursimulation und Systemidentifikation, dem sogenannten LES/SI Ansatz, zu analysieren. Der letzte Teil dieser Arbeit ist der Entwicklung einer Methode zur Quantifizierung von Unsicherheiten gewidmet, die sowohl epistemische als auch aleatorische Unsicherheiten im dynamischen Flammenantwortmodell quantifizieren kann. Mit diesem Ansatz soll untersucht werden, wie sich die Empfindlichkeit der Betriebsbedingungen auf die Vorhersagen des Flammenmodells mit der LES/SI Methode und damit auf die Berechnung der thermoakustischen modalen Instabilität auswirkt.

Um die Antwort von Sprühprozessen auf die Akustik zu verstehen, wurde eine analytische Formulierung entwickelt. Mit dieser Formulierung wird untersucht, wie die Bewegung und Verdampfung von Tropfen auf Änderungen der Schallgeschwindigkeit stromaufwärts reagiert. Das vorgeschlagene analytische Modell liefert explizite Ausdrücke, um zu beschreiben, wie die Bewegung der verdampfenden Tröpfchenpopulation auf Geschwindigkeitsänderungen durch die Modulation der Anzahldichtewelle und der Sprühverdampfungsrate reagiert. Der Quellterm für die Modulation der Sprühverdampfungsrate wird dann in eine eindimensionale konvektiv-diffusive Transportgleichung eingesetzt, um die zeitliche Entwicklung von Fluktuationen im Äquivalenzverhältnis zu analysieren. Die Verdampfungsdynamik wird durch eine Übertragungsfunktion beschrieben, die von der Frequenz der Störungen abhängt. Der Vergleich des Frequenzgangs der analytischen Übertragungsfunktion mit dem einer eindimensionalen numerischen Strömungssimulation zeigt eine gute Übereinstimmung. Darüber hinaus zeigt die Analyse die Tiefpasscharakteristik des Systems und die inhärente Zeitverzögerung, die für die Stabilitätsanalyse thermoakustischer Systeme von entscheidender Bedeutung sind.

Im folgenden Teil der Arbeit wird versucht, die Korrelation zwischen der instationären Wärme-freisetzung und der stromaufwärts gerichteten akustischen Störung durch eine Flammenübertragungsfunktion zu quantifizieren, die mit Hilfe des LES/SI Ansatzes einer turbulenten Sprühflamme gewonnen wird. Der Injektor ist hierbei ein GE Avio PERM (Partially Evaporating and Rapid Mixing)-Injektor für Flugzeugtriebwerke. Die aus der Kombination von LES und Systemidentifikation abgeschätzte Flammentransferfunktion stimmt qualitativ gut mit den experimentellen Trends überein und zeigt ein typisches Verhalten im Niederfrequenzbereich.

Das dynamische Flammenmodell, das aus der LES/SI-Methode abgeleitet wird, ist mit Unsicherheiten behaftet, die durch aleatorische Unsicherheiten aufgrund verrauschter Daten und

epistemische Unsicherheiten aufgrund mangelnder Kenntnis der Randbedingungen, wie z.B. der thermischen Randbedingungen des Sprays oder der Wand in einer CFD-Simulation, verursacht werden. Um beide Arten von Unsicherheiten im Flammenmodell zu quantifizieren, wird ein neuartiges datengetriebenes univariates Gauß-Prozess (GP) Ersatzmodell vorgeschlagen. Das univariate GP-Modell basiert auf den Finite Impulse Response (FIR) Modellen, die mit LES/SI bei verschiedenen thermischen Wandgrenzbedingungen erhalten wurden. Anschließend wird ein Bootstrapping-Verfahren verwendet, um die Variabilität der FIR-Koeffizienten zu quantifizieren. Das trainierte GP-Modell, das auf den FIR-Datensatz angewendet wird, der mit variierenden thermischen Randbedingungen der Wand berechnet wurde, sagt eine finite Impulsantwort mit einem breiteren Konfidenzintervall voraus, da es sowohl aleatorische als auch epistemische Unsicherheiten berücksichtigt. Das GP-Modell sagt die FIR-Koeffizienten bei neuen Parameterwerten, die nicht Teil des ursprünglich untersuchten Bereichs waren, effektiv voraus, was die Fähigkeit des GP-Modells zeigt, die zugrundeliegende LES-Flammenreaktion auf Änderungen der Wandrandbedingungen erfolgreich zu erfassen.

Acknowledgements

The research work presented in this thesis was conducted in the School of Engineering and Design and in the group of Thermo-Fluid Dynamics. I would like to kindly acknowledge the financial support provided by the Marie-Curie Sklodowska Initial Training Network MAGISTER, Grant No. 766425.

Firstly, I would like to express my heartfelt thanks to Prof. Wolfgang Polifke for giving me a unique opportunity to conduct research on spray combustion and thermoacoustics. Today, this thesis is made possible by his unwavering support, technical insights at critical junctures, and timely interventions when the research veered off course. The COVID-19 pandemic and delayed experimental investigations affected my research goals. However, his assistance enabled me to pursue multiple options toward obtaining a third paper. I hope that one day the TFD group will be able to complete the unfinished business of my third paper. I very much look forward to reading the results of that research. I am also profoundly grateful for Wolfgang's flexibility during the pandemic, which allowed me to work remotely, perform secondments without travel and visit my family in India during those challenging times.

I would like to extend my deepest gratitude to Dr. Camilo Silva, a co-author and a mentor, who was always there to resolve any doubts and provided much needed direction when I was "lost". I enjoyed our frequent, albeit confusing and seemingly never-ending discussions on formulating analytical expressions for droplet dynamics. In this regard, I would also like to thank the late Javier Achury. His work on droplet dynamics provided the foundation for the analytical work presented in the second publication of this doctoral thesis. During the latter part of my research, I had a chance to interact with Prof. Andreini and his group at University of Florence on performing spray flame computations. I like to thank Daniele Pampaloni and Simone Paccati from Andreini's group who provided CAD files, boundary condition and other important suggestions to successfully perform simulations with Ansys Fluent.

During my time at the chair, I had a chance to share the room partly with Shuai Guo with whom I had engaging discussions ranging from probability theory to his fascination about corgi dogs and partly with Alexander Eder - who now I refer to as a paper writing machine! Thanks to Thomas Hofmeister and Felix Schily for all the *English-Deutsch* translation duties and their help to find a decent living space in Munich. I had great fun with my ITN fellows (Alireza Javarehshkian, Guillaume Fournier, Michael McCartney and Naman Purwar) traveling to different cities before Covid-19 pandemic happened. I would like to additionally thank now Dr. Guillaume Fournier! for all the help I received during the submission of this thesis. Special mentions to Marcel Desor - the IT guy, Marcin Rywik, Edoardo Scoletta, Moritz Merk, Max Meindl, Matthias Häringer, Felicitas, Gary and Simon van Buren with whom I had memorable

time during the WTP Klausur and at the chair. Finally, it was a great experience to be a part of the SoTiC 2021 where I had fun organizing the event with Gerrit, Stephen and Prof. Sattelmayer. I also like to thank Frau Helga Bassett and Frau Sigrid Schulz-Reichwald for assisting me with German Bureaucracy and paperwork.

Being in a Marie-Curie ITN project, I had chance to meet talented researchers from across Europe not just from MAGISTER, but also from the ANNULIGHT project at different venues for project meetings. Many thanks to Jim Kok and James Dawson for coordinating these events where I was happy to meet my fellow ESRs: Varun, Alireza Ghasemi, Edmond, Sara, Ermanno and big names of the academia: Thierry Poincot, Tim Lieuwen, Laurent Gicquel, Benedicte Cuenot, Matthew Juniper and many others.

This thesis would not have been possible without my Munich family: Garima, Sneha, Prajeet, Farheen who were there as a family to share every moment with us. Thanks to all the late night conversations, trips and constant yet subtle reminders to complete my thesis. I am deeply grateful to my childhood friends: Anup, Arun and Shashidhar who made sure that I get much needed break away from academia from time to time. Special mention to my friend turned family, who I can now proudly call as Dr. Krishna with whom I shared so many memories talking about control theory, crypto, cricket during my doctoral journey.

I would like to express my deepest gratitude to my parents, for their love, and encouragement throughout my academic journey. Their belief in my abilities has been a constant source of motivation which has allowed me to reach this milestone. I also want to express my heartfelt appreciation to my dear brother for his constant support and encouragement. His belief in me and his willingness to lend an ear during challenging times have been invaluable. I am also very grateful to my father and mother-in-law for their belief in my capabilities and who inspire me to scale new heights. Finally, I would like to thank my beloved wife Ashwini, whose unwavering faith, love and encouragement have been the cornerstone of my PhD journey. I am deeply grateful for the countless sacrifices you have made personally while pursuing your own master's degree. At the beginning of my PhD, when I found it difficult to continue, you stood with me despite your own problems that you were facing both personally and academically. I am also very grateful for your words of encouragement, especially during the final phase of completing this thesis. This thesis would not have been possible without your support and you deserve it as much as I do. Thank you!

Contents

1	Introduction	1
2	Flame Dynamic Response	5
3	Response of spray to acoustics	7
3.1	Analytical Formulation	8
4	Estimation of flame dynamic response using LES simulations	12
4.1	Overview of LES methods	14
4.2	Overview of LES models for spray flames	16
4.2.1	Droplet Vaporization	17
4.2.2	Droplet Injection	18
5	Uncertainty Quantification and Surrogate Modeling	19
5.1	Gaussian Process for combined uncertainty using Bootstrapping methodology .	22
5.2	System Identification in Thermoacoustics	24
5.2.1	Input excitation signal generation	25
5.2.2	Selection of model structure	26
5.2.3	Estimation of model coefficients	27
5.2.4	Assessment of model quality	27
6	Contextualization and Discussion of Publications	29
6.1	Response of Monodisperse Droplets to Velocity Perturbations	29
6.2	Quantification of Mixed Uncertainties in the Flame model	31
7	Estimation of Spray Flame dynamics using LES/SI	33
7.1	Combustor Configuration	33
7.2	Numerical Setup	34
7.3	Preliminary Results	36
7.3.1	Axial velocity and temperature field	36
7.3.2	Droplet distribution and evaporation	37
7.3.3	Mixing and Flame stabilization	38
7.3.4	Flame Transfer Function	40
7.4	Conclusion	42
8	Summary and Contributions	44
8.1	Response of Spray Number Density and Evaporation Rate to Velocity Oscillations	44

8.2	Confidence in Flame Impulse Response Estimation From Large Eddy Simulation With Uncertain Thermal Boundary Conditions	45
9	Outlook	46
9.1	Response of motion of droplets and evaporation to velocity oscillation	46
9.2	Estimation of spray flame transfer function using LES/SI	46
9.3	Quantification of aleatoric and epistemic uncertainties in the flame response model	47
Appendix A	Reproduction of Papers	48
A.1	PAPER-EVAPORATION RESPONSE	49
A.2	PAPER-TOTAL UNCERTAINTY	60

1 Introduction

The aviation industry is expected to grow significantly despite the restrictions brought about by the recent pandemic. A recent estimate by the aviation industry's United Nations (UN) regulator- ICAO suggests that the demand for air transport will increase by an average of 4.3% per year over the next 20 years [1]. The burgeoning rise in the air demand leads to increased fossil-fuel burn from the contemporary aircraft engines and accelerates the production of green house gases: carbon dioxide, nitrous oxides, and water contrails. Increased green house gases correlates to a rise in global temperatures, which causes catastrophic changes to the natural environment. At this point, the aviation industry stands at the crossroads of growth and rising emissions. With increased pressure from the recent emission norms set out in the Paris Agreement ¹: the industry must respond to address its impact on the environment with continued improvement of existing technologies, while investing in the greener and sustainable solutions.

In recent years, disruptive and sustainable aviation propulsion technologies have been considered for the commercial and passenger air transportation sectors. Notably, electric propulsion, buoyed by the success in the automotive industry and hydrogen fuelled aero-engines that are already under advanced research and development phase. Each of these technological paths have their fair share of disadvantages along with obvious advantages. Electric propulsion provides improved efficiency in the energy conversion process and, depending on the origin of the materials used, can be seen as a technology with minimal emissions. Introducing electric propulsion to ground based transportation devices seems to be simple as they are relatively unaffected by the added weight of energy storage devices. Conversely, aircrafts are highly sensitive to the additional weight brought on by the batteries. The state-of-the-art mass specific energy density offered by the Lithium-ion batteries is in the range of 150-250 Wh/kg while the jet fuel has mass specific energy density of $\sim 10^4$ Wh/kg [2]. Bills et al [3] showed that the average short-haul flights (~ 900 km) would require 600 Wh/kg of battery density, medium-haul (~ 2000 km) would need 820Wh/kg and long-haul ($>\sim 4000$ km) a staggering 1,280Wh/kg. They also concluded that the current battery technology is not capable of servicing commercial airliners and one needs to move beyond the current state-of-the-art to either Lithium-air or Lithium-flourinated carbon chemistries.

Shifting to hydrogen as a fuel for aero-engines is not without challenges. The biggest deterrent is the extra weight required for the fuel storage, be it in gaseous or liquid form. For liquid hydrogen, efforts needs to be put in producing lightweight vacuum insulated tanks that maintain hydrogen below its boiling point of 20 K. Whereas gaseous hydrogen which has low volumetric energy density of 0.01 MJ/L at atmospheric pressure requires heavy weight tanks to be built that can withstand pressures of 250-300 bar [4] at which gaseous hydrogen's volumetric energy density exceeds that of kerosene. Although liquid hydrogen offers a higher mass-specific energy density (142 MJ/kg) than aviation fuel (44 MJ/kg), much of that energy could be spent in cryo-

¹https://unfccc.int/sites/default/files/english_paris_agreement.pdf

genic cooling ($\sim 45\%$) and thus delivers less energy for thrust (low tank-to-wing efficiency). Nevertheless, the development history hints that these technologies need another 20–30 years to mature and be certified for safe air travel. In this transition phase, conventional liquid jet fuel along with sustainable aviation fuels produced from sustainable raw materials will satisfy the increasing demand of the aviation sector.

As a result of increasing environmental protection regulations, aero-engine combustors are forced to operate in a lean combustion regime to reduce pollutant emissions. Operating in a lean combustion regime makes the engine susceptible to thermoacoustic combustion instabilities [5–8]. Thermoacoustic instabilities pose a severe technological hindrance in the development of the gas turbine engine. These instabilities occur due to the feedback loop between the acoustic waves, flow and flame. The gases traveling through the flame expand leading to pressure fluctuations propagating as acoustic waves. These acoustic waves interact with system boundaries and cause flow perturbation which then impinge on the flame leading to heat release fluctuations. When constructive interference between acoustic waves, unsteady combustion, and flow occurs, the amplitude of the pressure fluctuations can grow in time to a level that interferes with engine operation and, in extreme cases, leads to failure of the system due to excessive structural vibration and heat transfer [9].

A key ingredient in the feedback loop of thermoacoustic instabilities is the dynamic response of flame to acoustic forcing i.e flame dynamics. Flame dynamics is mainly described in the frequency domain using transfer functions that characterize the variations in the unsteady heat release rate to upstream velocity fluctuations. Different approaches have been employed in the literature to deduce the frequency response of a flame. These approaches range from highly resolved and expensive measurements [10] or CFD of reacting flows [11] to inexpensive simple mathematical models based on the kinematic balance between the flame and flow velocity [12].

Dynamic response of premixed gaseous flames has been well researched over the years with some focus on gaseous non-premixed flames in the recent years. Whereas modeling of spray flame dynamics has received sparse attention as the determination of spray flame response to acoustic oscillations is not straightforward compared to gaseous fuels due to several competing mechanisms involved in spray combustion. Several studies using experimental and numerical techniques have highlighted the complexities that arise in the estimation of the dynamic response of the spray flame and in subsequent analysis of thermoacoustic stability of liquid-fueled combustors [13–16]. The complexities arise because, in the event of a combustion instability in liquid-fuelled combustors, the spray processes such as atomization, droplet convection, droplet-turbulence interaction, and evaporation are perturbed [17–19] and could control the flame dynamic response. Specifically, the acoustic velocity fluctuations caused by an instability directly modify the flame surface area and generate heat release rate oscillations similar to the instability mechanism in gaseous fuel combustion. In liquid-fuelled combustion additional mechanisms are at play where the acoustic velocity fluctuation modifies the fuel atomization, evaporation and mixing processes resulting in spatial and temporal variations in the equivalence ratio. Equivalence ratio variation causes heat of reaction changes over the flame surface and flame speed, giving way to additional pathways for overall heat release rate variation in the thermoacoustic feedback loop.

Compared to gaseous fuel combustion, there are multiple mechanisms, as seen before, contributing to thermoacoustic instability in a liquid fueled combustor. Understanding how these

mechanisms respond to velocity fluctuations is imperative in the development of aero engine as it enables the designer the means to stabilize the combustor. In this thesis an inexpensive analytical tool is developed to study the acoustic response of the droplet motion and evaporation. This theoretical study extends the work of Achury and Polifke [19] on the response of a single droplet to acoustic excitation to the population of droplets with evaporation. A specific closed-form formula is derived for the inhomogeneous and time-varying change in droplet concentration, referred to as the number density wave. This is then followed by an analysis of how an evaporating spray responds to fluctuations in acoustic velocity, and a description of the evaporation dynamics using a transfer function is presented. Such a theoretical formulation gives the possibility of carrying out parametric analysis with respect to different fuels, spray, and gas boundary conditions. Therefore, such analytical approaches enable quick characterization and turnaround needed at the early development stages of the engine.

One of the ways to evaluate the thermoacoustic stability of the system is through "divide and conquer" approach. Such an approach requires a flame response model as an input to an acoustic solver to deduce the growth rate and frequencies of the thermoacoustic modes of the system. The flame response in terms of the finite impulse response in the time domain is typically obtained from the CFD/SI procedure [20]. The flame response identified from CFD/SI procedure will be uncertain due to epistemic and aleatoric uncertainties. Epistemic uncertainties arise due to lack of knowledge of boundary conditions, such as spray boundary conditions after primary breakup of liquid, which are generally not modeled. Aleatoric uncertainties arise due to the application of the statistical SI procedure on time series data corrupted by turbulent noise. Figure 1.1 pictorially depicts the location of the occurrence of epistemic and aleatoric uncertainties in the CFD/SI flame model identification procedure.

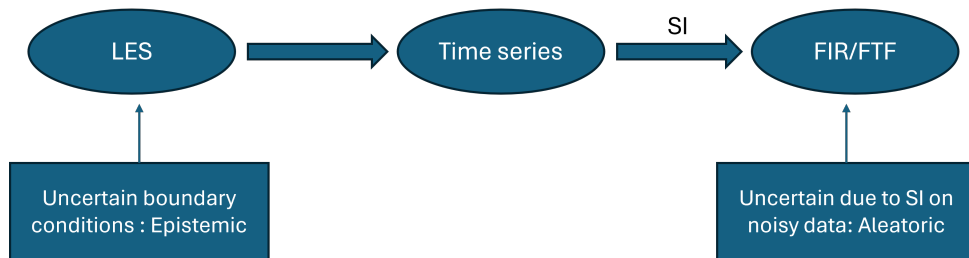


Figure 1.1: Identification of FIR/FTF is impacted by different sources of uncertainties in the LES/SI procedure

The second section of the thesis presents the assessment of epistemic and aleatoric uncertainties in the flame response model. Previous works focused on quantifying either epistemic [21] or aleatoric uncertainties [22] in the estimated flame model. To quantify both types of uncertainties in the impulse response flame model, a data-driven univariate Gaussian Process surrogate model is developed. This model is trained on the Finite Impulse Responses (FIRs) obtained from the LES/SI procedure under various boundary conditions. Additionally, a bootstrapping procedure is employed to address the variability of the estimated FIR coefficients. The surrogate model provides a robust approach to not only predict the FIR at any test location but also to provide combined epistemic and aleatoric uncertainty in the associated prediction of the impulse response.

In the concluding section of the dissertation, initial findings from the Large Eddy Simulation

(LES) of a turbulent spray flame generated by the GE Avio PERM (Partially Evaporating and Rapid Mixing) injector for aero-engine application, along with the FTF derived from using the SI method, are presented. The examination of how the spray flame reacts to acoustic forcing is based on the insights obtained from the analytical investigations conducted in the initial section of the thesis. The Large Eddy Simulation (LES) is utilized as a framework to implement the Gaussian Process surrogate technique established in this thesis to assess the influence of uncertain spray boundary conditions on the flame model.

The purpose of the thesis is to give an overview of the Gaussian process surrogate method used in this work to quantify mixed uncertainties, describe the LES setup of the PERM injector and preliminary results of the FTF and provide the context and summary of how different publications connect to this thesis.

2 Flame Dynamic Response

Flame dynamic response also known as combustion dynamics, is the response of the flame to upstream acoustic fluctuations which plays a key role in the thermoacoustic instability. Mathematically, this relates how global heat release rate fluctuation \dot{Q}' is linked to a driving factor such as the upstream velocity, equivalence ratio that causes these fluctuations. In a simple case of perfectly premixed flames that are velocity sensitive, global heat release rate fluctuations \dot{Q}' due to velocity perturbations u' upstream of the flame can be characterized in terms of either flame frequency response or flame transfer function, such that

$$\frac{\dot{Q}'(\omega)}{\bar{Q}} = \mathcal{F}(\omega) \frac{u'(\omega)}{\bar{u}} \quad (2.1)$$

or by corresponding flame impulse response $h(t)$

$$\frac{\dot{Q}'(\omega)}{\bar{Q}} = \frac{1}{\bar{u}} \int_0^T h(\tau) u'(t - \tau) d\tau \quad (2.2)$$

The $(')$ denotes deviation of a quantity from its mean value $(\bar{\cdot})$. The symbols ω and τ denote angular frequency and time delay respectively. T corresponds to the duration of the impulse response $h(t)$. A variety of models with different levels of complexity can be found in the literature to describe the FTF. One of the earliest and simple model of FTF is the $n - \tau$ model introduced by Crocco and Cheng [23]. In this model, the global heat release rate responds with a gain n for an acoustic disturbance produced upstream of the flame after a time delay of τ . This can be represented for a wide range of frequencies as

$$\mathcal{F}(\omega) = n(\omega) \exp(i\omega\tau(\omega)) \quad (2.3)$$

The flame transfer function is valid only in the limit of small acoustic fluctuations and thus cannot be used to determine the limit cycle amplitude of the thermoacoustic instability. Large amplitude oscillations trigger non-linear response and require a non-linear description of the flame dynamic response in terms of a Flame Describing Function [24]. In this work, the flame impulse response identified from LES and system identification procedure is used to emphasize the effect of inherent uncertainties that are associated with this widely used procedure.

As mentioned in the introductory section, combustion instabilities arise from the constructive interference between the flame and acoustics, which can be characterized by a suitable FTF. Figure 2.1 illustrates a general feedback loop for combustion instabilities. This loop consists of: 1) fluctuations in flow and mixture leading to fluctuations in heat release rate, 2) fluctuations in heat release rate inducing acoustic disturbances, and 3) these acoustic disturbances subsequently creating velocity fluctuations as described in step 1, thus completing the feedback loop. Depending on the energy added and the acoustic losses, the amplitude of the oscillations may decay, remain constant or grow non-linearly until limit cycle regime.

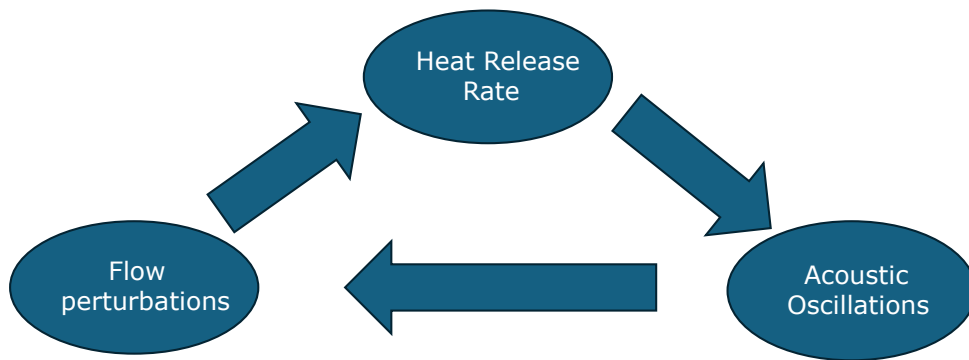


Figure 2.1: Schematic of the feedback processes responsible for thermoacoustic instabilities

Thermoacoustic instabilities can be driven by many mechanisms depending on the fuel used. Figure 2.2 shows different flow and flame processes that cause thermoacoustic instabilities in gas turbines. As the figure suggests, combustion instabilities in gaseous flames can be driven

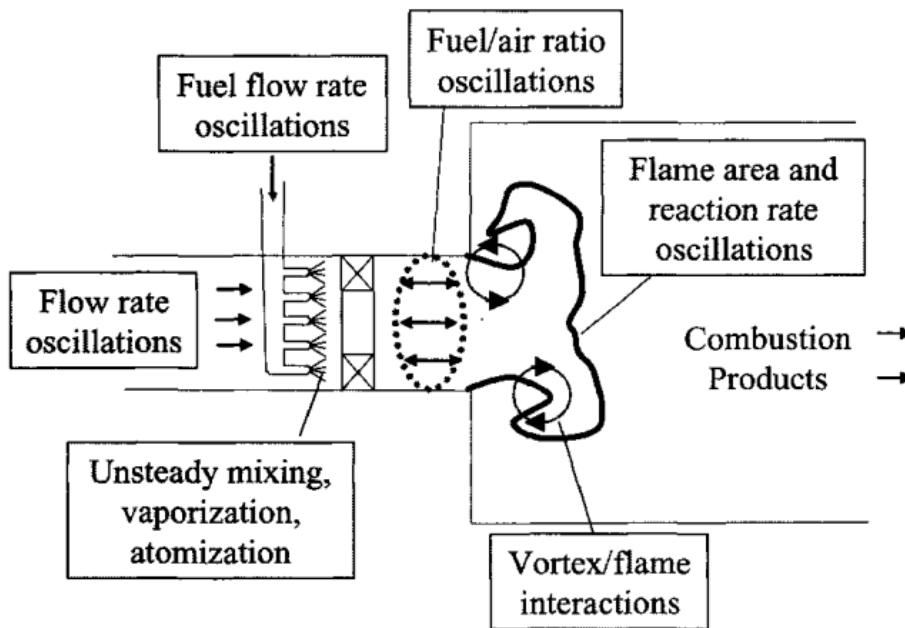


Figure 2.2: Illustration of different processes that can cause combustion instabilities. Courtesy Lieuwen et al. [25]

by many processes except for the vaporization and atomization which only occurs in a liquid fuel combustor. Because of the introduction of liquid fuel, acoustics interact with the injection, transport, and evaporation of liquid fuel to cause periodic release of gaseous vapor. This causes fluctuations in the equivalence ratio and perturbs the heat release rate. Depending on the time delay of the atomization, evaporation processes involved, and the distance of the reaction zone to the liquid fuel injector, the combustion instability can be driven by this additional pathway. The physical mechanisms driving combustion instabilities in gaseous fuels have been reviewed by [7, 25, 26]. However, the literature is sparse on the mechanisms driving combustion instabilities in liquid fuel combustion systems [13, 14, 27] due to the additional complexities caused by the liquid fuel combustion processes described earlier.

3 Response of spray to acoustics

A key component of the thermoacoustic instability process is the perturbation of the unsteady heat release rate by acoustic pressure. For an acoustically compact flame, the flame is insensitive directly to acoustic pressure fluctuations p' . However, fluctuations in acoustic pressure p' indirectly through fluctuations in gas velocity u' cause a disturbance in the global heat release rate. For gaseous flames, the perturbation of u' breaks the flow-flame kinematic balance and results in flame wrinkling. As a result of flame wrinkling, the flame curvature increases, and consequently increases the local flame speed. Enhanced flame speed further causes flame wrinkling by kinematic restoration [12]. In the case of swirl-stabilized combustors, vorticity waves are generated and in combination with acoustic waves again cause fluctuations in the flame area [28].

In liquid fuel combustion, as both the liquid phase and the gas phase exist, the mechanisms discussed above for gas phase interactions are supplemented by the acoustic wave and liquid spray interaction. As shown in Figure 3.1, the fluctuations in the inlet velocity modify the atomization process, causing a variation in the droplet sizes. Further, the differently sized droplets, while being convected downstream with the oscillating gas flow, also simultaneously evaporate. As a result, all of these processes contribute to the spatial and temporal variations of the equivalence ratio field. Perturbations in the equivalence ratio result in heat of reaction variations over the flame surface, giving rise to heat release rate oscillations.

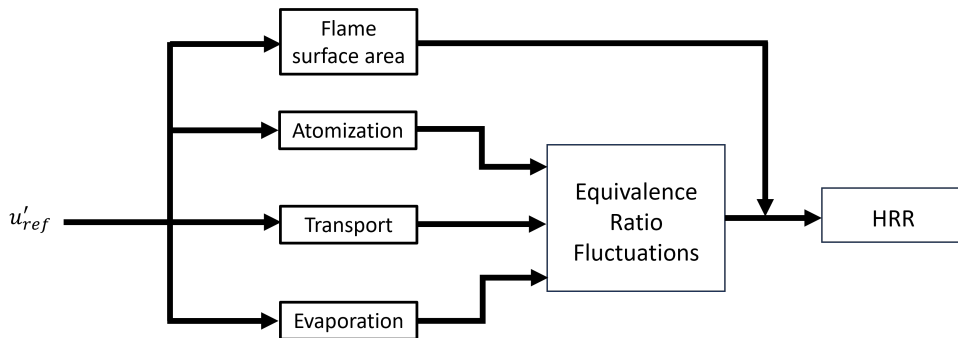


Figure 3.1: Schematic of the acoustic velocity coupling mechanism generating heat release rate oscillation for spray flames

One of the approaches used for thermoacoustic stability analysis is the construction of a theoretical description of the response of the flame to acoustic perturbations. Such analytical descriptions facilitate rich parametric analysis at a fraction of cost compared to numerical or experimental analysis. These analytical tools provide great help in the early combustor design phase and reduce the amount of time spent performing costly numerical and physical experiments. In any combustor, the overall heat release rate fluctuations due to acoustic perturbations

is governed by different mechanisms such as flame area changes, flame roll-up, flame stretching and so on. Extensive studies [12, 29] have been conducted to quantify analytical flame transfer functions for gaseous laminar and turbulent flames of different flame shapes. However, comprehending the contribution of different mechanisms towards the global spray flame response to velocity disturbances has received little attention due to the difficulties that arise when taking into account the two-phase nature of the problem. In recent years, there has been emphasis on numerical modeling of the response of a single droplet evaporation to an acoustic field [30–34]. Some studies have used the theoretical approach using the Euler-Lagrange framework to quantify the response of a single droplet to velocity oscillations [19, 35]. Recently, Moriniere [36] also introduced an analytical framework to describe the response of the droplet population to the perturbation of the upstream velocity using the Euler-Euler formulation. An analytical description of the acoustic response of a monodisperse droplet population (spray) within Euler-Lagrange has not been well documented, and this knowledge is important to build an analytical FTF of spray flames similar to premixed gaseous flames. In this section, a detailed derivation of the response of a population of monodisperse droplets with evaporation is introduced, which is used in the PAPER-EVAPORATION RESPONSE.

3.1 Analytical Formulation

In both the CFD and theoretical contexts, there are two approaches to model multiphase flows: Euler-Euler or Euler-Lagrange. For an analytical description of the response of a population of droplets to velocity perturbations, the Lagrange-mass point approach is considered to be a reasonably low-cost alternative, compared to methods that resolve the particle-fluid interface. Lagrangian approach requires modeling all the forces acting on the droplet to determine its velocity and location. The Lagrangian equation of motion for a spherical droplet with mass m_d and velocity \mathbf{u}_d is given by:

$$\frac{d\mathbf{u}_d}{dt} = \underbrace{\mathbf{g}}_{\text{body: gravity}} + \underbrace{\frac{1}{\gamma} \left(\frac{D\mathbf{u}_c}{Dt} - \mathbf{g} \right)}_{\text{undisturbed flow}} + \underbrace{\frac{3C_D}{4\gamma D} |\mathbf{u}_c - \mathbf{u}_d| (\mathbf{u}_c - \mathbf{u}_d)}_{\text{steady state drag}} + \underbrace{\frac{\Delta_A}{2\gamma} \left(\frac{D\mathbf{u}_c}{Dt} - \frac{d\mathbf{u}_d}{dt} \right)}_{\text{virtual mass}} + \mathbf{F}_{\text{Basset}} \quad (3.1)$$

In liquid fuel-air combustion systems, the density of the liquid is much higher than that of air ($\rho_{liq} \gg \rho_{gas}$) and in such cases, the virtual mass and Basset forces become negligible. The effect of gravitational acceleration on the droplet is also neglected. In the overarching context of constructing an analytical spray flame transfer function, the work described here introduces a simplified 1D approach, which nevertheless addresses the basic physics involved. For 1D flow in the Stokes flow regime, the Lagrangian equation of motion reduces to:

$$\frac{d\mathbf{u}_d}{dt} = \frac{1}{\gamma} \left(\frac{\partial u_c}{\partial t} + u_c \frac{\partial u_c}{\partial x} \right) + \frac{18\nu_c}{\gamma D^2} (u_c - u_d) \quad (3.2)$$

For the theoretical description of the response of droplets to velocity oscillations, the droplet motion equation is solved with the fluctuating carrier gas velocity u_c :

$$u_c = \bar{u}_c + \hat{u}_c \sin(\omega t + \phi), \quad (3.3)$$

3.1 Analytical Formulation

Droplets are continuously being injected with a velocity of u_d in the fluctuating gas velocity environment resembling droplet injection from an atomizer. In Eq. 3.3, \bar{u}_c is the mean velocity, \hat{u}_c is the fluctuating component of the gas velocity, $\omega = 2\pi f$ is the angular frequency, and ϕ is the phase angle of the flow oscillation, which is included to generalize the solution. In this work, droplets are injected into an oscillating flow of an incompressible medium at the mean gas velocity, corresponding to the zero slip velocity with respect to mean gas velocity ($u_d = \bar{u}_c$). Substituting the gas velocity equation 3.3 in Eq. 3.2 gives:

$$\frac{du_d}{dt} = \frac{1}{\gamma} (\hat{u}_c \omega \cos(\omega t + \phi)) + C (\bar{u}_c + \hat{u}_c \sin(\omega t + \phi)) \quad (3.4)$$

where $C = 18\nu/\gamma D^2$. As we are interested in the trajectory of the particle from the injection time t_i until some measurement time t , the above differential equation can be solved by assuming that a general solution is of the form e^{ct} and integrating in the limit from t_i to t :

$$\int_{t_i}^t \frac{d(e^{ct} u_d)}{dt} = \int_{t_i}^t \frac{1}{\gamma} (\hat{u}_c \omega \cos(\omega t + \phi)) + (\bar{u}_c + \hat{u}_c \sin(\omega t + \phi)) \quad (3.5)$$

Applying integration by parts on the right hand side terms and the integration limits we get:

$$u_d = C_3 \left[\sin(\omega t + \phi) \left(\frac{\omega^2}{\gamma} + C^2 \right) + \omega C \cos(\omega t + \phi) \left(\frac{1}{\gamma} - 1 \right) \right] + \bar{u}_c - \bar{u}_c e^{C(t_i-t)} + u_{d0} e^{C(t_i-t)} + C_3 \left[\omega C e^{C(t_i-t)} \cos(\omega t_i + \phi) \left(\frac{1}{\gamma} - 1 \right) - e^{C(t_i-t)} \sin(\omega t_i + \phi) \left(C^2 + \frac{\omega^2}{\gamma} \right) \right] \quad (3.6)$$

with C_3 defined as:

$$C_3 = \frac{\hat{u}_c}{\omega^2 + C^2} \quad (3.7)$$

Integrating the droplet velocity equation above gives the droplet trajectory equation:

$$x_d = C_3 C \left[\sin(\omega t + \phi) \left(\frac{1}{\gamma} - 1 \right) - \cos(\omega t + \phi) \left(\frac{C}{\omega} + \frac{\omega}{\gamma C} \right) \right] + \bar{u}_c t + \bar{u}_c e^{C(t_i-t)} - u_{d0} e^{C(t_i-t)} - C_3 \left[\omega e^{C(t_i-t)} \cos(-\omega t_i + \phi) \left(1 - \frac{1}{\gamma} \right) - e^{C(t_i-t)} \sin(\omega t_i + \phi) \left(\frac{\omega}{\gamma C} + \frac{C}{\omega} \right) \right] + C_1 \quad (3.8)$$

The trajectory equation can be written in a compact way:

$$x_d = C_1 + C_2 e^{C(t_i-t)} + \bar{u}_c t + C_3 C \left(\sin(\omega t + \phi) \left(\frac{1}{\gamma} - 1 \right) - \cos(\omega t + \phi) \left(\frac{C}{\omega} + \frac{\omega}{\gamma C} \right) \right) \quad (3.9)$$

with,

$$C_2 = C_3 \omega C \left(\cos(\omega t_i + \phi) \left(\frac{1}{\gamma} - 1 \right) + \left(\frac{\omega}{\gamma C} + \frac{C}{\omega} \right) \right) + \frac{\bar{u}_c - u_{d0}}{C} \quad (3.10)$$

The integration constant C_1 in Eq. 3.8 is obtained by substituting initial conditions: at $t = 0$, $x_d = 0$ and $u_d = u_{d0}$:

$$C_1 = C_2 - C_3 C \left(\frac{C}{\omega} + \frac{\omega}{\gamma C} \right) \quad (3.11)$$

Equation 3.9 represents the dimensional droplet trajectory equation for mono-disperse droplets injected in an oscillating flow field. The first term of the droplet position equation (Eq. 3.9) is a constant, the second term describes an exponential decay where the droplets "lose" the influence of the initial condition as time progresses, the third term represents the mean convection of droplets which increases linearly with time and the fourth term describes the modulation of the droplet positions due to flow oscillation.

In the work of PAPER-EVAPORATION RESPONSE, the droplet is injected into the gas stream close to the wet bulb temperature of the liquid at the given temperature and pressure of the gas phase. Thus, the droplet heating time is negligible. In practical scenarios, significant droplet heating may occur, leading to additional droplet heating duration that could be crucial in the analysis of thermoacoustic stability.. The following analytical work adopted from Lupo and Duwig [37] shows the calculation of the droplet heat up time that can be included in the theoretical framework.

When the droplet is injected into the gas phase, the droplet evolution is characterized by two regimes:

1. Initial transient period until the droplet heats up to the wet bulb temperature T_{wb} .
2. Evaporation at constant wet bulb temperature T_{wb} under the d^2 -law.

In the transient regime, when the initial liquid temperature T_{l0} is less than the wet bulb temperature T_{wb} , the heat is transferred from the gas to the liquid in part to raise the droplet temperature to T_{wb} and partly it is used as latent heat of vaporization. In this work, a rapid mixing model is assumed in which the liquid field is treated as uniform and at constant temperature. Such an assumption is applicable in the case of a strong internal circulation or a small Biot number. With the rapid mixing model, the droplet temperature evolution for a droplet of initial diameter d_0 and at initial temperature T_{l0} can be written as

$$\frac{dT_l}{dt} = \frac{\beta_1}{\tau_h} [(T_\infty - T_l) - \beta_2] \quad (3.12)$$

where $\tau_h = d_0^2/4\alpha_0$ and α_0 is the thermal diffusivity of the liquid. The solution for the above differential equation is given by:

$$T_l = T_\infty - \beta_2 - [(T_\infty - T_{l0}) - \beta_2] e^{-\beta_1 t/\tau_h} \quad (3.13)$$

with β_1 and β_2 given as:

$$\beta_1 = \frac{\ln(1 + B_{M0})}{Le_0} \frac{1}{B_{T0}} \frac{\bar{\kappa}_0}{\kappa_{l0}} \quad (3.14)$$

$$\beta_2 = \frac{\Lambda_0 B_{T0}}{\bar{c}_{p0}} \quad (3.15)$$

In the above equations, B_{M0} and B_{T0} correspond to initial Spalding mass transfer and heat transfer number respectively. For a droplet convecting through the gas phase, the Spalding mass and heat transfer numbers are given by:

$$B_M = \frac{Y_s - Y_\infty}{1 - Y_s} \quad (3.16)$$

$$B_T = (1 + B_M)^{1/Le} - 1 \quad (3.17)$$

3.1 Analytical Formulation

where Y_s and Y_∞ represent the droplet mass fraction at the surface and far away from the surface respectively and Le is the Lewis number of the liquid. The droplet heat up time to reach the wet bulb temperature is given by:

$$\tau_{wb} = \frac{\tau_h}{\beta_1} \ln \left(\frac{(T_\infty - T_{l0}) - \beta_2}{(T_\infty - T_{wb}) - \beta_2} \right) \quad (3.18)$$

Finally, the overall lifetime of the droplet is given by adding the heat up time and the droplet vaporization time at constant T_{wb} using the d^2 -law:

$$\tau_{life} = \tau_{wb} + \frac{d_s^2}{K_{wb}} \quad (3.19)$$

where K_{wb} is the evaporation coefficient.

4 Estimation of flame dynamic response using LES simulations

Combustion instability is one of the critical issues that affects the stable operation of a lean combustion gas turbine engine. As we have seen earlier, these instabilities are the result of constructive interference of pressure oscillations and unsteady heat release rate, which eventually damages the engine components and reduces the life span of the engine. Therefore, the prediction of the thermoacoustic stability of the system in the early design phase becomes important. For a successful prediction of the thermoacoustic behavior, a thorough understanding of the flame dynamics and its driving mechanisms is necessary. Generally for gaseous flames, its dynamic response to acoustic perturbations is quantified by a flame transfer function if the level of perturbations is small. The FTF over the desired range of frequencies is derived from applying a broadband excitation to the flame in a high fidelity LES simulation coupled with System Identification methods [20]. The FTFs identified from the LES/SI procedure are combined together with an acoustic model to determine the thermoacoustic eigenmodes of the system.

Quantifying an FTF for spray flames is rather complex due to the effect the acoustic perturbations may have on various processes such as atomization, evaporation, transport, and mixing. As seen in the earlier work - PAPER EVAPORATION RESPONSE [38], the perturbation in velocity gives rise to periodic variation of the droplet size distribution and equivalence ratio which consequently produces heat release rate oscillations. The physical processes involved in the combustion of liquid fuel are intertwined, and further research is necessary to understand these interactions accurately.

The following review of the literature highlights the important driving mechanisms involved in liquid fuel dynamics. Tachibana et al. [14] performed LES of a self-sustained instability event of a swirled spray flame at elevated pressure and noticed the importance of the time delay introduced by evaporation and proposed a simple acoustic velocity mechanism as a driving factor of the thermoacoustic instability in their LES study. Pillai et al. [39] showed the effect of temporal variation of the droplet diameter distribution on the instability behavior of a backward-facing step combustor. Vignat et al. [13] in their study also show various mechanisms such as fluctuation of the swirl number due to acoustics, fluctuations of the fuel flow rate resulting from the response of the injector to acoustics and together with the fluctuation of the total mass flow rate drives the fluctuation of the heat release rate. These processes give rise to a combined time delay of the injector response, convection time, and chemical conversion time. Interestingly, vaporization time is not included, as it happens simultaneously with convection. Kitano et al. [15] remarked that in their high equivalence ratio flame, reaction dominates droplet evaporation, as the surrounding rich fuel gas mixture consumption leads to enhanced droplet evaporation. They also concluded that the thermoacoustic mode is affected by the initial diameter of the droplets, which controls the release of fuel vapor. Recently, Lo Schiavo et al. [40] showed the importance

of the liquid fuel injection angle and the liquid film dynamics on the stability of the SICCA combustor. These studies with high fidelity LES simulations show the existence of different mechanisms and how they contribute in driving combustion instabilities while highlighting the complexity that comes in predicting combustion instability of liquid fuels.

Another approach to evaluate thermoacoustic stability of the system is to use the "divide and conquer" approach, also known as the hybrid approach as elucidated in the previous chapter of this thesis. For the hybrid approach, a flame model is required, which is generally represented by a flame transfer function. Numerous works exist in the literature on the estimation and measurement of FTF of gaseous fuels, whereas few investigations have been carried out on the estimation and measurement of FTF of liquid fuel flames mainly due to the complexities involved. Concerning the FTF of liquid fuel, Eckstein et al. [41] indicated that for air-assisted atomizers, in the limit of negligible prevaporization, the heat release rate is directly proportional to the droplet evaporation rate. It was noted that with low-frequency combustion oscillations, increases in air velocity result in a corresponding increase in heat release rate oscillations. This establishes a direct relation between heat release rate and the droplet diameter. Andreini et al. [42] investigated different formulations of liquid flame FTF to reproduce the flame behavior obtained from an aeroengine liquid fuel PERM injector and concluded that simple FTF formulations are inadequate to capture the dynamic flame behavior generated from the PERM injector, which has been shown to be strongly dependent on operating conditions [43].

As simple FTF formulations are insufficient to describe the dynamic behavior of the flame produced by the PERM injector, an alternate way of estimating the flame dynamics from the CFD/SI method described earlier can be employed. Zhu et al. [44] performed RANS of a spray flame of a simplified domain and computed the transfer behavior of the system by estimating the coefficients of the infinite impulse response filter in the low-frequency regime. They observed that the rate of combustion increases in the primary zone when the air velocity upstream is high, consistent with the findings of Eckstein and Sattelmayer at a later time. At high frequencies, the combustion lags the quasi-steady response through a simple time lag. Badhe and coworkers [45] conducted flame dynamics studies using LES of the SICCA burner, which had been previously studied for self-excited instabilities. They applied harmonic acoustic forcing at varying frequencies to analyze the Flame Transfer Function (FTF) using LES/SI methods and to explore how the injection angle affects flame dynamics. It was observed that when the inlet was forced, the level of acoustic velocity fluctuation obtained prior to the swirler was inconsistent with the experiments indicating inadequate acoustic resolution of the domain. While the outlet forcing matches the results with inlet forcing, there is an overall mismatch with the measured data. In another study, Innocenti et al. [46] performed URANS of a spray flame produced by GE Avio PERM injector with $\beta - PDF$ combustion model and estimated the FTF using System Identification techniques. Through the CFD/SI procedure, they showed the sensitivity of the flame dynamics to the liquid fuel properties and the wall thermal boundary condition. They found that constant or variable liquid fuel properties as a function of temperature impacted the evaporation location and velocity. Similarly, adiabatic and isothermal combustor back plane boundary condition changed the FTF qualitatively and quantitatively. Overall, qualitative trend of the FTF was in agreement with the measured data. Quantitatively, a mismatch with experimental data was observed particularly in the low-frequency region which could be due to multiple modeling assumptions: value of the combustor wall temperature, liquid fuel injection boundary condition and reaction mechanism of the fuel.

One of the objective of the current thesis is to identify FTF of both gaseous and spray flames using LES/SI method which is to be used for different investigations. For the flame models to be determined via SI techniques, the input-output time series data needs to be generated through LES simulations and this constitutes as a first step in the overall FTF identification and uncertainty quantification procedure. In the current work both compressible and incompressible reactive LES is used for data generation step.

4.1 Overview of LES methods

One of the major challenges in solving fluid dynamical flows computationally is to accurately resolve turbulent structures. There is no universal model for turbulence and it is often geometry-dependent. In a turbulent flow, large turbulent structures exist which are often dependent on the geometry of the fluid containment and the kinetic energy continuously transfers from larger structures to smaller structures until the energy is dissipated at the smallest Kolmogorov scales. For homogeneous isotropic turbulence the energy transfer happens through a constant dissipation rate. This energy cascade process is shown in Figure 4.1 Resolving different scales in a

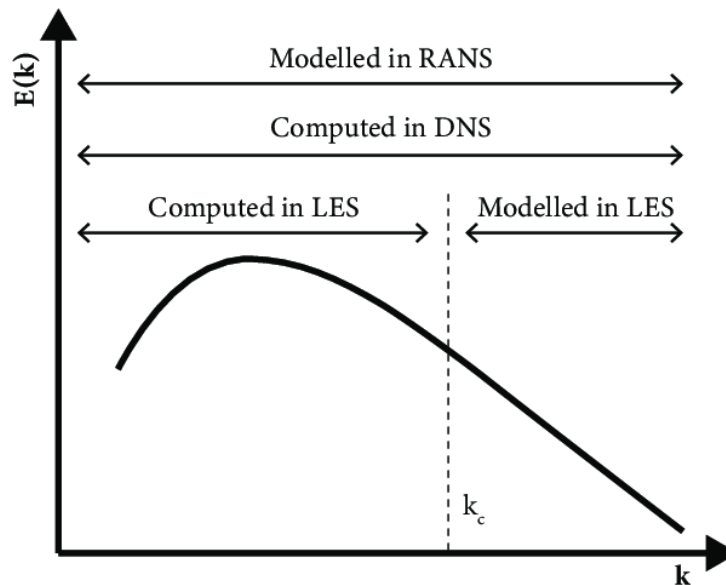


Figure 4.1: Different turbulence modeling approaches visualized through turbulent energy spectrum against wave numbers

CFD simulations gives rise to different modelling approaches. On one extreme end is the RANS approach where all the scales are modeled resulting in statistical mean flow quantities that are dissipative and do not represent temporal nature of the quantities of interest. On the other extreme end is the DNS approach, where all the scales down to the smallest Kolmogorov scales are resolved via a highly refined mesh. Such a highly resolved simulation is practically not possible for engineering problems due to the high computational demand of the DNS approach. Another approach is the LES method, which utilizes best of both the RANS and DNS methods. In LES, large-scale geometry-dependent turbulent structures that contain most of the energy are resolved by the computational grid filtering out the small scales. The filtered small scales that

4.1 Overview of LES methods

exhibit universal characteristics are modeled using the information of the resolved scales with a suitable subgrid scale (SGS) model. In this work, subgrid stresses exerted by the smallest scales are modeled using the Wall Adapting Linear Eddy (WALE) model as:

$$\bar{\tau}_{ij}^{sgs} = -\bar{\rho} (\widetilde{u_i u_j} - \widetilde{u_i} \widetilde{u_j}) \quad (4.1)$$

A turbulent viscosity is used to model the viscous stress as:

$$\bar{\tau}_{ij}^{sgs} = \bar{\rho} \nu_t \left(\frac{\partial \widetilde{u_j}}{\partial \widetilde{x_i}} + \frac{\partial \widetilde{u_i}}{\partial \widetilde{x_j}} \right) - \frac{2}{3} \bar{\rho} \nu_t \left(\frac{\partial \widetilde{u_k}}{\partial \widetilde{x_k}} \delta_{ij} \right) \quad (4.2)$$

In the WALE model, the turbulent viscosity is modelled as:

$$\nu_t = (C_w \Delta_x)^2 \frac{(S_{ij}^d S_{ij}^d)^{3/2}}{(\widetilde{S}_{ij} \widetilde{S}_{ij})^{5/2} + (S_{ij}^d S_{ij}^d)^{5/4}}, \quad (4.3)$$

with

$$S_{ij}^d = \frac{1}{2} \left[\left(\frac{\partial \widetilde{u_i}}{\partial \widetilde{x_j}} \right)^2 + \left(\frac{\partial \widetilde{u_j}}{\partial \widetilde{x_i}} \right)^2 \right] - \frac{1}{3} \left(\frac{\partial \widetilde{u_k}}{\partial \widetilde{x_k}} \right)^2 \delta_{ij}, \quad (4.4)$$

and

$$\widetilde{S}_{ij} = \frac{1}{2} \left(\frac{\partial \widetilde{u_j}}{\partial \widetilde{x_i}} + \frac{\partial \widetilde{u_i}}{\partial \widetilde{x_j}} \right) \quad (4.5)$$

$C_w = 0.4929$ is the model constant. Unresolved species fluxes and energy fluxes are closed using turbulent Schmidt and Prandtl numbers, respectively.

In turbulent reactive systems, the flame thickness produced by the fuel/air combustion is smaller than the grid size for the given operating conditions, pointing out the need for a subgrid scale combustion model. A Thickened Flame Model (TFM) is used as a subgrid scale combustion model in this work. As the adopted mesh is larger than the laminar flame thickness, the flame front is artificially thickened to be able to resolve it on the LES grid. Thickening is achieved while preserving the laminar flame speed by increasing the thermal diffusivity D_{th} and reducing the reaction rate exponent A by a factor F named thickening factor for a single step reaction. Scaling the diffusivity and reaction rate exponent gives a constant laminar flame speed S_L^0 and increased flame thickness δ_L^0 as:

$$S_L^0 \propto \sqrt{D_{th} A} \xrightarrow{\text{Thickening}} \sqrt{F D_{th} \frac{A}{F}} = \sqrt{D_{th} A} \quad (4.6)$$

$$\delta_L^0 = \sqrt{\frac{D_{th}}{A}} \xrightarrow{\text{Thickening}} \sqrt{F D_{th} \frac{F}{A}} = F \sqrt{\frac{D_{th}}{A}} \quad (4.7)$$

With appropriate values of F , the reaction zone can be sufficiently resolved on the adopted mesh. Typically, F is used such that 5-7 mesh points lie inside the flame zone. Constant values of F cannot be used in regions where no reactions occur. To limit the thickening to regions around the flame only, a sensor factor S is used to detect premixed reaction zones and apply the thickening [47]. This approach is known as a dynamically thickened flame model. The value of S is calculated from the flame front characterizing reaction rate equation for the global one-step

and two-step reaction schemes. The Value of S needs to be adjusted when multistep reaction schemes are used. Artificial thickening of the flame causes a reduction in the Damköhler number Da , altering the rates of wrinkling of the flame and fuel consumption. To compensate for reduced Da , the thermal diffusivity and reaction rate are multiplied by an efficiency function E adopted from the work of Colin et al. [48]. The efficiency function is the wrinkling ratio of the non-thickened flame to the thickened flame. The TFM model is used with a two-step global mechanism for kerosene/air combustion developed by Franzelli et al. [49] for the LES simulations in this work.

4.2 Overview of LES models for spray flames

There are two approaches when it comes to numerical simulation of multiphase flows: Euler-Euler approach, where different phases are treated as interacting continuum and equations are solved for the phase volume fraction, which is a continuous function of space and time, and the sum of different phases always reaches unity. For LES applications, governing equations are filtered and suitable subgrid scale modeling is employed where necessary; in Euler-Lagrange approach that is used in this thesis, fluid phase is treated as continuum characterized by the Navier-Stokes equation, while the dispersed phase is solved by tracking large number of particles/droplets through the continuous fluid phase. The dispersed phase can exchange mass, momentum, and energy with the continuous fluid phase. In the Euler-Lagrange approach, no subgrid-scale modeling or ensemble averaging is used, thus making it suitable for tracking polydisperse sprays.

In the Euler-Lagrange approach, the spray droplets are assumed to be discrete spherical droplets, which are smaller than the Kolmogorov length scales. The trajectory of particles is computed by integrating the momentum equation, which is written in Lagrangian reference frame as:

$$\frac{du_p}{dt} = F_D(u - u_p) + F_x \quad (4.8)$$

where F_x represents additional forces (added mass, Basset history force) that act on the droplet. The force of gravity is neglected. In combustion applications where the density difference between liquid and gas is high ($\rho_{liq} \gg \rho_{gas}$), these force terms become irrelevant and only drag forces are significant. F_D is the drag force per unit particle mass given by:

$$F_D = \frac{18\mu}{\rho_p d_p^2} \frac{C_D Re}{24} \quad (4.9)$$

Here, u is the fluid phase velocity, u_p is the discrete phase velocity, μ is the molecular viscosity of the fluid, ρ is the density of the fluid, ρ_p is the density of the discrete phase and d_p is the diameter of the particle. Re is the relative Reynolds number defined as:

$$Re = \frac{\rho d |u_p - u|}{\mu} \quad (4.10)$$

Equation 4.8 is integrated in time over discrete time steps to yield the velocity of the particle at each point along the particle trajectory. Particle trajectory itself is calculated by integrating

the velocity. Particle velocity and trajectory equation are coupled ordinary differential equations and can be cast in general form as:

$$\frac{du_p}{dt} = \frac{1}{\tau_p} (u - u_p) + a \quad (4.11)$$

with

$$\tau_p = \frac{\rho_p d_p^2}{18\mu(1 + 0.15Re^{0.687})}$$

$$\tau_g = \frac{\mathbf{l}_g}{\mathbf{u}_g}$$

$$St = \frac{\tau_p}{\tau_g}$$

where a includes acceleration due to all the other forces except drag force, \mathbf{l}_g and \mathbf{u}_g represents gaseous phase space and time scales, τ_p is the particle relaxation time, τ_g is the flow time scale and St is the Stokes number which is ratio of two time scales.

The steady-state drag force F_D needs drag coefficient, C_D information. C_D is a complex function of flow parameters, turbulence level, particle shape etc. For a spherical shape particle, C_D is calculated according to Morsi and Alexander [50] which is valid over a large of Reynolds numbers:

$$C_D = a_1 + \frac{a_2}{Re} + \frac{a_3}{Re^2} \quad (4.12)$$

where model coefficients, a_1, a_2, a_3 are defined for large range of Reynolds numbers as defined in [50].

4.2.1 Droplet Vaporization

Ansys FLUENT uses a simple heat balance equation to relate particle temperature T_p to convective heat transfer. Radiation heat transfer is not considered in this work.

$$m_p c_p \frac{dT_p}{dt} = h A_p (T_\infty - T_p) \quad (4.13)$$

where m_p is the mass of the particle, c_p is the specific heat capacity of the particle, A_p is the surface area of the particle, h is the convective heat transfer coefficient. Equation 4.13 assumes that there is no temperature gradient within the particle, i.e., the particle is at a uniform temperature throughout. The convective heat transfer coefficient required in Eq. 4.13 is calculated using the Ranz and Marshall correlation [51]:

$$Nu = \frac{h d_p}{k_\infty} = 2 + 0.6 Re_d^{1/2} Pr^{1/3} \quad (4.14)$$

When the rate of vaporization is slow, the vaporization is controlled by the difference in the concentration of the fuel vapor at the droplet surface and droplet concentration in the bulk gas and the vaporization rate is given by:

$$N = k_c (C_s - C_\infty) \quad (4.15)$$

where N is the molar flux of vapor, C_s is the concentration of fuel vapor at the droplet surface, C_∞ is the concentration of fuel vapor in bulk gas and k_c is the mass transfer coefficient. The mass transfer coefficient is calculated from the Sherwood correlation as:

$$Sh_{AB} = \frac{k_c d_p}{D_{i,m}} = 2.0 + 0.6 Re_d^{1/2} Sc^{1/3} \quad (4.16)$$

where $D_{i,m}$ is the diffusion coefficient of vapor in bulk and Sc is the Schmidt number. For high vaporization rates, the convective flow of the vapor from the surface to the bulk becomes important, known as the Stefan flow. In such cases, the droplet evaporation rate is given by:

$$\frac{dm_p}{dt} = k_c A_p \rho_p \ln(1 + B_m) \quad (4.17)$$

where B_m is the Spalding mass transfer number:

$$B_m = \frac{Y_{i,s} - Y_{i,\infty}}{1 - Y_{i,s}} \quad (4.18)$$

with mass transfer coefficient given by Eq. 4.16.

4.2.2 Droplet Injection

To represent the polydisperse spray, it is necessary to obtain information on the particle size distribution. The droplet size distribution information can be obtained from measurements. In numerical simulations, the droplet size distribution is conveniently represented by the Rosin-Rammler expression. The complete range of sizes is divided into an adequate number of discrete bins; each represented by a mean diameter for which trajectory calculations are performed:

$$Y_d = e^{(-d/\bar{d})^n} \quad (4.19)$$

where \bar{d} is the mean diameter and n is the spread parameter. The values of these parameters can be obtained by fitting the measured spray size distribution data to the Rosin-Rammler equation. However, often size measurement data are not available, and the users need to guess these parameters such that certain performance indicators from the simulations agree with the measurement. This gives rise to uncertainty in the droplet injection conditions.

Once the droplet size distribution is known, the location and type of injection of the droplet need to be fixed. Ansys FLUENT allows as many as 11 different injection types (single, surface, pressure-swirl-atomizer, etc.). In this thesis, the surface injection type is used where droplets are released from the chosen surface(s) with user-defined velocity, temperature, and total liquid mass flow rate. The chosen surface represents the lip of the atomizer in experiments where atomization of the liquid fuel occurs. The droplet injection location, temperature, velocity, and droplet size distribution constitute spray injection boundary conditions. The spray boundary conditions significantly affect liquid penetration in the combustion chamber [52], liquid/vapor distribution, flame stand-off distance and overall heat release rate. In the context of thermoacoustic stability analysis, lack of knowledge of the physical spray boundary conditions and model parameters causes unreliable flame response and thermoacoustic stability predictions.

5 Uncertainty Quantification and Surrogate Modeling

Computer simulations have become an indispensable part of the design development and analysis of engineering problems. Courtesy of advancement in computing power and algorithms, computational models that mimic the underlying physics facilitate valuable insights of the system. However, performing numerical simulations is not straightforward as the various models involved in the simulations are fraught with uncertainties. Simulating a model with uncertainties may cause the outcomes to differ from reality, leading to unreliable simulations. To quote George Box, "all models are wrong, but some are useful". Utilizing these "imperfect" models effectively relies on the significance of uncertainty quantification. This process aids in measuring the influence of variability and randomness within the models, thereby facilitating the analysis of how uncertainties affect the outcomes of simulations.

In reality, performing reliable simulations is a nontrivial task, as various sources of uncertainties corrupt the reliability of the results. These sources of uncertainties can be broadly categorized into the following two types: aleatoric and epistemic uncertainties.

- **Aleatoric uncertainty** arises due to inherent randomness in the system being modelled. It is also known as stochastic uncertainty. Aleatoric uncertainty cannot be reduced by additional information of the experiment. Due to the randomness of the uncertainty, aleatoric uncertainty is studied using probabilistic framework. In the context of this thesis, aleatoric uncertainties appear in the FIR model identified via LES/System Identification methodology. The FIR model coefficients are uncertain due to the statistical nature of the SI process, low signal-to-noise ratio, etc. and are characterized by the confidence interval of each coefficient. Generally, uncertainties of the FIR coefficients are estimated using residual analysis.
- **Epistemic uncertainty** arises from the limited knowledge or information available about the system being modeled. Unlike aleatoric uncertainty, epistemic uncertainty can be reduced through additional data. In other words, it is a measure of how well we understand a system. Epistemic uncertainty can be represented as a lack of information about model parameters, boundary and initial conditions or limited knowledge of the underlying physical phenomena. In the context of this thesis, epistemic uncertainties are taken into account due to unknown thermal boundary conditions or spray boundary conditions (injection angle, droplet size distribution etc.).

Typically, an assessment of the impact of these sources of uncertainties on the variation of the outputs is carried out using a sampling-based Monte Carlo method. This procedure involves drawing random samples from the input probability distributions and then using the

chosen computational model to calculate the corresponding response for each sample. Uncertainty statistics of the output can then be inferred based on the ensemble of the results. This method is non-intrusive and has gained widespread usage due to its easy implementation. Although this method is simple and effective, it suffers from slow convergence as the estimation error of the mean of a random variable with the N number of samples converges rather slowly on the order of $N^{-1/2}$ [53]. Due to slow convergence behavior, Monte Carlo can be expensive when dealing with quantifying the impact of uncertainties in already computationally expensive LES simulations.

To alleviate the high computational cost associated with the Monte Carlo method, the surrogate modeling methodology is explored in this thesis [54]. In particular, we employ Gaussian Process (GP) as a surrogate model, which is a form of supervised machine learning algorithm that aims to obtain a cost-efficient surrogate model by learning the input-output relationship of the underlying computer simulation [55]. Monte Carlo method is then applied on this efficient surrogate model to attain the uncertainty estimates. In addition, like most regression algorithms, the GP model not only provides point estimates, but also quantifies the uncertainties in the prediction resulting from possible measurement and parameter estimation procedure. In the following, the fundamentals of GP are described, which lay the foundation for the bootstrapping GP method used in the work of PAPER - TOTAL UNCERTAINTY [56].

For a supervised learning algorithm, the core problem lies in trying to learn a mapping $y = f(\mathbf{x})$ that is a black-box representation of the input-output relationship. The general solution approach is to find a best guess $f^*(\mathbf{x})$ for the black box mapping f based on the known output values $f(\mathbf{x}^i)$ that result from a set of input values $\mathbf{x}^i, i = 1 \dots N$. Unlike other models, the process of constructing a surrogate model is non-parametric in nature where a Gaussian prior over the function f is defined and this assumed prior is updated using the training dataset to arrive at the posterior of the function f .

The Gaussian prior is defined over the function output values at arbitrary points x_1, \dots, x_N such that each output $f(\mathbf{x}_i)$ and their ensemble $f(\mathbf{x}_1), \dots, f(\mathbf{x}_N)$ is a realization of a random process and can be denoted using a set of random vectors:

$$\mathbf{f} = \begin{bmatrix} f(\mathbf{x}_1) \\ \vdots \\ f(\mathbf{x}_N) \end{bmatrix}$$

This random distribution is defined by a mean $\mathbf{1}\mu$ where $\mathbf{1}$ is a column vector of ones of size $N \times 1$. In practice, the mean μ is simply set as some unknown constant m . We assume that the output random variables which are being predicted are correlated, smooth, and continuous over the input space. We express the correlation among the random variables using a basis function. Among the different basis functions available we use a Gaussian basis function or "kernel" to define the correlation among the function outputs at two different input locations.

$$Cor[f(\mathbf{x}_i), f(\mathbf{x}_l)] = \exp\left(-\sum_{j=1}^k \theta_j |x_j^{(i)} - x_j^{(l)}|^2\right) \quad (5.1)$$

where θ_j represents the hyperparameter that controls the spatial correlation between the locations within the input dimension j . The Gaussian kernel definition (5.1) is used to populate the

$N \times N$ correlation matrix Ψ of all the observed data as:

$$\Psi = \begin{pmatrix} \text{cor}[f(\mathbf{x}^{(1)}), f(\mathbf{x}^{(1)})] & \cdots & \text{cor}[f(\mathbf{x}^{(1)}), f(\mathbf{x}^{(N)})] \\ \vdots & \ddots & \vdots \\ \text{cor}[f(\mathbf{x}^{(N)}), f(\mathbf{x}^{(1)})] & \cdots & \text{cor}[f(\mathbf{x}^{(N)}), f(\mathbf{x}^{(N)})] \end{pmatrix} \quad (5.2)$$

and a covariance matrix \mathbf{K} which measures the correlation between two random variables as:

$$\mathbf{K} = \sigma^2 \Psi \quad (5.3)$$

where σ is the process variance. From Eq. 5.1 we see that the correlation between random variables depends on the distance between the sample points and the hyperparameter. Figure 5.1 shows how the value of θ affects the degree of correlation. A low value of θ represents a slow rate of decay of correlation among the variables in that given dimension, suggesting that the function is rather "inactive" along that dimension. Whereas a high value of θ in the figure suggests a high rate of decay of correlation among the variables in the given dimension, thus indicating that the function is "active" along that dimension. By examining the elements of θ one can determine which are the most important input variables that helps in dimensionality reduction.

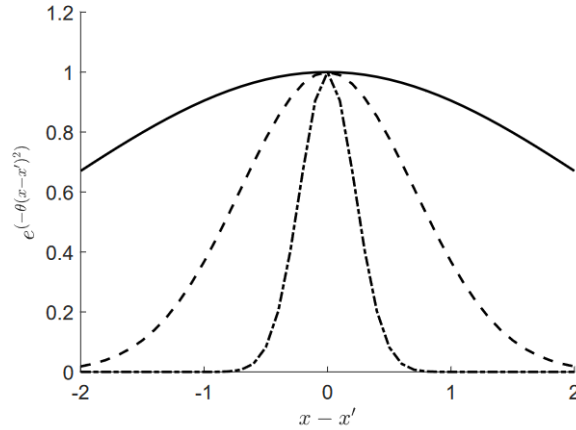


Figure 5.1: Effect of varying θ on correlation

The kernel parameters θ and σ^2 along with the mean function m are estimated from the observed data using the likelihood approach. In the likelihood approach the parameters are estimated in such a way that the likelihood of obtaining the observations is maximized. For given parameters (m, σ^2, θ) , the likelihood function L is defined as:

$$L = \frac{1}{(2\pi\sigma^2)^{N/2} |\Psi|^{1/2}} \exp \left[-\frac{(\mathbf{y} - \mathbf{1}m)^T \Psi^{-1} (\mathbf{y} - \mathbf{1}m)}{2\sigma^2} \right] \quad (5.4)$$

In practice, the logarithm of Eq. 5.4 is maximized to avoid round-off error to give:

$$\ln(L) = -\frac{N}{2} \ln(2\pi) - \frac{N}{2} \ln(\sigma^2) - \frac{1}{2} \ln|\Psi| - \frac{(\mathbf{y} - \mathbf{1}m)^T \Psi^{-1} (\mathbf{y} - \mathbf{1}m)}{2\sigma^2} \quad (5.5)$$

For maximum estimation, setting the derivatives of Eq. 5.5 to zero, we obtain the maximum likelihood estimate for \hat{m} and σ^2 :

$$\hat{m} = \frac{\mathbf{1}^T \Psi^{-1} \mathbf{y}}{\mathbf{1}^T \Psi \mathbf{r}^{-1} \mathbf{1}} \quad (5.6)$$

$$\hat{\sigma}^2 = \frac{(\mathbf{y} - \mathbf{1} \hat{m})^T \Psi^{-1} (\mathbf{y} - \mathbf{1} \hat{m})}{N} \quad (5.7)$$

The values of θ , are further estimated by solving an auxiliary optimization problem:

$$\hat{\theta} = \underset{\theta}{\operatorname{argmax}} \left[-\frac{N}{2} \ln(\hat{\sigma}^2) - \frac{1}{2} \ln(|\Psi|) \right] \quad (5.8)$$

The values of θ cannot be solved analytically and instead an optimization technique is employed. Generally, a local optimization approach (e.g., gradient-based methods) or a global optimization approach (e.g., evolutionary algorithms) are used. Local optimization methods tend to converge faster and are computationally inexpensive, but may yield local minima. Whereas global optimization approaches are computationally expensive, but are robust against local minima and are able to find global minima. In the current thesis, a multi-start global optimization approach is adopted to find the optimum θ .

Given the observed training dataset $\mathcal{D} = (\mathbf{x}^i, f(\mathbf{x}^i), i = 1 \dots N)$ and the estimation of hyperparameters discussed above, one can make a prediction $\hat{\mathbf{f}}$ at \mathbf{x} in such a way that the prediction is consistent with the observed data and therefore with the correlation parameters found before. Hence the idea is to choose a prediction which maximizes the likelihood of the observed data given the estimated correlation parameters. This is achieved by augmenting the observed data \mathbf{y} with a new prediction \hat{y} which is to be determined to yield $\tilde{\mathbf{y}} = \{\mathbf{y}^T, \hat{y}\}^T$. We can also construct the associated augmented correlation matrix:

$$\tilde{\Psi} = \begin{pmatrix} \Psi & \boldsymbol{\psi} \\ \boldsymbol{\psi}^T & 1 \end{pmatrix} \quad (5.9)$$

where $\boldsymbol{\psi}$ is the correlation matrix between the observed data and new prediction. Again using the likelihood maximization estimate, the prediction \hat{y} can be obtained as:

$$\hat{y}(\mathbf{x}) = \hat{m} + \boldsymbol{\psi}^T \Psi^{-1} (\mathbf{y} - \mathbf{1} \hat{m}) \quad (5.10)$$

where \hat{m} is the prediction mean. The prediction covariance matrix is defined as:

$$\hat{\sigma}^2 (\Psi_P - \boldsymbol{\psi}^T \Psi^{-1} \boldsymbol{\psi}) \quad (5.11)$$

where Ψ_P is the correlation matrix between the testing samples.

5.1 Gaussian Process for combined uncertainty using Bootstrapping methodology

The GP formulation derived above has been used by Guo et al. [57, 58] to quantify the impact of aleatoric uncertainties in the flame model on the prediction of the growth rate of a thermoacoustic mode. In the present thesis, the GP formulation shown above is used to predict

the mean of the FIR distribution and then use the bootstrapping methodology to determine the aleatoric uncertainty, which includes the model approximation uncertainty and the FIR estimation uncertainty. Further, the effect of epistemic uncertainty (unknown wall boundary conditions) is taken into account by performing Monte Carlo procedure on the already configured GP model to obtain the comprehensive uncertainty estimate at any test location within the range considered. The bootstrapping methodology was developed and implemented in the work of PAPER-TOTAL UNCERTAINTY. The workflow discusses an example to quantify epistemic uncertainty (unknown wall temperature boundary condition) and aleatoric uncertainty (stochastic nature of system identification) in the flame model that is typically obtained from a CFD/SI procedure.

Step 1: Generate FIR ($h \sim (\mathbf{m}, \mathbf{C})$) models from LES/SI at different wall temperatures (T_w). FIRs at different temperatures constitutes as training dataset. A visual representation of a training dataset of FIRs is shown below.

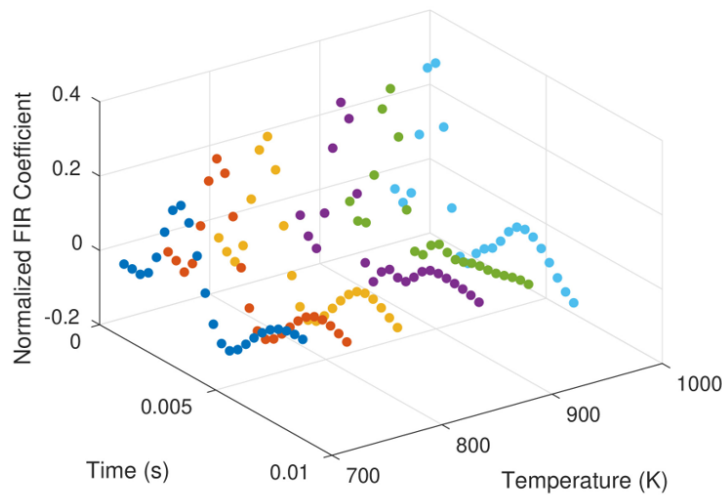


Figure 5.2: Training dataset of FIR flame models obtained at different wall temperatures

Step 2: Train a univariate GP model on the mean values of FIRs at different temperatures ((T_w, \mathbf{m})) to determine the nominal FIR GP hypersurface. An example of a trained GP hypersurface is shown in Figure 5.3:

Step 3: To predict an FIR distribution at a test location the nominal GP hypersurface is used from step 2. The corresponding uncertainty is determined by aggregating the uncertainties due to FIR coefficient uncertainty, model approximation and unknown temperatures. This is done in steps:

- Due to the stochastic nature of the FIR identification process, the identified FIRs have an associated uncertainty estimate. To capture the uncertainty given by the SI procedure, multiple realizations (p) of the training data are generated within the FIR coefficient uncertainty given by the SI procedure.
- At each realization generated in the previous step, the GP model hyperparameters are re-calculated. The re-calibrated GP model is then leveraged to predict at any test location.

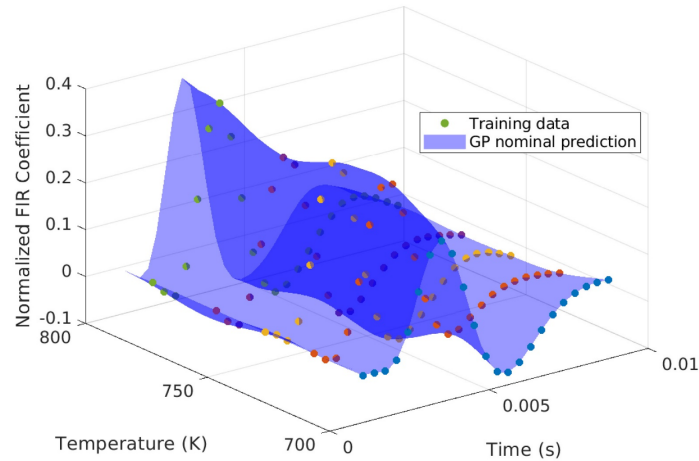


Figure 5.3: Illustration of a GP hypersurface

- The GP model prediction at any test location is uncertain as the model is only approximating the FIR distribution at the test location. This uncertainty estimate is obtained by generating multiple realizations within the covariance matrix of the GP model prediction 5.11. This is shown with an example sketch in Figure 5.4

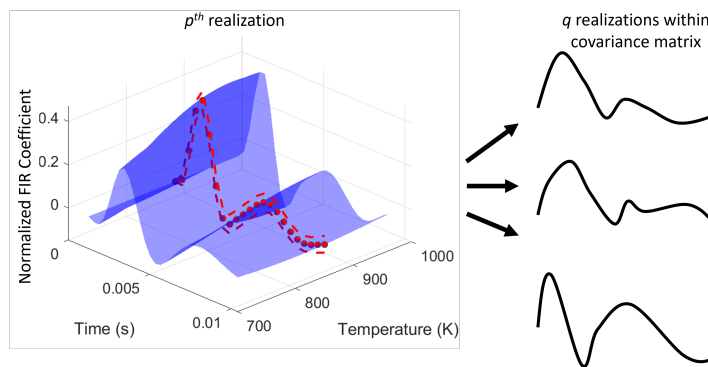


Figure 5.4: Illustration of uncertainty aggregation in the bootstrapping procedure

Step 4: All the uncertainty estimates generated in different items listed in step 3 are aggregated to derive the comprehensive uncertainty containing aleatoric and epistemic uncertainty.

5.2 System Identification in Thermoacoustics

This section introduces the theoretical background of system identification in general. This is followed by the discussion on the four step identification procedure that is used in estimation of a flame model: general of excitation signal, model structure, estimation of model coefficients and assessment of model quality.

More often than not, real world processes are too complex to be understood using first principles. In such scenarios, a practical alternative is to understand the process through an *empirical* approach that is based on the analysis of observations in contrast to first principles modelling. System identification is one such method that attempts to describe the process using a suitable mathematical model based on observed/experimental data. This method, although introduced in the mid-1960s, has gained traction in recent years due to increasing access to sensor data and as well as computational power. Figure 5.5 pictorially depicts the identification of a mathematical model representative of the underlying process using input-output data.

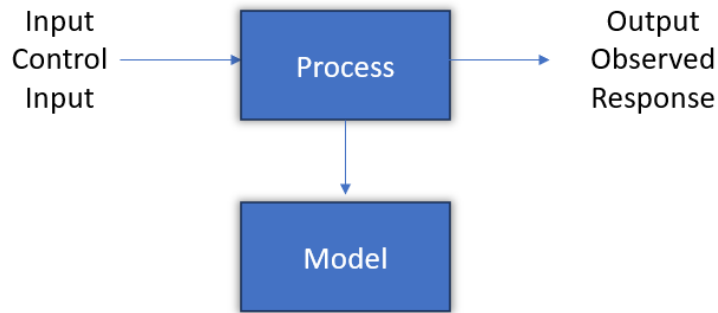


Figure 5.5: Schematic of the identification process using input-output data. Courtesy of Tangirala [59]

In the context of thermoacoustics, a system representing the flame can be considered as a linear time-invariant system. For any linear time-invariant system, velocity fluctuations at a given reference position u'_{ref} describe the total heat release rate \dot{Q}' by

$$\dot{Q}'(t) = G \cdot u'_{ref}(t) \quad (5.12)$$

wherein, the *plant model* G can be associated with a flame transfer function since it establishes a causal relation between the input velocity fluctuations $u'_{ref}(t)$ and output heat release rate fluctuations $\dot{Q}'(t)$. Thus, the objective of the SI procedure is to estimate the plant model G . Identification of such a model consists of four steps: 1. generation of the input excitation signal 2. selection of model structure 3. determination of model coefficients using an optimization algorithm, and finally 4. model quality assessment. In the following sub-sections, these steps are briefly described.

5.2.1 Input excitation signal generation

SI is a method that attempts to estimate a model based on input and output. In this thesis, LES is used to generate input-output time series through acoustic forcing of the LES. Generally, a characteristic signal f_{in} applied at the inlet produces a system response in terms of heat release rate fluctuations. This system can then be characterized by its response to the input excitation signal. The transfer behavior or the FTF at a particular frequency can be estimated by exciting the flame with that particular mono-frequency input signal. Repeated simulations with mono-frequency excitation would be needed to determine the FTF across a given frequency range. In

the context of LES, this would be rather expensive as for each excitation frequency multiple forcing cycles need to be computed. Instead of performing simulations repeatedly with distinct mono-frequency excitation signals, one can perform only a single simulation with a broadband excitation signal, which contains spectral energy across a specified frequency range. With the resulting input-output time series from broadband excitation, the FTF can be estimated across a complete frequency range with the help of the SI techniques. As a single simulation with broadband forcing yields a transfer function that is valid in the complete complex plane, this technique significantly reduces the computational effort in LES.

Different types of signals are possible for broadband excitation. To ensure a reliable and accurate identification of the flame response, in this thesis the in-going characteristic wave based on Daubechies wavelets [60] is used, which is optimized for the estimation of FTF. This type of signal offers certain advantages for use in LES. First, the amplitude of the signal is bounded. This makes certain that no non-linear flame response is triggered by the input signal forcing. Second, the spectral energy is constant up to a specified cut-off frequency, after which the spectral energy monotonically decreases. Finally, the Daubechies wavelet exhibits minimal auto-correlation in the time domain. Otherwise, strong auto-correlation of the input signal corrupts the identification procedure. A typical broadband input-output time series generated by LES is shown in Figure 5.6.

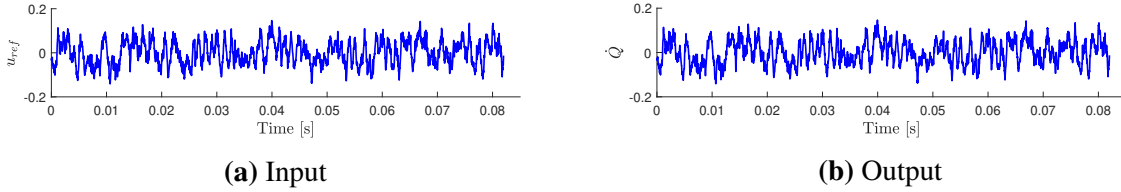


Figure 5.6: Normalized broadband input-output time series generated by LES

When generating an excitation signal for LES, one should pay attention to the amplitude of the signal and the cutoff frequency. First, care should be taken to choose an optimal signal amplitude, as a lower value might cause low signal-to-noise ratio, while a higher value might trigger non-linear flame response. Second, the cut-off frequency should ideally be higher. However, a higher cutoff frequency results in a wide spread of the spectral energy, lowering the spectral energy content per frequency, which hampers the identification accuracy.

5.2.2 Selection of model structure

After input-output data are generated, a model structure needs to be selected. The general polynomial model structure is defined as:

$$A(q, \theta) \dot{Q}'(t, \theta) = \frac{B(q, \theta)}{F(q, \theta)} u'_{\text{ref}}(t) + \frac{C(q, \theta)}{D(q, \theta)} e(t) \quad (5.13)$$

wherein A, B, C, D and F are polynomials with time shift operator q^{-i} :

$$q^{-i} u'(t) = u'(t - i\Delta t) \quad (5.14)$$

By including or excluding some of the polynomial filters A, B, C, D and F , different model structures can be obtained. One of the well established model structure used to analyze the flame dynamic response is the Flame Impulse Response model (FIR) [20, 61, 62]. The FIR model structure can be obtained from the general model structure by setting polynomial filters A, C, D and F to unity

$$\dot{Q}'(t, \theta) = B(q, \theta) u'_{\text{ref}}(t) + e(t) \quad (5.15)$$

This means that, the output \dot{Q}' is the result of convolution of the model coefficients $\theta = \{b_0, b_1, \dots, b_{n_b}\}$ with the prior inputs of $u'_{\text{ref}}(t)$. In principle, an infinite number of model coefficients must be considered, which specifies the number of prior inputs that are taken into account for convolution. As an infinite number of model coefficients are used, such a model structure is called the Infinite Impulse Response (IIR) model. Practically, only a finite number of model coefficients ($\theta = n_b$) are sufficient to describe the system leading to a Finite Impulse Response (FIR) model. The number of model coefficient times the time step size ($n_b \Delta t$) gives the characteristic convective time of the system. As polynomials C and D are set to unity, no noise model is inferred. Therefore, the noise contribution is assumed to be Gaussian white noise. However, when the source models for combustion noise is to be identified, then a more general Box-Jenkins model structure is suitable [63]. It is important to mention that when both model structures are applied to the same input-output data, they tend to yield similar results for short time series. [63].

5.2.3 Estimation of model coefficients

After a model structure is chosen, model coefficients $\theta = \{b_0, b_1, \dots, b_{n_b}\}$ need to be estimated. As input-output data exist, a least-squares optimization problem can be setup as:

$$\arg \min_{\theta} \sum (\dot{Q}' - \widehat{Q}'(\theta))^2 \quad (5.16)$$

where \widehat{Q}' denotes the actual output. Model coefficients are estimated using correlation analysis, where in the likelihood of obtaining the observations is maximized, thereby minimizing the cost function. Regularization might be applied when the length of the time series used are very short to avoid over-fitting by adding constraints to the cost function.

It should be emphasized here that the model estimation procedure discussed above is an empirical approach in which only observed data are used to deduce input-output transfer behavior. No first-principle approach was used to identify the models. As the input-output transfer behavior is deduced by minimizing the error between the model prediction and the observed output, SI can also be classified as a supervised learning algorithm. Advantages of such data-driven models is that their reliance on physical modeling information is negligible and is not limited to a specific problem, e.g., to a certain combustion, flame shape, etc.

5.2.4 Assessment of model quality

The final aspect of the model identification procedure is the quality assessment of the model. The quality of the identified model generally depends on the selected model structure and the

model order. The chosen model structure must represent the physics of the process. Inaccurate model structure gives rise to a biased estimate, where a systematic error is introduced, thus preventing the identified model to converge to the true solution even with infinitely long time series. The model order impacts the variance and generalization behavior of the identified model, similar to the bias-variance trade-off problem encountered in machine learning problems. In case of system identification, if the chosen model order is too small, then the identified model cannot capture the average response of the system. However, if the model order is higher than necessary, then the identified model attempts to capture the noise in the system. The fitting of noise leads to high variances of the model coefficients. As a result of overfitting to a particular dataset, the model cannot generalize and would perform poorly on a test dataset, as the noise components would be different in the test dataset.

To find whether a chosen model order is sufficient, Akaike's Information Criterion (AIC) and residual analysis are used. For more information on these methods, please refer to [64]. These methods help in assessing the quality of the identified model. Typically, a good identified model should have a lower AIC value (meaning low model order and model inaccuracy) and should pass the *Independence Test* and *Whiteness Test*. Both these tests are based on the residuals, which is the difference between the predicted output and the measured output. According to the independence test, a model is considered good if the residuals are uncorrelated to their past inputs. Evidence of correlation suggests that the model does not describe how part of the output relates to the corresponding input. According to the whiteness test, a good model should have no auto-correlation of the residuals. Significant auto-correlation means that the residuals exhibit prediction of the residual dynamics (e.g. colored noise contribution) that are not related to input signal.

6 Contextualization and Discussion of Publications

This chapter discusses the publications connected to the present thesis and clarifies the context among them. First, *Analytical modeling of response of spray to external forcing* discusses the development of an analytical formulation for the assessment of droplets' motion and the response of evaporation rate to acoustic excitation. Second, *Uncertainty quantification in the flame model* proposes a strategy to quantify mixed uncertainties (epistemic and aleatoric) in the estimated flame response model.

6.1 Response of Monodisperse Droplets to Velocity Perturbations

Numerous works described in the literature have aimed at characterizing the effect of acoustics on the behavior and evaporation of a single droplet. Duvvur et al. [30] investigated the burning of a single droplet in a standing acoustic wave. It was observed that droplet vaporization may drive longitudinal instability based on the fuel vapor flow direction caused by the acoustic velocity with respect to the bulk flow direction and in certain frequency ranges. Another important conclusion from this study was that the amplitude of the pressure fluctuation had little effect on the droplet vaporization and the system response. This implies that even a low-amplitude pressure fluctuation can cause unsteady heat release rate, leading to growing thermoacoustic instability. Sujith et al. [18] observed that acoustics modifies the fuel evaporation rate as observed by Carvalho et al. [65] and that the evaporation rate increases with increasing acoustic driving frequency. While Prud'Homme et al. [33] also observed enhanced evaporation through a theoretical investigation of the droplet vaporization response to acoustic oscillations, they also noticed that the internal thermal exchange inside the droplet model is critical factor in the context of thermoacoustic instabilities.

Single droplet approaches are insightful, but such models cannot be generalized to describe the complex physics comprising of population of droplets (spray). In practical situations such as aero engines, the dynamics of the droplet or spray population is important. Dubey et al [66] experimentally studied the acoustic response of ethanol spray. As seen in the single droplet studies, the evaporation rate in the spray increased, causing a reduction of the Sauter Mean Diameter (SMD). The acoustic interaction with spray not only enhances evaporation but also impacts atomization and transport. For large droplets ($\approx 2 \text{ mm}$) secondary atomization can be caused by acoustic forces acting on the droplets. With smaller droplets that are of relevance in aero-engine combustors, the spray exhibits droplet number density fluctuation caused by the impact of the oscillating flow on the atomization process and transport of droplets [27]. Stud-

ies from different fields have also identified the inhomogeneous and time-varying change in droplet concentration, also known as the number density wave subjected to acoustic perturbations. Katoshevski et al. [35] attributed the creation of nodes and antinodes of particle clusters to the local relaxation of particles to the relative gas phase velocity depending on their position in the standing acoustic wave. Li et al. [34] using the Euler-Euler two-phase numerical model identified two types of droplets clustering: first formed by relaxation of the particle velocity from its mean value to the instantaneous gas velocity, and second due to modulation of the particle velocity by the acoustic wave introduced at the inlet. Such particle clustering regimes were also observed by Achury and Polifke [67]. Multiple experimental investigations [13, 68–71] performed on the response of spray to acoustic excitation have validated the formation of a droplet number density wave due to the effect of oscillating flow on the transport of droplets. Recently, Aradhey et al. [72] performed reacting spray measurements in a lean direct ignition geometry to reveal droplet coupling mechanisms during a combustion instability event. They proposed a new combustion instability pathway which includes droplet surface area rate parameter instead of droplet diameter ($SMD : D_{32}$) as SMD does not take into account the droplet number density. These experimental and numerical works shed light on the response of various mechanisms involved in the spray formation, transport and evaporation that eventually perturb the heat release rate of the spray flame. Nevertheless, general conclusions from these studies are hard to ascertain unless elaborate parametric studies are performed. Parametric evaluations with experimental campaigns and numerical investigations are time-consuming and expensive. However, a theoretical framework based on simple mathematical formulation yet with desired physics gives an opportunity to perform inexpensive parametric studies and enable quick characterization of the system.

To facilitate inexpensive parametric studies and enable quick characterization of the system, Kulkarni et al. developed an analytical formulation based on the Lagrangian point mass approach to quantify the response of monodisperse droplets and their simultaneous vaporization behavior to acoustic oscillations. The work was developed based on the single droplet study of Achury and Polifke [19] and extended to a population of evaporating droplets. Kulkarni and co-workers deduced an analytical solution from the Maxey-Riley equations of motion [73] in the linear drag regime for the response of the monodisperse droplet population to acoustic excitation in terms of the droplet number density. The analytical solution of the droplet population dynamics was extended by incorporating the effect of evaporation to describe an oscillatory evaporation rate.

The analytical study shows that the oscillatory evaporation rate profile inherits the characteristics of the number density wave without any phase lag. As a consequence, the oscillatory evaporation rate causes the formation of a vapor wave, which convects downstream at the mean flow speed and manifests itself in the form of equivalence ratio perturbations in space and time. The equivalence ratio oscillation determined by solving a 1D droplet transport equation with appropriate Green's function shows good agreement with the results from the 1D Euler-Lagrange CFD simulation. Kulkarni and co-workers also show that the evaporation dynamics calculated by a transfer function follows a low-pass behavior and that the evaporation process introduces a characteristic time delay in the fluctuation of the equivalence ratio. Thus, future studies with polydisperse and detailed evaporation models could facilitate accurate determination of additional time delays that could be critical for thermoacoustic stability analysis.

6.2 Quantification of Mixed Uncertainties in the Flame model

Section 6.1 introduces a theoretical framework to assess the response of different mechanisms of spray combustion to acoustic excitation. The understanding of the results and the analysis of the theoretical framework can be leveraged in the larger context of analyzing the spray flame response to acoustic excitation. Generally, the flame response to acoustic excitation is calculated by computing FTF through a data-driven LES/SI approach [74]. However, the FTF calculated from such an approach is uncertain due to aleatoric and epistemic uncertainties. The following work presents a surrogate modeling methodology to propagate these uncertainties on the flame response model.

The model for the acoustic response of the flame plays a major role in the hybrid approach that is often used to determine thermoacoustic stability of a system. As shown in numerous works, LES/SI is an efficient way to estimate a flame response model in terms of a FIR [44, 62, 75]. The flame model derived from LES/SI of a turbulent flame is typically characterized by uncertainties, which are partially attributed to epistemic uncertainties arising from insufficient understanding of operating conditions [76], such as spray boundary conditions [77] and thermal wall boundary conditions [62], and partially stemming from aleatoric uncertainties resulting from employing SI on systems affected by combustion noise produced by turbulent flames [61]. Previous works have focused on propagating only aleatoric uncertainties in the estimated FIR model to the thermoacoustic modal growth rate [22]. Avdonin and Polifke [21] proposed the polynomial chaos method to quantify epistemic uncertainties caused by uncertain operating conditions in the estimated FIR of LES / SI of a laminar flame. To quantify both epistemic and aleatoric uncertainties in the FIR model, a Gaussian Process (GP) based surrogate model is developed in this thesis. The novelty of the method lies in the way the surrogate model is constructed. First, a univariate GP model is employed to account for two inputs and one output where each of the FIR model coefficients is a function of time delay and uncertain temperature. Second, bootstrapping methodology is used to capture the variability of the estimated FIR coefficients.

The univariate bootstrapping GP model trained on the FIR models generated from LES at different back plate temperatures showed to successfully approximate the complex response surface of the FIR. The GP model when applied on the entire investigated range shows a FIR with wider confidence interval due to the aggregation of both epistemic and aleatoric uncertainties. In addition, a key feature of the developed GP methodology is that the trained GP model can be leveraged to interpolate FIR coefficients with uncertainty at locations not seen during the training phase. Such a feature could be used to determine a more accurate value of the uncertain variable which best fits the validation data such as experiment or LES results.

In summary, the two papers discussed above contribute towards understanding and quantifying spray flame dynamics with confidence. The first work contributes to understanding and modeling of the physical mechanisms involved in the response of spray to acoustics. Although the physical mechanisms that are responsible for response of gaseous flames have been well documented in the literature, works on modeling of response of spray sub-processes such as droplet motion and evaporation are relatively scarce. The analytical framework on the response of a population of monodisperse droplets presented in section 6.1 showed the formation of a num-

ber density wave, modulation of the evaporation rate and the characteristic time delay involved in the dynamic response of the evaporation that is important in the thermoacoustic stability analysis. While the first work focuses on understanding the physical mechanisms that are necessary to describe the dynamic response of spray, the second work carried out in this thesis contributes to estimation of a dynamic flame response model from the LES/SI procedure in the presence of both types of uncertainties (aleatory and epistemic). Previous studies focused on either propagating aleatoric uncertainties in the flame model to the growth rates of the thermoacoustic modes or quantifying epistemic uncertainties in operating conditions on the flame model. The work presented in section showed the quantification of both types of uncertainties in the flame model using a novel Gaussian Process surrogate model. This work allows for the trained GP method to deduce uncertain variable that was previously unknown. The initial findings outlined in the chapter 7 and the knowledge gained from the two works described in this section, enable the analysis of the dynamic response of spray flames with a reliable level of statistical certainty.

The two studies described above establish the foundation for forthcoming research. The knowledge obtained from the analytical model investigating the response of droplet evaporation to velocity oscillations can be applied to examine the spray flame response derived from LES/SI. Additionally, the approach developed in the uncertainty quantification study can be utilized to evaluate the influence of uncertain liquid boundary conditions in the droplet injection model of an LES simulation on the predicted spray flame response model.

7 Estimation of Spray Flame dynamics using LES/SI

This work presents the preliminary results on the dynamics of the spray flame generated by the GE Avio PERM injector obtained from LES simulations using Thickened Flame Model. The PERM lean injection system was previously investigated by Innocenti et al. [46] through URANS simulations. The FTF obtained from the URANS simulation was quantitatively not in good agreement with the experiments and also presented strong dependence on the wall thermal boundary conditions. The goal of this work is to better estimate the FTF through LES/SI approach during which following objectives will be realized: (1) to demonstrate an incompressible Large Eddy Simulations of a lab-scale combustor equipped with PERM atomizer using a dynamically thickened flame model is able to capture the correct flame shape, (2) assess the liquid fuel statistics such as spray penetration depth using the statistically steady fields; (3) perform LES with isothermal wall boundary conditions and upstream velocity perturbations to generate time series data of the heat release rate oscillations and velocity perturbations for the estimation of Flame Impulse Response using System Identification methods. The objectives were realized in collaboration with the group of Prof. Andreini at University of Florence. In the following section a brief description of the investigated combustor is given followed by the preliminary results of the LES/SI investigation and the outlook.

7.1 Combustor Configuration

As mentioned in the introduction, the aim of the project was to perform an incompressible LES simulation of the lean spray flame generated by the GE Avio PERM injection system in lab-scale combustor and validate the dynamic response of the lean spray flame to acoustic perturbation against the measurement data of Gikadi [78] using the LES/SI approach.

A schematic of the GE Avio PERM injector is shown in Figure 7.1. The injector has a double radial co-rotating swirler, where liquid is injected in a pre-filming airblast fashion. The injected fuel forms a film of fuel on the inner surface of the lip that separates the two swirling flows. Primary atomization is achieved when the film reaches the edge of the lip. Due to the double swirler configuration, fine droplets and rapid mixing is achieved. For stable operation, the airblast injector is coupled with a hollow cone pressure atomizer located at the center of the primary swirler which generates a pilot flame to stabilize the combustion process. When operating at atmospheric pressure setting, the atomizer is operated only using the pilot fuel injection. The injected pilot fuel at low pressures, does not evaporate instantly and the droplets hitting the inner surface forms a liquid film as shown in Figure 7.1.

The flame produced by the PERM injector was investigated using an atmospheric test rig built at

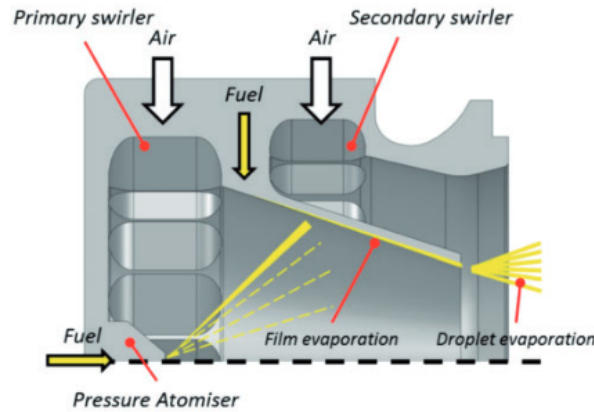


Figure 7.1: Schematic of PERM injector

TU Munich by Gikadi as part of the KIAI European Project. In the test rig, the PERM injector is fed by an upstream plenum with circular cross section as shown in Figure 7.2. A highly homogeneous reacting fuel mixture is produced by the PERM injector and a flame is stabilized in the combustion chamber which has a square cross section. The walls of the combustion chamber are cooled using impinging air jets. Flame Transfer Function of the spray flame was obtained with perforated screen at the outlet by measuring the acoustic transfer matrices with two-source technique [79]: by measuring the acoustic pressures and velocities of the burner with and without the flame. The FTF measurement at atmospheric pressure will be used to validate the FTF estimated from the LES/SI method used in this work.

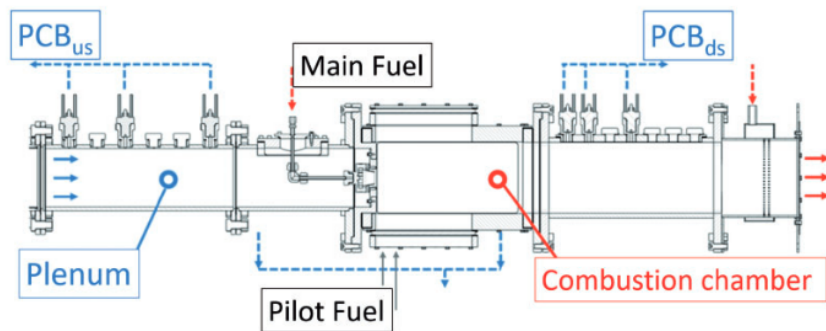


Figure 7.2: Sketch of the test rig at TU Munich

7.2 Numerical Setup

The test rig with PERM injector sketched in Figure 7.2 is a single burner swirled spray with kerosene/air configuration. The incompressible form of the LES-filtered Navier-Stokes equations are solved using the Ansys Fluent 2021.R2 code. From the previous work of Innocenti et al. [43, 46] it can be seen that the flame is acoustically compact and the heat release rate due to velocity oscillations is dominant while the effect of pressure oscillations are rather weak. Therefore, the flame dynamics is governed by the hydrodynamic processes and can be tackled

by incompressible solvers [80]. The computational domain of the test rig is shown in Figure 7.3 which has circular cross-section for the plenum and square cross-section for the combustion chamber and a converging section at the outlet to ensure no-recirculation at the outlet. The computational domain is first discretized with 29 million cells (unstructured tetrahedral and quad elements) with further mesh refinement in the flame region and swirler to correctly reproduce liquid fuel evolution and flame dynamics. However, performing two-phase simulation on a 29 million mesh for about 150 ms as demanded by the LES/SI procedure for FTF identification results in very long run times. To alleviate this, the unstructured mesh was converted to poly mesh while preserving the accuracy [51] using the built-in algorithm of Ansys Fluent 2021.R2. Finally, the LES-filtered incompressible Navier-Stokes equations are solved on a poly mesh of 11 million elements as shown in Figure 7.4. It is to be noted that during this mesh conversion process the accuracy of the flow field was conserved. To further perform LES simulations, ac-

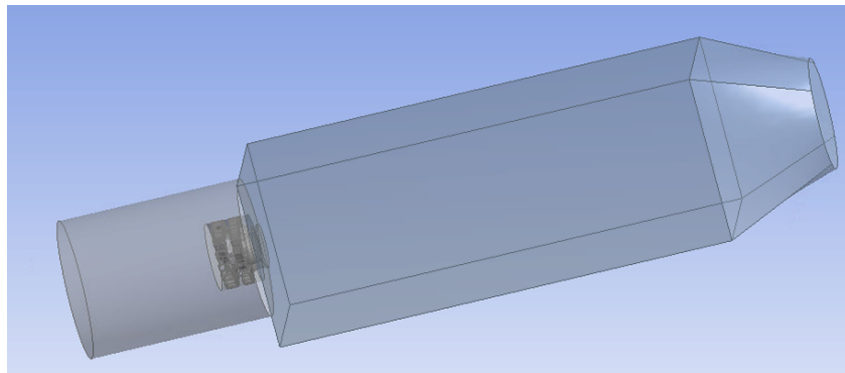


Figure 7.3: Computational domain of the test-rig

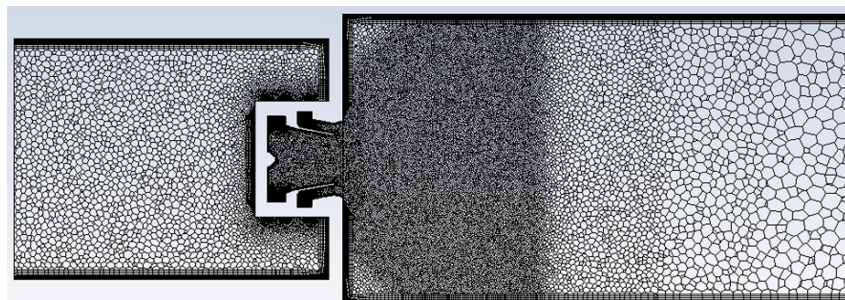


Figure 7.4: Polyhedral mesh visualized on the mid-longitudinal plane

ording to the best practice guidelines from Ansys Fluent, a steady-state RANS solution with liquid fuel injection on the poly mesh was calculated. The RANS solution was used to assess the turbulence resolution of the mesh for the LES and accordingly further refinement was carried out. The refinement procedure led to a mesh with sufficient turbulence energy resolution measured by the LES quality index [81] as shown in Figure 7.5 where a value greater than 0.7 shows more than 70% turbulence energy resolution. The effect of non-resolved eddies was taken into account using the WALE subgrid scale model [82]. Two-phase simulation and spray dynamics is realized using Eulerian-Lagrangian formulation. Explicit modelling of primary and secondary breakup is not included to reduce the computational effort. Hence, the liquid droplets are injected directly from the lip where the primary breakup occurs. This is done using a surface

injection over the circular area of the lip. Liquid droplets are injected at 0° injection angle and at a temperature of 25°C following the Rosin-Rammler distribution with mean droplet size of $6.32\ \mu\text{m}$ and a spread parameter $q = 2$.

Gaseous and liquid phase interaction are taken into account using the two way coupling approach with the exchange of mass, momentum and energy source terms. For the liquid phase momentum equation, only drag and gravity terms are included where the drag is calculated according to Morsi and Alexander [50]. Secondary breakup effect is enabled through Taylor Analogy Breakup (TAB) model [83] as the Weber number for the given boundary condition is less than 100. Turbulent dispersion of the liquid droplets is taken in to account using the random walk model of Gosman and Ioannides [84]. Droplet evaporation is modelled using uniform temperature model of Abramzon and Sirignano [85] where the effect of Stefan flow on the mass transfer is included according to formulation of Sazhin [86]. Temperature dependent liquid fuel properties are used as suggested in the work of Innocenti et al. [46]. Turbulence-chemistry interaction is modeled using the TFM model as described in Section 4.1.

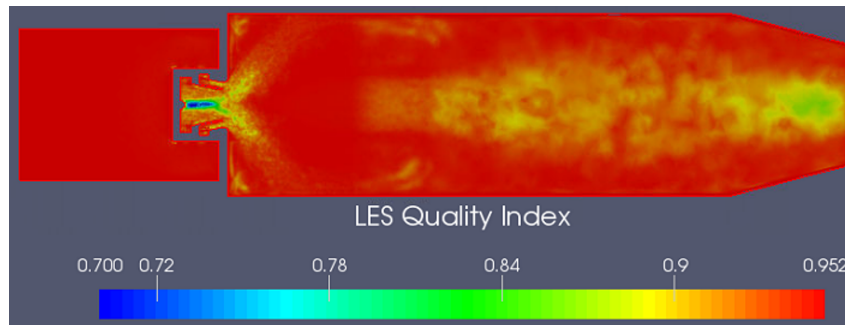


Figure 7.5: Contour of LES quality index on the mid-longitudinal plane

Pressure based solver with SIMPLEC algorithm for pressure-velocity coupling was used. The LES-filtered equations are solved using a bounded second order implicit scheme for time and Green-Gauss node-based method for space. Bounded Central Differencing for momentum and Second-Order Upwind schemes were used for all other equations. A constant time step size of 1×10^{-6} s was used to ensure a CFL number below 0.7 in the simulation.

7.3 Preliminary Results

7.3.1 Axial velocity and temperature field

After obtaining a mesh with sufficient turbulence energy resolution for the LES, directly reactive simulations were performed. Due to the absence of cold flow measurements, the velocity field could not be validated in the absence of flame. The time averaged statistics for axial velocity and temperature were obtained after running the simulation for two flow through times. Figures 7.6 show the instantaneous and time averaged normalized axial velocity with iso-contours of zero axial velocity. Normalization was performed based on the maximum obtained in the simulation on the mid-longitudinal plane.

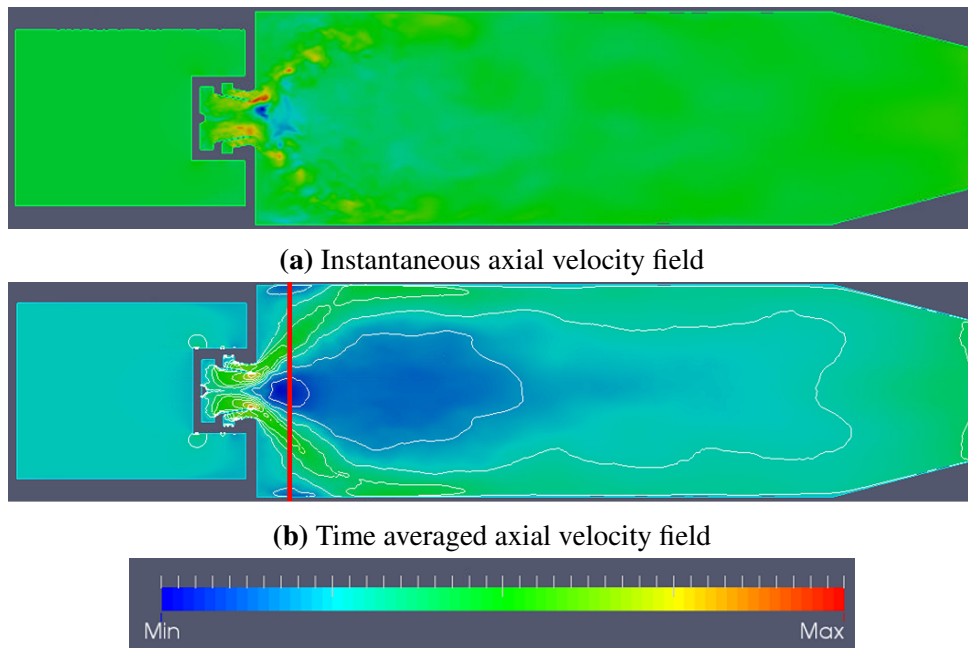


Figure 7.6: Instantaneous and time averaged velocity field on the mid-longitudinal plane

From the contours of axial velocity, a typical flow field can be observed where the flow expands into the combustor with high velocity jets impinging on the walls of the combustor. This creates two outer recirculation regions. Due to the nozzle, pressure drop arises giving rise to a central recirculation region which extends downstream in to the combustion chamber. The central recirculation region helps in sucking hot gases back and aids in droplet heat up and evaporation. From the temperature field (Figure 7.7) it can be observed that high temperature regions occur within the lower external recirculation region and low temperatures in the swirling jet region coming from the nozzle. In the central recirculation region temperature of 1400-1500 K exists. Furthermore, cooling due to isothermal wall boundary conditions can be seen at the walls i.e., $T \sim 1200$ K close to the side windows and $T \sim 1000$ K at the combustor dump plane.

7.3.2 Droplet distribution and evaporation

The droplets injected from the injector lip are immediately trapped in the highly vitiated flow before impinging on the liner wall. From the contour of the droplet diameter distribution (Figure 7.8) it can be seen that the droplets reflect off the surface of the liner and penetrate deeper into the combustion chamber. However, looking only at the droplet diameter contour (Figure 7.8) may be misleading as it shows that only a few large droplets survive the hot reaction zone without evaporating and travel further downstream. This can be evidenced by the liquid volume fraction (Figure 7.9) field, where it can be seen that most of the evaporation occurs before the droplets hit the wall of the liner and only a small amount of evaporation happens downstream due to the presence of larger droplets.

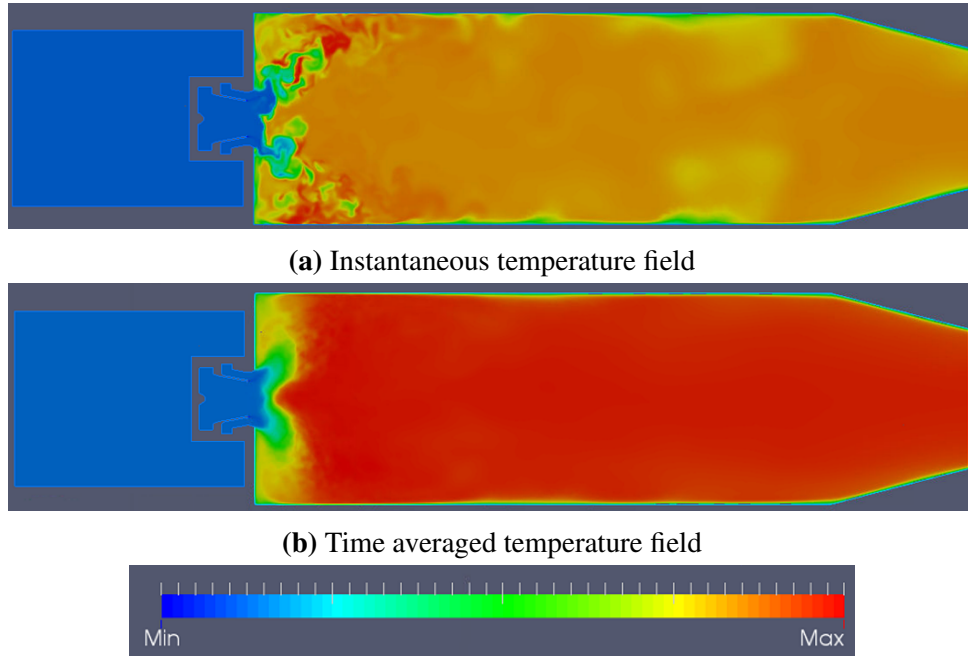


Figure 7.7: Instantaneous and time averaged temperature field on the mid-longitudinal plane

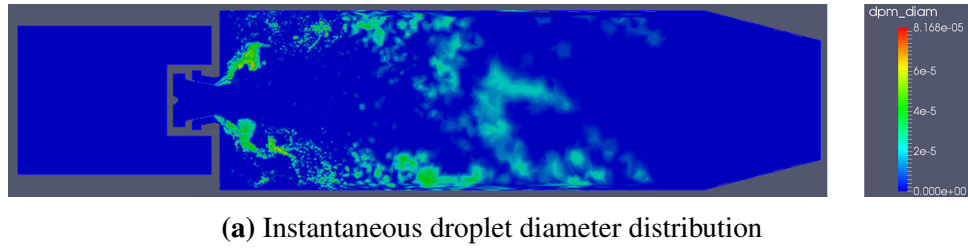


Figure 7.8: Contour of droplet diameter distribution visualized on the mid-longitudinal plane

7.3.3 Mixing and Flame stabilization

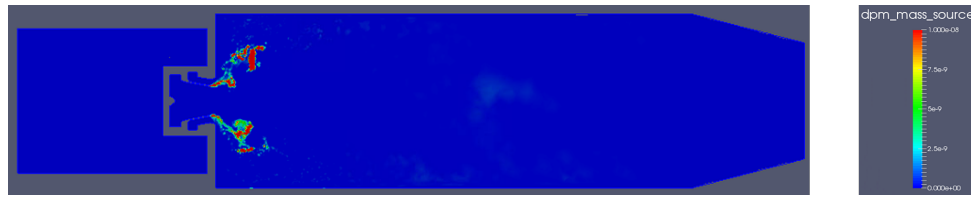
Flame stabilization plays a key role in the design of a stable and safe combustion chamber of an aero-engine. Flame stabilization is not only governed by the vaporization in a liquid fuelled combustor but also the mixing of the fuel vapour with the incoming oxygen in the air. To analyse the mixing behaviour, the mixture fraction definition based on the elemental mass fraction from Bilger et al. [87] is introduced:

$$Z = \frac{2 \frac{Y_C}{M_C} + \frac{1}{2} \frac{Y_H}{M_H} + \frac{Y_{O,ax} - Y_O}{M_O}}{2 \frac{Y_{C, fuel}}{M_C} + \frac{1}{2} \frac{Y_{H, fuel}}{M_H} + \frac{Y_{O,ax}}{M_O}} \quad (7.1)$$

where Y_C , Y_H and Y_O are the elemental mass fractions of the elements C , H and O respectively. The quantity Z , mixture fraction varies from $Z = 0$ in the oxidizer stream and $Z = 1$ in the fuel stream. The stoichiometric value is given by:

$$Z_{st} = \frac{\frac{Y_{O, ax}}{M_O}}{2 \frac{Y_{C, full}}{M_C} + \frac{1}{2} \frac{Y_{H, fuel}}{M_H} + \frac{Y_{O, ax}}{M_O}} \quad (7.2)$$

7.3 Preliminary Results



(a) Time averaged liquid evaporation mass source distribution

Figure 7.9: Time averaged mass source distribution visualized on the mid-longitudinal plane

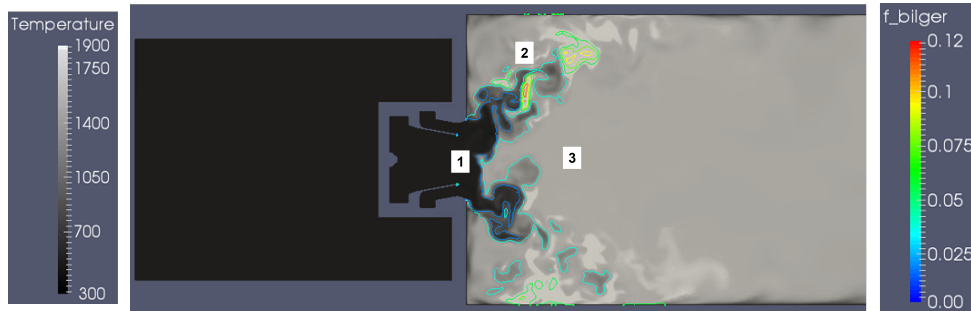


Figure 7.10: Instantaneous temperature field superimposed with isocontours of mixture fraction

For the investigated condition, the stoichiometric value of the mixture fraction in the burner yields $Z_{st} = 0.063$. Figure 7.10 displays the instantaneous temperature field along with the mixture fraction field according to Eq. 7.1. From the figure different zones can be seen:

1. Unmixed region: It is the region close to the exit of the injector that is only covered by the oxidizer from air stream. In this zone, no droplet evaporation occurs as no heat is supplied from the combustion products.
2. Flame region: Highest temperatures are encountered in this region ($T > 1700$ K) where the mixture fraction is close to the stoichiometric value of 0.06 (green lines). In this region majority of the fuel evaporation takes place and is being continuously mixed by the hot combustion products through the external recirculation regions. At the same time these hot combustion products are cooled by the side and bottom plate of the combustion chamber.
3. Upper mixing zone: In this zone mixing is aided by the central recirculation. Hot gases together with unburnt droplets are cooled slightly by the side walls and then transported back towards the nozzle in the central region.

In summary due to the action of the upper and central recirculation regions, hot combustion products provide a constant source of energy to continuously ignite the incoming reactants after being sufficiently mixed by the swirling motion created by the swirlers. Due to the transport of hot combustion products back to the flame root, the flame stabilizes in the shear layer along the mean spray trajectory resulting in a v-shaped flame on a time-averaged basis as shown in Figure 7.11

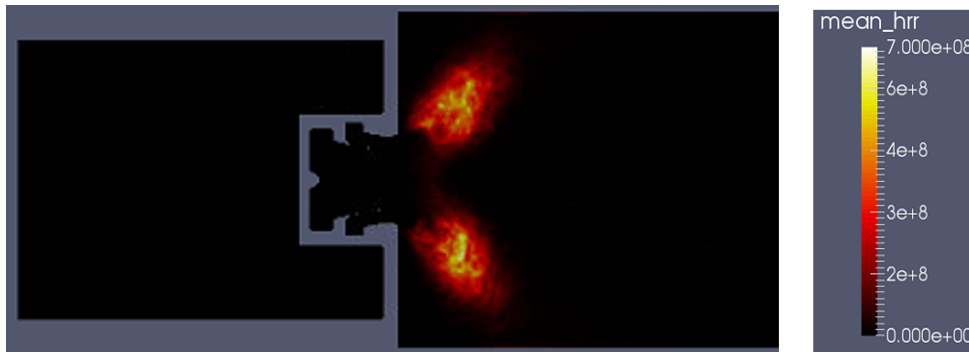


Figure 7.11: Time averaged field of heat release rate visualized on the mid-longitudinal plane

7.3.4 Flame Transfer Function

In this section, the LES simulation is leveraged to obtain the flame impulse response model for flame dynamics according to the procedure discussed in the Section 5.2. According to the four step flame model identification process, a Daubechies wavelet signal with 10 % excitation amplitude and constant power spectral density up to a cut-off frequency of 1000 Hz is used as the experimental FTF shows flame behaviour to drop after 800 Hz. The excitation signal is applied for 150 ms to generate the time series of acoustic velocity and heat release rate perturbations. This data is then subsequently used to infer the FIR coefficients via System Identification techniques of correlation analysis as described earlier. Time series length of 150 ms corresponds to roughly 15 times the length of the impulse response. Even though in practice longer time lengths have been used for premixed flame analysis, it was observed that increasing the time series length from 100 to 150 ms did not change the FIR coefficients and hence a signal length of 150 ms was deemed sufficient for this study.

Figure 7.12 illustrates the flame transfer function derived by utilizing the z -transform on the FIR model, which is obtained through the LES/SI process with isothermal wall boundary conditions for the combustor side walls and combustor dump plane. The FTF obtained with LES/SI procedure is shown in blue solid lines and the uncertainty of the estimation is given by the shaded area. The raw data of the experimental FTF was not available and hence the FTF was reconstructed from Figure 18 of Innocenti et al. [46] and is shown in black markers. The FTF obtained by Innocenti et al. [46] with isothermal wall boundary conditions is shown in green unfilled circles (reconstructed due to lack of raw data). The trend of the FTF gain has the typical shape of a premixed flame response where the response of the flame to acoustic fluctuations decreases with the frequency showing low-pass behaviour of the flame. While, the trend obtained from the simulations for FTF gain is in good agreement with the measurement data, the steeper slope in the FTF phase compared to measurement suggests that the flame length computed with the thickened flame model might be shorter than in the measurement. As there was no experimental data on the temperature field and heat release rate, the flame length could not be validated. The same trend for phase is also observed for the FTF of Innocenti et al. with the isothermal wall boundary conditions.

The trend of the FTF (both gain and phase) in the current work matches the experimental FTF at high frequencies. Nevertheless, a discrepancy in the trend of the FTF at low frequencies is seen when compared with the FTF from Innocenti's work and experiments. In particular, a ma-

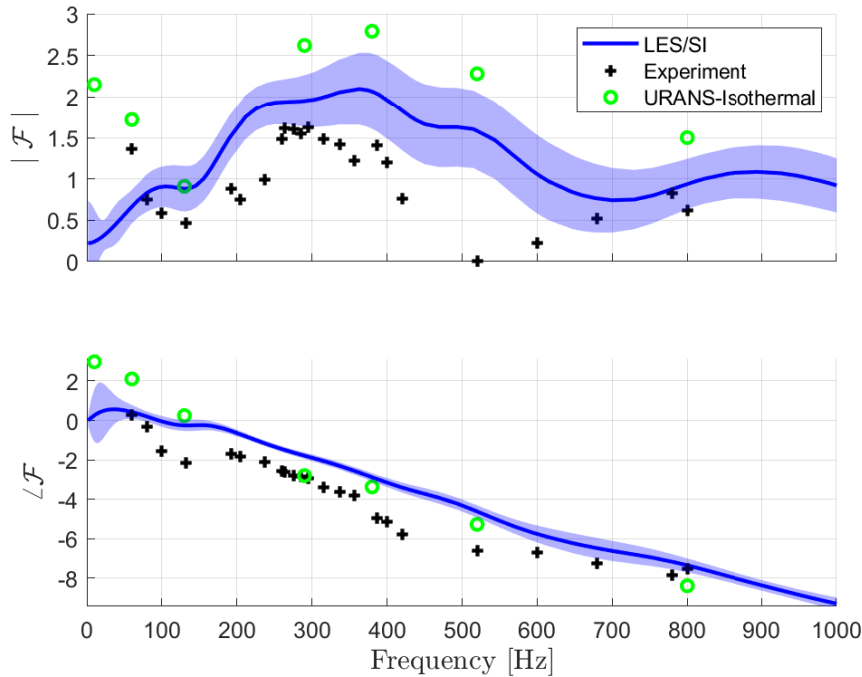


Figure 7.12: Comparison of FTF (blue) inferred from LES time series data against measured FTF (black) and FTF from URANS with isothermal wall boundary conditions (green, Figure 18 of [46])

jor difference is observed in the low-frequency behaviour. The FTF from the current work with LES/SI differs from the FTF of Innocenti et al. obtained with isothermal wall boundary conditions, where the gain at low frequencies tends to two. Although the trend of the experiments seems to suggest an FTF gain higher than one at low frequencies, it should be noted that measurements below 100 Hz are inaccurate due to a poor pressure signal recorded with downstream excitation for the calculation of the transfer matrix [88]. Recent experimental investigations on swirling spray flames show that the FTF gain tends to zero as the frequency goes to zero [89, 90]. This was also recently confirmed through an analytical function for a planar isothermal spray flame by Morinere [36]. Such an observation is valid for spray flames with stiff fuel injection: once all the transients have died out, the overall effect of adjustments in fuel vapour release, flame speed, position etc., must result in an unchanged total heat release rate, because the rate at which fuel is injected is fixed. Regarding the phase at low frequencies, Prieur [89] and Mirat et al. [90] through experiments have argued that the low-frequency behaviour of spray flames is similar to that of technically premixed flames. Many studies appear to have different low-frequency limits of the phase for spray flames or technically premixed flames. For example, recent works[91–94] show that the low-frequency limit of the phase is π , whereas Morinere [36] through a series expansion of the analytical transfer function at zero frequency deduced the phase of the FTF to be $\pi/2$. In Figure 7.12 the URANS work of Innocenti et al. [46] suggest that the phase tends to π at zero frequencies, while the phase from LES/SI tends to zero. As the gain of the transfer function tends to zero at steady-state limit, description of the phase becomes physically meaningless, and there can be no unique solution to the phase at steady-state limit. For spray flames or technically premixed flames, the overall flame transfer function has two

leading contributors: velocity and equivalence ratio fluctuations. Depending on the time delay of both the velocity and the equivalence ratio fluctuation in reaching the flame, it is possible to obtain a different low-frequency limit for the phase of the overall FTF. Therefore, discrepancies of phase at low-frequency is not further investigated.

Apart from discrepancies in the low-frequency region, the overall trend of the FTF estimated from the LES/SI differs from the FTF identified from URANS of the $1/4^{th}$ sector of the same geometry. The variations could be due to differences in the turbulence model, turbulence-chemistry interaction, and the chemical reaction scheme used. The table 7.1 outlines the key similarities and differences between the present study and the URANS study by Innocenti et al. [46]. Droplets in both studies are injected from a given surface representing the lip of the atomiser with the Rosin-Rammler droplet size distribution and 0° injection angle. Due to the better resolution of the turbulence in LES simulation, the particle dispersion in LES is different from the URANS study. Additionally, because of the isothermal combustor wall temperature, liquid fuel evaporates more quickly in the LES, resulting in a shorter flame length and short flame lift-off height from the combustor back plane. However, a longer flame length and reduced product formation were achieved in the URANS study by modifying the reaction order of the dominant reaction. As a result of the detailed reaction mechanism, there could be additional time delays from "slow" reactions. Furthermore, because of the different time scales of the chemistry of the detailed reaction scheme and the URANS turbulence model, the Damköhler number is different. This causes a change in the reaction rate and overall heat release rate. In terms of the combustion model, the URANS work uses the $\beta - PDF$ combustion model, which infers the thermochemical state from the lookup table with a detailed reaction mechanism and does not calculate the heat release rate directly. Instead, the heat release rate is calculated in the post-processing step, and the FTF obtained consequently cannot be directly compared with the heat release rate predictions from the LES.

Table 7.1: Comparison of models between present study and Innocenti's URANS study

	Present Study	Innocenti et al.[46]
Turbulence	LES	URANS
Combustion	TFM	β -PDF
Reaction Scheme	2 step BFER	39 reactions scheme of Kundu
Droplet Size Distribution Model	Rosin-Rammler	Rosin-Rammler
Spray Injection	Surface	Surface
Wall Boundary Condition	Isothermal, $T_w = 600$ K	Isothermal, $T_w = 600$ K

7.4 Conclusion

In this study, the dynamics of the spray flame generated by PERM injector was studied using LES simulations with thickened flame model. The time series from LES simulation was used to infer the FTF using SI techniques. The FTF obtained from LES/SI highlighted the difference between the FTF obtained from Innocenti et al using isothermal wall thermal boundary conditions. However, the validity of the FTF trend could not be derived due to lack of measurement data. This study also lays platform to perform uncertainty quantification studies to assess the

7.4 Conclusion

impact of liquid boundary conditions on the flame topology and thereby on the flame dynamics. The UQ methodology developed in the work of PAPER TOTAL UNCERTAINTY [56] could be leveraged to find a right wall thermal boundary condition such that the FTF phase is in good agreement with the measurement.

8 Summary and Contributions

8.1 Response of Spray Number Density and Evaporation Rate to Velocity Oscillations

Label: PAPER- EVAPORATION RESPONSE

Outcome: In this publication, an analytical solution for the response of a monodisperse population of droplets to acoustic excitation in terms of a number density wave was developed. The analytical formulation was further extended to incorporate the evaporation of droplets, resulting in a theoretical description of the oscillatory evaporation rate. It was further shown that the oscillatory evaporation rate convects at the mean flow speed, causing equivalence ratio fluctuations in space and time. Such an analytical formulation facilitated the construction of a transfer function to characterize the evaporation response to velocity oscillations. The evaporation transfer function exhibits low-pass behavior. The work lays the foundation for future investigations on the effect of transient droplet heating, which might introduce additional time delay and that might impact the thermoacoustic stability of the system.

Relevance for the thesis: This paper introduces a theoretical model for the response of motion of a population of droplets and their evaporation to velocity oscillations that occur typically in an aero-engine combustor. This paper demonstrates how an analytical framework for evaporation response aids in the development of a low-order representation of the spray combustion system.

Contribution: The conceptualization of the topic was formulated by Camilo Silva and Wolfgang Polifke based on the single droplet studies of late Javier Achury. I contributed in reformulating the analytical equations for the droplet population and evaporation modulation and introducing analytical Green's function formulation for 1D convection-diffusion process. I set up the Euler-Lagrange CFD simulations in OpenFOAM for validation of the analytical approach. The manuscript was written by me followed by a rebuttal for the journal publication. Significant feedback on the analytical formulation was given by Wolfgang Polifke and Camilo Silva. Proof-reading and suggestion for improvement were given by all co-authors.

Status: Published in *International Journal of Spray and Combustion Dynamics*

Comment: A first version of this manuscript was first presented and published in the proceedings of the Symposium on Thermoacoustics: Industry meets Academia, 2021 (SoTiC 2021).

Review Process: Peer-reviewed, Scopus listed.

Reference: Sagar Kulkarni, Camilo F. Silva, and Wolfgang Polifke. Response of Spray Number Density and Evaporation Rate to Velocity Oscillations. *Int. J. Spray Comb. Dynamics*, 14(1-2):107–117, 2022. DOI: 10.1177/17568277221085957. Reproduced on p. 49ff.

8.2 Confidence in Flame Impulse Response Estimation From Large Eddy Simulation With Uncertain Thermal Boundary Conditions

Label: PAPER- TOTAL UNCERTAINTY

Outcome: The present work investigated the impact of epistemic uncertainties that are caused by the lack of knowledge of boundary conditions (uncertain combustor wall temperature) and aleatoric uncertainties that are caused by the stochastic nature of the system identification procedure that is used to determine the flame model. To account for total uncertainties (epistemic and aleatoric) in the flame model, a novel univariate Gaussian Process surrogate model with bootstrapping technique was developed. The trained Gaussian Process surrogate model was able to approximate the response surface of FIRs obtained from LES/SI at different training locations (wall temperatures) and interpolate the FIR coefficients with reasonable accuracy along with total prediction uncertainty. The trained GP model was used to find a wall temperature where the flame model matched the experimental results satisfactorily.

Relevance for the thesis: This work contributes to the quantification of mixed uncertainties in the estimated flame model from the LES/SI approach. The confidence intervals shown in the spray flame FTF (7) only accounts for uncertainties due to the application of system identification procedure on a noisy time series data. The UQ methodology developed in this paper not only accounts for the aleatoric uncertainty, but also accounts for epistemic uncertainties. Such a methodology provides a tool to explore the impact of unknown operating/boundary conditions on the flame dynamics and thermoacoustic stability analysis.

Contribution: The research objective of quantifying the uncertainties from LES and SI in the flame model was formulated by Wolfgang Polifke. The concept of using Gaussian Process for the UQ analysis was a result of discussion between the lead author and Shuai Guo based on the previous works of Shuai Guo. The lead author along with Shuai Guo implemented the Gaussian Process surrogate model with bootstrapping strategy in Matlab to quantify total uncertainties in the FIR prediction. I performed LES simulations in AVBP at different combustor wall temperatures to generate the data for subsequent UQ analysis. The lead author performed further data post-processing, analyzing and composing the manuscript, preparing rebuttal and presentation at the virtual conference. All other co-authors provided significant suggestions for the improvement of the manuscript and the study.

Status: Published in *Journal of Engineering for Gas Turbines and Power*

Comment: A first version of this manuscript first appeared in the Proceedings of the ASME Turbo Expo 2021: Turbomachinery Technical Conference and Exposition, Online

Review Process: Peer-Reviewed, Scopus Listed

Reference: Sagar Kulkarni, Shuai Guo, Camilo F. Silva, and Wolfgang Polifke. Confidence in Flame Impulse Response Estimation From Large Eddy Simulation With Uncertain Thermal Boundary Conditions. *Journal of Engineering for Gas Turbines and Power*, 143(12):121002, December 2021. DOI: 10.1115/1.4052022. Reproduced on p. 60ff.

9 Outlook

This thesis research was carried out with the broad objective of understanding the response of a spray flame to acoustic perturbation through analytical and numerical modeling. In particular the objective is classified into three tasks which focuses on i) an analytical model to understand the response of various spray mechanisms such as evaporation and transport to velocity oscillations that impact the eventual flame response, ii) determination of spray flame response to acoustics via FTF using LES/SI method, and iii) data driven surrogate model to quantify both the aleatoric and epistemic uncertainties in the flame response model identified from LES/SI method. In the following, conclusion and possibilities for future work for each of these three tasks are discussed:

9.1 Response of motion of droplets and evaporation to velocity oscillation

An analytical formulation for the response of a mono-disperse population of droplets is developed and extended to include evaporation effects. The analytical formulation describes the oscillatory evaporation rate which further gives rise to equivalence ratio fluctuations. The dynamic response of equivalence ratio fluctuations is characterized by a transfer function. Although the transfer function is arrived at by simplifying approximations, the results are in good agreement with 1D Euler-Lagrange CFD simulation results. With the validation of the analytical model, this work can be extended to more realistic conditions, first by including the effect of droplet heating, which introduces a time delay, and might play a critical role in the thermoacoustic stability of the system. Second, the effect of varying the droplet size as produced by a typical atomizer can be incorporated by evaluating the analytical model on the size distribution of the droplets. Finally, the analytical model with increased complexity can be validated against a DNS study by Pera and Reveillon [95] of the spray flame produced by a bunsen-type injector or with the recent study of Moriniere on an monodisperse isothermal spray using Euler-Euler formulation.

9.2 Estimation of spray flame transfer function using LES/SI

To understand the dynamic spray flame response to acoustic velocity oscillations, LES of a spray flame generated by the GE Avio PERM injection system is performed. The flame transfer function estimated by applying system identification techniques on the time series data generated by LES reveals a low-pass behavior similar to the response of gaseous fuels with a low frequency limit of zero. Although the FTF estimated from LES/SI agrees qualitatively with the

measurement, some disagreement in the phase at low frequencies against measurement is recognized. The results of the current LES study deviate from the results of the same setup with URANS by Innocenti et al. [46] in the low frequency limit. As discussed in the chapter(7), the variation in the results may arise due to differences in the turbulence resolution, combustion model, reaction mechanism, and the system identification technique. As the URANS solution of Innocenti et al. with adiabatic wall thermal boundary condition matches the current LES solution with isothermal wall boundary condition, this warrants another LES study with adiabatic wall thermal boundary condition to clarify the differences. Further, a Dynamic Mode Decomposition (DMD) analysis on the time series obtained with Gaussian pulses can be performed to identify the dominant modes at various frequencies.


9.3 Quantification of aleatoric and epistemic uncertainties in the flame response model

Many UQ studies have focused on propagating only aleatoric uncertainties in the flame model to eigenmode predictions. The current work extends this approach by propagating epistemic uncertainties due to lack of knowledge of operating conditions and aleatoric uncertainties caused by performing SI on LES data corrupted by noise on the FIR coefficients that represent the flame dynamics. This mixed uncertainty is quantified using a univariate bootstrapping Gaussian Process model. The trained GP surrogate model successfully approximates the complex response surface of the FIRs and interpolates the FIR model at unseen test locations. The GP surrogate model in the current study is trained on the FIRs obtained from LES/SI from uniform sampling space, which can be computationally expensive. This can be alleviated by employing an active learning scheme in which fewer training points are needed with longer simulation times to gain the same information. This scheme improves the efficiency of the surrogate model training procedure and helps to reduce the computational cost of the UQ procedure. The current work provides a platform for using the LES results of the forced spray flame response carried out in this thesis to quantify the impact of uncertain liquid fuel boundary conditions on the dynamic spray flame response.

A Reproduction of Papers

The publications related to the present thesis are reproduced in the following appendices.

Response of spray number density and evaporation rate to velocity oscillations

Sagar Kulkarni¹ , Camilo F. Silva¹ and Wolfgang Polifke¹International Journal of Spray and
Combustion Dynamics
Volume 0: 1–11
© The Author(s) 2022
Article reuse guidelines:
sagepub.com/journals-permissions
DOI: 10.1177/17568277221085957
journals.sagepub.com/home/scd


Abstract

A theoretical investigation of the effect of gas velocity oscillations on droplet number density and evaporation rate is presented. Oscillations in gas velocity cause a number density wave, i.e. an inhomogeneous, unsteady variation of droplet concentration. The number density wave, as it propagates downstream at the mean flow speed, causes modulation of the local evaporation rate, creating a vapour wave with corresponding oscillations in equivalence ratio. The present work devises an analytical formulation of these processes. Firstly, the response of a population of droplets to oscillations in the gas velocity is modelled in terms of a number density wave. Secondly, the formulation is extended to incorporate droplet evaporation, such that an analytical expression for the evaporation rate modulation is obtained. Subsequently, the droplet ID convection-diffusion transport equation with the calculated evaporation source term is solved using an appropriate Green's function to determine the resulting equivalence ratio perturbations. The dynamic response of equivalence ratio fluctuations to velocity oscillations is finally characterized in terms of a frequency-dependent transfer function. The aforementioned analytical approach relies on a number of simplifying approximations, nevertheless it was validated with good agreement against ID Euler-Lagrange CFD simulations.

Keywords

Droplet Number Density Wave, evaporation, equivalence ratio fluctuations, transfer function

Date received: 23 November 2021; accepted: 22 February 2022

Introduction

The economic and environmental requirements for aero-engines continue to push for combustors operating in lean combustion regimes to reduce NO_x emission. Due to energy density requirements, liquid fuels are used for aero-engines. Operating liquid fuelled engines in lean conditions may give rise to combustion instabilities.^{1–6} Combustion instabilities occur due to the coupling of pressure and velocity oscillations with unsteady heat release rate. In liquid fuelled systems affected by combustion instabilities, the gas velocity oscillations modulate the evaporation rate and thereby, the equivalence ratio. Equivalence ratio fluctuations cause heat release fluctuations,^{7,8} which make the overall system prone to combustion instabilities. Investigating spray combustion involves the modelling of several interacting phenomena – such as atomization, evaporation and transport of droplets – that occur over a wide range of spatial and temporal scales. Among the various sub-processes of spray formation and transport, droplet evaporation is particularly important, because it is often rate controlling. Additionally, the unsteady evaporation

rate may lead to various burning regimes – from premixed to non-premixed – thus impacting the flame structure.⁹ As a result, the dynamic response of evaporation is a key constituent of spray combustion dynamics that needs to be modelled accurately.

As droplet evaporation plays an important role in spray combustion, previous works have assessed the impact of acoustics on a single evaporating droplet. Tong et al.¹⁰ numerically studied the effect of travelling acoustic waves on droplets that are injected at regular intervals into a combustor. It was observed that the overall droplet evaporation rate is enhanced and that the gain of the droplet vaporization response function is sufficiently large to sustain instability in the combustor. In a similar study, Duvvur et al.¹¹

¹School of Engineering and Design, Technical University of Munich, Garching, Germany

Corresponding author:

Sagar Kulkarni, School of Engineering and Design, Technical University of Munich, D-85747, Garching, Germany.
Email: kulkarni@tfd.mw.tum.de

numerically investigated the effect of acoustic standing waves on the droplet vaporization process with an improved droplet evaporation model. It was seen that only in certain frequency ranges the droplet vaporization process was able to drive combustion instabilities in the combustor and the amplitude of the oscillation had minimal impact on the vaporization rate compared to changes in the fuel volatility. Sujith et al.¹² examined the effect of an axial acoustic field on the behaviour and evaporation of the droplet. The conclusion from this study was that the droplet evaporation rate increases with the increase of acoustic velocity frequency. Prud'Homme et al.¹³ conducted a theoretical investigation of the droplet dynamic vaporization response to acoustic oscillations with a droplet evaporation model accounting for finite thermal conductivity inside the liquid phase of the droplet. Enhanced evaporation rate due to the application of acoustic waves was observed. It was concluded that the internal thermal exchange inside the droplet is an important factor in modelling the droplet evaporation rate in the context of combustion instabilities.

Adequate studies have been carried out on the response of a single droplet to acoustic oscillations. However, in realistic situations we are more concerned with response of a population of droplets. The following discussion reviews some works concerned with response of a spray to acoustic oscillations. The effect of acoustic field on an ethanol spray flame was experimentally studied by Dubey et al.¹⁴. The Sauter mean and arithmetic mean diameters of the spray were seen to decrease in the presence of an acoustic field by 15% and 20%, respectively, due to enhanced evaporation rate of the spray. Gurubaran et al.¹⁵ observed droplet clustering and a variation of droplet mean diameter downstream of the injector and concluded that the acoustic pressure amplitude has a significant effect on the particle size distribution. Gajan et al.¹⁶ experimentally investigated the behaviour of a spray downstream of an aero-engine injector submitted to acoustic excitation and noticed the formation of a spray droplet density wave. With numerical analysis, the droplet density wave was shown to have two origins: due to the atomization process and due to the effect of oscillating flow on the transport of droplets. Apeloig et al.¹⁷ experimentally studied the unsteady interaction of a kerosene spray downstream from a multi-point injector with the flame, where the liquid jet was injected into the air as a crossflow. During an instability cycle, different droplet concentration were seen, leading to heat release rate oscillations. In a recent, similar experimental study by Bodoc et al.¹⁸ the formation of an alternating dense and diluted zones of two-phase flow was observed downstream of the multipoint jet-in-crossflow injector.

On the one hand, experimental and numerical studies^{19–22,2} of the response of a single droplet or a population of droplets to an acoustic field have been carried out. Nevertheless, general conclusions from these studies

cannot be drawn unless an elaborate parametric analysis is performed. Such parametric analysis in experimental campaigns and numerical studies might be expensive. On the other hand, theoretical study on the response of a population of droplets to an acoustic field may lead to a simple mathematical formulation and facilitate a rich and inexpensive parametric analysis of the number density wave and subsequent modulated evaporation rate. In the present work, we aim to devise an analytical formulation of the response of a population of droplets with and without evaporation to an acoustic field. The goal of formulating an analytical description of the response of population of droplets to acoustic oscillation comprises of three objectives: (1) analytical formulation of number density wave without evaporation, (2) analytical formulation of the evaporation spray response, and finally (3) description of the evaporation spray dynamics using a transfer function.

Previous studies have observed droplet clustering¹⁵ and the formation of a droplet density wave^{23,16} downstream of the injector through experiments and simulations. Achury and Polifke²⁴ proposed a theoretical approach to study the response of a single droplet to acoustic oscillations. The current work extends this work from a single droplet to a population of droplets by proposing an analytical formulation of the Number Density (ND) wave. Such a ND wave results from modulating the gas velocity with continuous injection of mono-disperse droplets.

Prior studies^{11,10,25} have dealt with the response of droplet(s) to large acoustic pressure oscillations leading to an oscillatory response of the evaporation. However, in those studies the implicit role of velocity fluctuations was not taken into account. Velocity oscillations cause an ND wave, where droplets exhibit a heterogeneous distribution, which leads to a spatio-temporal oscillation of evaporation rate and the formation of a fuel vapour wave. The vapour wave is convected downstream at the mean flow speed causing equivalence ratio fluctuations. A theoretical development, based on the concept of solving the droplet motion equation by perturbation theory, was used to incorporate droplet evaporation to the spray number density wave by Katoshevski et al.²⁶. In the present work, instead, we extend the analytical formulation of the ND wave by incorporating the droplet evaporation. Furthermore, we model the equivalence ratio fluctuations caused by the propagation of the vapour wave by analytically solving the 1D convection-diffusion equation by means of a Green's function. The oscillatory evaporation response is then characterized by an analytical transfer function of the evaporation. The results of the analytical approach are validated against 1D Euler-Lagrange CFD simulations.

Modelling the spray as a collection of sub-systems comprising of a given droplet ND wave, evaporation and fuel vapour transport facilitates the development of a so-called network model²⁷ for the response of a flame to acoustic wave. A Network model is a low-order representation of

all the involved sub-systems characterised by blocks with associated inputs and outputs, which subsequently can be interconnected forming a global system (investigated spray) that can be described analytically by a transfer function. Such a method of studying acoustic response via network modelling may be useful when studying realistic sprays with increased complexity.

In the next section, an analytical formulation of the number density wave is deduced from the droplet motion equation. This is followed by the Evaporative Spray Response section, which shows the formation of evaporation rate fluctuations caused by the ND wave. Finally, the Equivalence Ratio Fluctuations section describes the formation of equivalence ratio fluctuations and subsequent characterisation of the evaporation response in terms of an analytical transfer function.

Droplet Dynamics

In the present study, we aim at analytically determining the response of a population of droplets to velocity oscillations that typically occur in liquid-fuelled combustors. In pressure-swirled atomizers used in gas turbine combustors, due to the hydrodynamic instabilities involved in the breakup process, primary atomization occurs. In this region, the spray is quite dense and its velocity and temperature do not substantially change from their injection values.²⁸ Further break-up of the droplets occurs downstream due to the interaction with the turbulent gaseous flow in the secondary atomization process. Droplet heating and vaporization occurs only downstream from the primary atomization region, once the droplet dispersion causes the spray to become dilute to allow for the droplets to receive thermal energy from the surrounding gas. As a consequence, atomization, spray formation, vaporization and combustion can be studied independently. In the following discussion, we focus on the dynamics of the droplets' motion and simultaneous vaporization behaviour due to fluctuating gas velocity occurring in the dilute downstream region where the liquid volume fraction is small. Due to small liquid volume fraction, the droplet-droplet interaction can be neglected and the modelling approach can be carried out with a "one-way" coupling approach as shown in the work of Elghobashi.²⁹ As seen in the previous studies,^{16,21} due to the oscillation of the gaseous field, droplets downstream of the injector concentrate inhomogeneously in space and time, thus giving rise to a droplet number density wave. Such a droplet number density can be analysed by studying the response of a population of droplets to acoustic forcing. In CFD, as well as theoretical approaches, the Lagrangian or mass-point perspective is well-suited to model dilute spray problems, as it is computationally inexpensive and easier to model than approaches that resolve droplet/fluid interfaces. In the Lagrangian framework, the droplet acceleration is balanced by the

forces acting on it, which need to be modelled for accurate droplet dynamics. The Lagrangian equation of motion for a spherical droplet with mass m_d and velocity \mathbf{u}_d is given by:

$$m_d \frac{d\mathbf{u}_d}{dt} = \mathbf{F}_B + \mathbf{F}_S, \quad (1)$$

where \mathbf{F}_B refers to body forces, such as gravity acting on the droplet, and \mathbf{F}_S refers to surface forces, such as pressure gradient and shear stress. Maxey and Riley³⁰ presented an equation of motion for a small rigid particle of diameter D immersed in a non-uniform flow field that resolves all the forces acting on the particle. In their hypothesis, forces can be split broadly into two categories: *undisturbed* and *disturbed* flow forces. The former represent the surface forces required to accelerate the fluid that would occupy the volume of the particle if the particle were absent.³¹ Maxey and Riley further classified undisturbed flow forces into *pressure gradient force* and *shear stress*. The latter \mathbf{F}_{uf} can be written as:

$$\mathbf{F}_{\text{uf}} = V_d \left(\underbrace{-\nabla p}_{\text{press.grad.}} + \underbrace{\nu_c \nabla^2 \mathbf{u}_c}_{\text{shearstress}} \right) = \frac{1}{\gamma} \left(\frac{D\mathbf{u}_c}{Dt} - \mathbf{g} \right), \quad (2)$$

where \mathbf{g} corresponds to buoyancy force, $\gamma = \rho_d/\rho_c$ represents the density ratio of the liquid to carrier fluid, ν_c represents the kinematic viscosity of the carrier fluid and V_d is the volume of the droplet. The disturbed flow forces \mathbf{F}_{df} correspond to the forces exerted due to the presence of the droplet. The disturbed flow forces can be sub-divided into *steady-state drag*, *virtual mass force* and *Basset* or history integral forces. The complete Maxey-Riley equation including all the surface forces is given as:

$$\begin{aligned} \frac{d\mathbf{u}_d}{dt} = & \underbrace{\mathbf{g}}_{\text{body : gravity}} + \underbrace{\frac{1}{\gamma} \left(\frac{D\mathbf{u}_c}{Dt} - \mathbf{g} \right)}_{\text{undisturbed flow}} \\ & + \underbrace{\frac{3C_D}{4\gamma D} |\mathbf{u}_c - \mathbf{u}_d| (\mathbf{u}_c - \mathbf{u}_d)}_{\text{steadystatedrag}} \\ & + \underbrace{\frac{\Delta_A}{2\gamma} \left(\frac{D\mathbf{u}_c}{Dt} - \frac{d\mathbf{u}_d}{dt} \right)}_{\text{virtualmass}} + \mathbf{F}_{\text{Basset}} \end{aligned} \quad (3)$$

where Δ_A is an empirical constant used to extend the approach to high Reynolds number flows. Added or virtual mass effects become important only when the particle/droplet density is comparable to the fluid density, for example when the 'particle' is a gas bubble in a liquid, and therefore can be neglected in this investigation. Similarly, Basset forces, which represent history acceleration effects, become insignificant when the density of the particle is very large compared to the gaseous phase density.³² In the current investigation, the particle density (water) is higher than the density of the gaseous medium (air) and therefore Basset forces can be neglected. The

drag force depends on the coefficient of drag, $C_D = 24f_1/Re_d$, where Re_d is the droplet Reynolds number defined as $Re_d = |\mathbf{u}_d - \mathbf{u}_c|D/\nu_c$. A non-linearity is introduced by the drag force³³ if the flow is outside the Stokes regime, then f_1 becomes a function of Re_d as shown below:

$$f_1 = \begin{cases} 1 & \rightarrow \text{Stokes flow, } Re_d < 1 \\ 1 + 0.15Re_d^{0.687} & \rightarrow \text{Schiller Naumann, } Re_d < 800 \end{cases} \quad (4)$$

In a 1D flow, with $\ddot{x}_d = \dot{u}_d$ and $\dot{x}_d = u_d$ and particle relaxation time $\tau_d = \gamma D^2/18\nu_c$, the equation of motion for particle position x_d in the Stokes flow regime ($f_1 = 1$) after neglecting the gravity, Basset and virtual mass forces reduces to:

$$\ddot{x}_d + \frac{f_1 \dot{x}_d}{\tau_d} = \frac{f_1 u_c}{\tau_d} + \frac{1}{\gamma} \frac{\partial u_c}{\partial t} \quad (5)$$

Droplet Population Response

In this section, an analytical description of the response of a population of droplets to velocity oscillations is introduced. Consider droplets with velocity u_d being continuously injected into the one dimensional domain with carrier gas velocity u_c (Eq. (6)) resembling droplets being sheared from an atomizer.

$$u_c = \bar{u}_c + \hat{u}_c \sin(\omega t + \phi), \quad (6)$$

where \bar{u}_c is the mean velocity, \hat{u}_c is the fluctuating component of the gas velocity, $\omega = 2\pi f$ is the angular frequency and ϕ is the phase angle of the flow oscillation, which is included to generalize the solution. In this work, droplets are injected into a pulsating flow (oscillation superposed on mean flow) of an incompressible medium at the mean gas velocity, corresponding to zero slip velocity with respect to

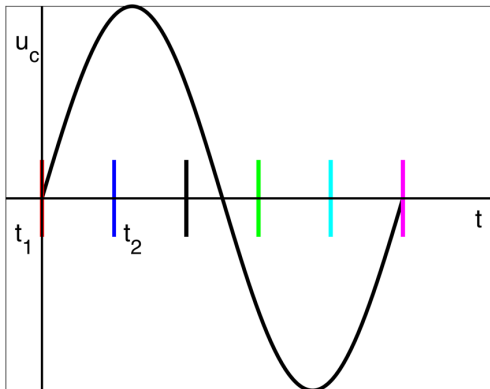


Figure 1. Droplet injection times t_i ($i=0,1,\dots,6$) marked by vertical coloured solid lines on the time axis

mean gas velocity ($u_d = \bar{u}_c$). Due to the application of pulsating flow, the domain under investigation is assumed to be acoustically compact, i.e. the droplet-acoustic interactions occur over a length considerably smaller than the acoustic wavelength. Therefore, acoustic velocity and displacement are homogeneous in the domain.

Due to the acoustic compactness of the problem, a non-dimensional equation can be derived from Eq. (5) by normalizing time with the oscillation time period, $\tilde{t} = t/\tau_d$ and velocity by the oscillation amplitude, $\tilde{u}_d = u_d/\hat{u}_c$. Under the dilute flow regime the governing equation can be written with relative amplitude of oscillation, $\varepsilon = \hat{u}_c/\bar{u}_c$, non-dimensional frequency $\tilde{\omega} = \omega\tilde{t}$ along with other dimensionless parameters which control the response to velocity oscillation¹²:

$$\frac{d\tilde{u}_d}{d\tilde{t}} = -\frac{f_1}{2\pi} \left(\tilde{u}_d - \sin(\tilde{\omega}\tilde{t}) - \frac{1}{\varepsilon} \right) + \frac{\tilde{\omega}}{\gamma} \cos(\tilde{\omega}\tilde{t}) \quad (7)$$

An analytical solution of Eq (7) is possible as the droplets are injected at the fluid mean flow velocity ($Re_d \sim 0$, $f_1 = 1$) and due to the application of oscillating flow (infinite acoustic wavelength). If the Schiller-Naumann extension for the drag law is accounted for, an analytical solution is not possible and is resolved numerically as discussed in Achury et al.²⁴.

In an acoustically compact domain, the number density wave, as reported previously in the works of Gurubaran et al.¹⁵ and Gajan et al.¹⁶, results from the interaction of the pulsating flow with the droplets at the injection time. When droplets are continuously injected into a pulsating flow, droplets at an asymptotic state (after a long time) convect at mean flow speed \bar{u}_c and oscillate around that for a given frequency, amplitude of oscillation, droplet size and fluid and gas

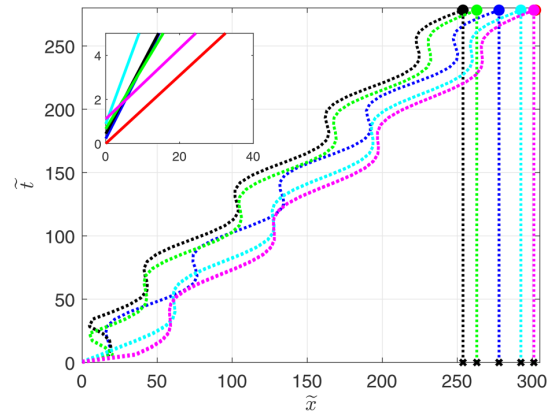


Figure 2. Individual trajectories of six droplets injected at t_i (c.f. Figure 1) according to Eq. (8). Black crosses show droplet positions at time $\tilde{t} = 280$. Dimensional parameters for this example: Droplet size $35 \mu\text{m}$, (Stokes number = 0.8), mean flow velocity $\bar{u}_c = 5 \text{ m/s}$, gas phase oscillation amplitude $\hat{u}_c = 2.5 \text{ m/s}$ and frequency $f = 250 \text{ Hz}$ ($T = 1/f = 0.004 \text{ s}$)

properties. When droplets are injected into the flow domain, each droplet experiences a different gas velocity corresponding to the relative phase of the fluctuating gas velocity. For example, in Figure 1 a droplet injected at instance t_2 (blue) sees a higher gas velocity, whereas a droplet injected at t_1 (red) sees a lower gas velocity. As droplets experience different gas velocity when injected, the trajectory of each droplet is different as shown by the dotted lines in Figure 2. Differences in droplet trajectories due to different injection times gives rise to differences in spacing of the droplets in the domain at any given observation time. This inhomogeneous distribution of droplets in space, as shown by black crosses in Figure 2, determines the Number Density wave.

In this work, we seek to obtain a closed form solution for the proposed number density wave. This is achieved by first assessing an individual droplet trajectory and then analysing the evolution of an ensemble of droplet positions with observation time to determine the ND wave function. In 1-D, to assess the response of a droplet to a given fluid excitation, one may solve Eq. (3) with flow excitation $u_c(x, t)$. Using the ansatz for $u_c(x, t)$ in the droplet motion equation, the analytical solution of the droplet positions x_d in the Stokes flow regime ($f_1 = 1$) can be obtained by integrating over the lifetime t of the particle. To identify relevant parameters that govern the droplet trajectories, the analytical solution is represented in a non-dimensional form with the droplet relaxation time τ_d and mean velocity \bar{u}_c as characteristic time and velocity scales.

$$\begin{aligned} \tilde{x}_d(\tilde{t}, \tilde{t}_i) = & \tilde{C}_1 + \tilde{C}_2 e^{-\tilde{t}-\tilde{t}_i} + \tilde{t} \\ & + \tilde{C}_3 \left[\frac{\gamma - 1}{\gamma} \sin(\tilde{\omega}\tilde{t} + \phi) - \left(\frac{1}{\tilde{\omega}} + \frac{\tilde{\omega}}{\gamma} \right) \cos(\tilde{\omega}\tilde{t} + \phi) \right] \end{aligned} \quad (8)$$

The coefficients \tilde{C}_1 and \tilde{C}_2 calculated using the initial condition $x_d(0) = 0$ and $\dot{x}_d(0) = u_{d0} = \bar{u}_c$ are also shown in non-dimensional form as:

$$\tilde{C}_3 = \frac{\hat{u}_c/\bar{u}_c}{1 + \tilde{\omega}^2} = \frac{\varepsilon}{1 + \tilde{\omega}^2} \quad (9)$$

$$\begin{aligned} \tilde{C}_2 = & \frac{\bar{u}_c - u_{d0}}{\bar{u}_c} \\ & + \tilde{C}_3 \left[\frac{1 - \gamma}{\gamma} \cos(\tilde{\omega}\tilde{t}_i - \phi) - \left(\frac{1}{\tilde{\omega}} + \frac{\tilde{\omega}}{\gamma} \right) \sin(\tilde{\omega}\tilde{t}_i - \phi) \right] \quad (10) \\ \tilde{C}_1 = & -\tilde{C}_2 e^{-\tilde{t}_i} \\ & + \tilde{C}_3 \left[\left(\frac{1}{\tilde{\omega}} + \frac{\tilde{\omega}}{\gamma} \right) \cos(\tilde{\omega}\tilde{t}_i - \phi) + \frac{1 - \gamma}{\gamma} \sin(\tilde{\omega}\tilde{t}_i - \phi) \right] \end{aligned} \quad (11)$$

The first term of the non-dimensional droplet position equation (Eq. (8)) is a constant, the second term describes an exponential

decay where the droplets “loose” the influence of the initial condition as time progresses, the third term represents the mean convection of droplets which increases linearly with time and the fourth term describes the modulation of the droplet positions due to flow oscillation. The trajectory of the individual droplets injected at different injection times: $t_i = 0, T/5, 2T/5, 3T/5, 4T/5, T$ of the 250Hz gas oscillation signal u_c , and for a given phase angle $\phi = 0$, is shown in Figure 2 by dotted lines at an observation non-dimensional time of 280. It is to be noted that, a high excitation amplitude (50%) and a low convection velocity, which is not typical of values seen in gas turbines, are used to distinctly visualize individual droplet trajectories in Figure 2 which otherwise would not be visible. However, higher velocity can be considered in the current analytical framework. Differences in the droplet trajectories due to different injection times can also be seen in the zoomed in view (inset) in Figure 8. Since the gas phase excitation is periodic, a periodic behaviour of the droplet trajectories is also reached asymptotically where they convect at mean speed and fluctuate at the oscillation frequency. This asymptotic behaviour can also be seen by zeroing the exponential term in Eq. (8), which results in an expression with terms involving convection at \bar{u}_c and oscillation (\tilde{C}_1 and \tilde{C}_3 without \tilde{C}_2), as given in Eq. (12):

$$\begin{aligned} \tilde{x}_d(\tilde{t}, \tilde{t}_i) = & \tilde{t} + \tilde{C}_3 \left[\frac{1 - \gamma}{\gamma} (\sin(B) - \sin(A)) \right. \\ & \left. - \left(\frac{1}{\tilde{\omega}} + \frac{\tilde{\omega}}{\gamma} \right) (\cos(B) - \cos(A)) \right], \end{aligned} \quad (12)$$

where $A = \tilde{\omega}\tilde{t} + \phi$ and $B = -\tilde{\omega}\tilde{t}_i + \phi$.

Definition of the Number Density Wave

Figure 2 shows that individual droplet trajectories differ from each other leading to different inter-droplet spacing at any given observation time, as shown by black crosses. Such a heterogeneous distribution of droplets in space results in a number density wave. The evolution of the number density wave can be obtained by tracking the change in spacing of droplets as time progresses. The change in spacing of droplets is inversely dependent on injection time t_i . Thus, the number density wave can be mathematically written as the inverse of time derivative $(dx_d/dt_i)^{-1}$. In order to obtain the inverse time derivative, we first differentiate the dimensional form of Eq. (8) to get dx_d/dt_i (Eq. (13)) and then take the inverse to get the expression for number density wave ($\rho(x_d(t_i), \phi)$):

$$\begin{aligned} \frac{d\tilde{x}_d}{d\tilde{t}_i} = & 1 - \left(\frac{\bar{u}_c - u_{d0}}{\bar{u}_c} \right) e^{-\tilde{t}_i} + \varepsilon (1 - e^{-\tilde{t}_i}) \\ & \left(\frac{\tilde{\omega}}{\gamma} \cos(-\tilde{\omega}\tilde{t}_i + \phi) + \sin(-\tilde{\omega}\tilde{t}_i + \phi) \right). \end{aligned} \quad (13)$$

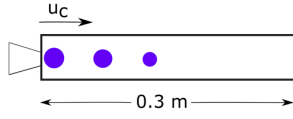


Figure 3. Schematic of the CFD domain with droplet injection

Table 1. Boundary conditions for the CFD simulations

Diameter, μm	\bar{u}_c (m/s)	\hat{u}_c (m/s)	u_{d0} (m/s)	T_{gas} (K)	T_{d0} (K)
30	5	2.5	5	700	300

$$\tilde{q}(\tilde{x}_d, \phi) = \dot{n}\tau_d \left[1 - \left(\frac{\bar{u}_c - u_{d0}}{\bar{u}_c} \right) e^{-\tilde{t}_i} + \varepsilon \left(\frac{\tilde{\omega}}{\gamma} \cos(\tilde{\omega}\tilde{t}_i - \phi) - \sin(\tilde{\omega}\tilde{t}_i - \phi) \right) (1 - e^{-\tilde{t}_i}) \right]^{-1} \quad (14)$$

where, \dot{n} is the rate of droplet injection and ϕ is the phase angle of the gas oscillation corresponding to the time when the droplet is injected into the domain. The number density wave fundamentally depends on x_d and time of injection t_i . It also depends on time t through the inverse function t_i and x_d . Equation. (14) is not yet useful as t_i is not known explicitly. By inspection of Eq. (8), it can be recognized that $x_d(t_i)$ is composed by the superposition of the trajectories due to the relaxation of the droplets to the mean flow and the oscillation induced by \hat{u}_c when $\hat{u}_c > 0$. An approximation for the inverse function to obtain t_i from Eq. (8) assuming small oscillation amplitudes is given by:

$$\tilde{t}_i(x_d) = \tilde{x}_d + \frac{\bar{u}_c - u_{d0}}{\bar{u}_c} + W(z), \quad (15)$$

where $W(z)$ is a Lambert W function, which can be expressed as a power series according to the Lagrangian inverse theorem in the following way:

$$W(z) = \sum_{n=1}^{\infty} \frac{(-n)^{n-1}}{n!} z^n, \quad \text{with} \quad (16)$$

$$z(\tilde{x}_d) = e^{-\frac{1}{\bar{u}_c}(\bar{u}_c - u_{d0} + \tilde{x}_d)} \left(\frac{u_{d0} - \bar{u}_c}{\bar{u}_c} \right).$$

As $t_i(x_d)$ is obtained, a closed form expression for the Number Density is obtained by combining Eqs. (14), (15) and (16). Before proceeding further, the analytical formulation of the obtained ND wave expression is validated against a 1D CFD simulation carried out in OpenFOAM.

Validation of the ND wave model

In this section, the number density wave is validated against a 1D CFD simulation with Lagrangian particle tracking scheme to obtain droplet statistics. Droplet position and

liquid mass flow data from the simulation are post-processed to validate the number density wave and evaporation rate modulation, which will be discussed in the next section.

The CFD setup consists of a 1D duct of length 0.3 m in the x direction and is discretized with 500 grid points. Water is used as the dispersed phase and air is used as the carrier phase. As the focus of the work is to demonstrate an analytical framework to capture the evaporation response of droplets to velocity oscillations, water is chosen as the material for dispersed phase, because compared to other fuels there is little ambiguity concerning the available thermophysical properties. The current framework can be used with typical fuels such as heptane, kerosene by considering respective thermophysical properties without altering the analytical framework. Mono-disperse droplets are injected continuously at the inlet of the domain ($x = 0$ m) as shown in the Figure 3, which are tracked using Lagrangian particle tracking method. To assess the response of a spray to velocity oscillations, the gas velocity at the inlet is modulated at a given frequency and amplitude. Other boundary conditions used for the simulation and analytical procedure are given in Tab. 1.

The transient simulation with time step of $\Delta t = 5 \times 10^{-4}$ of the laminar flow is carried out for 0.1 s. The Lagrangian data in terms of velocity, position in the domain at any given observation time, and number of droplets is recorded at each time step. The number density is obtained by using the histogram and the position information of the droplets. The normalized ND wave ($\bar{q} = q/q(\hat{u}_c = 0)$) calculated from the closed expression (Eq. 14) is in good agreement with the CFD simulation as shown in Figure 4.

Evaporative Spray Response

This section focuses on the characterisation of the evaporative spray response to a pulsating flow, where the

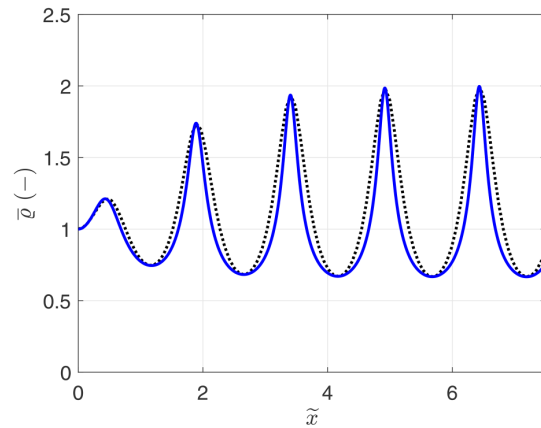


Figure 4. Comparison of analytical (—) and CFD (- - -) Normalized Number Density profile

previously developed theory regarding the formation of a number density wave for non-evaporating droplets is recalled and droplet evaporation is incorporated. This can be simply seen as the progressive reduction of the droplet size, along with the droplet convection. To include the effect of evaporation, we consider the D^2 model for evaporation of droplets injected with zero slip velocity with respect to mean velocity. We show later that for moderate amplitudes of excitation, the D^2 law can recover quite accurately the evaporation response as obtained with an advanced evaporation model employed in CFD. For a spherical droplet the rate of evaporation from D^2 law is expressed as:

$$\dot{m}_d = 2\pi D \rho_g \mathcal{D}_{AB} \ln(1 + B_M) \quad (17)$$

which yields the following equation for the droplet diameter evolution:

$$\frac{dD^2}{dt} = -\frac{8\rho_g \mathcal{D}_{AB}}{\rho_d} \ln(1 + B_M) \quad (18)$$

where ρ_g is the average gas density evaluated at film temperature and composition obtained using the $1/3^{rd}$ rule,³⁴ ρ_l is the density of the liquid, \mathcal{D}_{AB} is the binary diffusion coefficient and B_M is the Spalding mass transfer number. The droplet lifetime can then be calculated as:

$$t_d = \frac{D_0^2}{K} \quad (19)$$

where D_0 is the initial droplet size and K is the evaporation constant. As a first approach, the simple aforementioned D^2 law can be used in the number density wave to incorporate size variation. In this case the droplet size evolution can be resolved for initial injection size D_0 and constant evaporation coefficient K (Eq. (20)) which does not depend on the droplet Reynolds number. Please note that a constant evaporation coefficient can be justified in this case as the droplet is injected close to the wet-bulb temperature of water for the given gas phase temperature and pressure. Thus droplet heating time is negligible and the evaporation coefficient can be considered constant in time and can be deduced analytically. However, future work will consider extension of the theoretical framework to include non-negligible droplet heat up time analytically based on the liquid injection temperature, liquid material and gas phase temperature and pressure.

$$K = \frac{8\rho_g \mathcal{D}_{AB}}{\rho_d} \ln(1 + B_M) \quad (20)$$

The droplet size evolution can be further used in the Number Density equation (Eq. (14)) via the droplet relaxation time parameter τ_d . The function $x_d(t, t_i)$ gives the position of the droplets at a given observation time t , that were injected at injection time t_i . In order to obtain the droplet size evolution for all the droplets injected in the domain,

the D^2 law for size evolution can be written as:

$$D(t_i) = \sqrt{D_0^2 - Kt_i} \quad (21)$$

After having obtained the droplet size evolution equation for all the droplets, the droplet size evolution function is introduced in the ND wave Eq. (14) via parameter $\tau_d(D(t_i))$ which recursively depends on t_i .

The number density wave equation (Eq. (14)) contains an implicit function in $\tau_d(t_i)$, which is solved using a predictor-corrector scheme. In the first step, the initial droplet size D_0 is used to determine the $\tau_d(D_0)$ as done in the non-evaporative case. $\tau_d(D_0)$ is then used to obtain the t_i values. In the next step, the injection time t_i estimated in the first step is substituted in Eq. (21) to give the droplet size evolution.

Eq. (14) for the number density wave was derived for a constant droplet relaxation time τ_d . Inclusion of a variable $\tau_d(D(t_i))$ in the derivation of the number density equation (14) results in a problem that appears analytically intractable. Fortunately, given that the time scales of droplet relaxation and oscillation are smaller than the droplet life time t_d , a quasi-steady approximation for the oscillatory evaporation appears justified, which is obtained by simply inserting the time-varying τ_d in Eq. (14). The fact that results from the analytical approach are in good agreement with CFD (see below) provides a posteriori validation of the quasi-steady ansatz. The limits of the validity of this assumption will be explored in future work.

Finally, the parameter $\tau_d(D(t_i))$ is updated and then used in the evaluation of the ND wave (Eq. (14)). The profile of the evaporation rate (Eq. (17)) is extended with ND wave Eq. (14) to give the evaporative spray response:

$$\dot{m}(x_d(t_i)) = \underbrace{\frac{\pi}{4} \rho_d \sqrt{D_0^2 - Kt_i(x_d)}}_{\text{individual droplet}} \underbrace{\frac{dD^2/dt}{K}}_{\text{number density}} \underbrace{q(x_d(t_i), \phi)}_{\text{number density}} \quad (22)$$

The constant evaporation coefficient K for the analytical expression in Eq. (22) is obtained by the D^2 law for $Re_d = 0$. In the Lagrangian CFD solver, the film theory of Abramzon and Sirignano³⁵ is employed for the calculation of the evaporation of droplets. The evaporation rate in the CFD case is estimated as the local sum of the evaporated liquid which is added to the gas-phase system in the given time interval. This evaporation rate source term is extracted using a user-defined routine in OpenFOAM. The oscillating component of the gas velocity $\hat{u}_c > 0$, which elicits the formation of a ND wave, produces a local fluctuation of the droplet rate of evaporation. Droplet grouping caused by the ND wave in space and coupled with simultaneous evaporation of droplets gives rise to the spatio-temporal modulation of the evaporation rate. The evaporation rate in non-dimensional form

($\tilde{m}_d = \dot{m}_d / \rho_d A_{domain} \bar{u}_c$) with cross-sectional area A_{domain} , is shown in Figure 5.

Figure 5 compares the evaporation rate profile according to Eq. (22) with the CFD simulation. A good agreement is seen, except for the fact that the CFD case exhibits a gradual increase in oscillations at the start of the domain $\sim x = 0$, which is not reproduced by the analytical result. This is plausible due to the absence of droplet heating process in the analytical formulation. Another important takeaway message from Figure 5 is that the D^2 law used for the analytical prediction recovers the group evaporation response obtained with the more realistic Abramzon and Sirignano evaporation model. In summary, the timing of the injection of droplets and fluctuation velocity lead to the formation of a number density wave. As a result of the ND wave and simultaneous evaporation of droplets, the evaporation rate \dot{m} is also modulated.

Equivalence Ratio Fluctuations

In this section, we seek an analytical solution for the evaporation response of a population of droplets. We have seen from the previous section that due to the imposition of acoustic excitation, an inhomogeneous distribution of droplets occurs downstream of the injector to form a ND wave. As a result of the ND wave the rate of evaporation oscillates giving rise to the fuel vapour wave, which propagates downstream at mean convection speed.^{36,37} Oscillations in fuel vapour production lead to oscillations in the equivalence ratio. The fact that air velocity oscillations lead to oscillations in the equivalence ratio allows to construct a transfer function characterizing the evaporation response to velocity oscillations. Such a transfer function block for the evaporation process coupled with a transfer

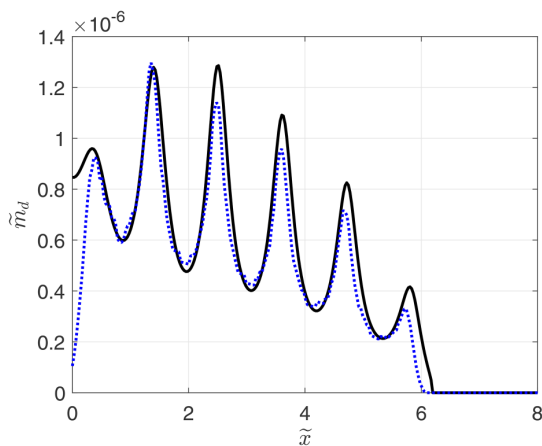


Figure 5. Comparison of analytical (—) and CFD (---) evaporation rate of droplets, $D = 30 \mu\text{m}$, $f = 250 \text{ Hz}$, $K = 7.7\text{e-}8 \text{ m}^2/\text{s}$, $T_{air} = 700 \text{ K}$, $T_{p0} = 300 \text{ K}$.

function for other processes, such as atomization and heat release rate dynamics, completes the low-order model of a spray flame for the study of combustion instabilities.

The evaporated mass flow feeds the gaseous phase with fuel vapour. Thus, the expression Eq. (22) for the evaporated mass flow rate obtained in the previous section can be utilized as a source term in a transport equation for gaseous fuel to determine the mass fraction modulation of fuel vapour:

$$\rho \frac{\partial Y}{\partial t} + \rho \bar{u}_c \frac{\partial Y}{\partial x} - \rho D \frac{\partial^2 Y}{\partial x^2} = \dot{m}. \quad (23)$$

Essentially, Eq. (23) captures the effect of acoustic modulation via the source term, while the transport of mass fraction ignores the fluctuations in the convective-diffusive transport. This is justified as the evaporated vapour convects at mean flow speed which allows to evaluate Eq. (23) using only the mean flow speed without oscillation. It is to be noted that the density ρ is out of the differential operators due to the combination of the conservative form of the transport equation and continuity equation, along with the assumption that density fluctuations are negligible due to compact acoustics and small vapour loading. This assumption is justified a posteriori, as the results from the analytical approach matches well with the CFD, where density variations are taken into account. The limit of the validity of such an assumption will be investigated in the future work.

We solve the 1D transport equation via the Green's function method for convection-diffusion problem with a source term.

$$Y(x, t) = \int_0^t \int_0^{\xi} G(\xi, \tau; x, t) \dot{m}(\xi, \tau) d\xi d\tau \quad (24)$$

Now, the problem turns to find a Green's function form that can solve Eq. (23). For the given 1D transport equation, where the source term \dot{m} is set to act in the domain $x \in 0 - \xi$ and during time $0 - \tau$, the Green's function³⁸ with mean flow can be derived as:

$$G(\xi, \tau; x, t) = \frac{H(t - \tau)}{\sqrt{4\pi D(t - \tau)}} \exp\left[-\frac{[\xi - x + \bar{u}_c(t - \tau)]^2}{4D(t - \tau)}\right], \quad (25)$$

where D is the diffusion coefficient and H is the Heaviside function. It is to be noted here that, first, the solution Y is evaluated at time t , which means the source (evaporation of droplets) is active in $0 - \xi$ until time $\tau = t$. The diffusion coefficient χ is set equal to the value used in the OpenFOAM CFD simulation to enable direct comparison of the results.

The mass fraction result obtained from solving Eq. (23) is validated against the mass fraction result obtained from CFD by post-processing the mass fraction in the flow domain. Figure 6 shows the mass fraction obtained from CFD and the analytical Green's function method with

only mean flow at a given time instance. The result of the analytical solution in terms of the oscillation amplitude and the diffusion of fuel vapour is in good agreement with the CFD results. The discrepancies between the analytical solution and CFD result could be due to the absence of an oscillating component in the Green's function solution of the transport equation Eq. (25).

The dynamic response of the equivalence ratio to air velocity oscillations can be studied by a evaporation transfer function as shown below:

$$F(\omega) = \frac{Y'_{H_2O}/\bar{Y}_{H_2O}}{u'_c/\bar{u}_c} = G(\omega)e^{i\varphi(\omega)} \quad (26)$$

where $G(\omega)$ and $\varphi(\omega)$ represent the gain and phase delay of the evaporation response. Such a transfer function enables one to characterize the response of the evaporation process across the relevant frequency spectrum.

In this study, the gain of the transfer function for both analytical approach and CFD simulations is calculated by taking the ratio of the normalized mass fraction fluctuation and air velocity fluctuation time series signals imposed at the reference inlet position. The phase is calculated by taking the phase difference between mass fraction fluctuation and air velocity fluctuation time series signals at the reference location.

The gain and phase are calculated for the boundary conditions given in Tab. 1 at different Strouhal number ($Sr = fL/\bar{u}_c$) where L is the axial length of the domain as shown in Figure 8. The evaporation process describes a low-pass behaviour meaning that the droplet evaporation process becomes unresponsive to rapid changes in the gas velocity similar to the observations made by Chaussonnet et al.³⁹ for the atomization process. Such an observation needs to be rigorously studied for the realistic poly-disperse spray,

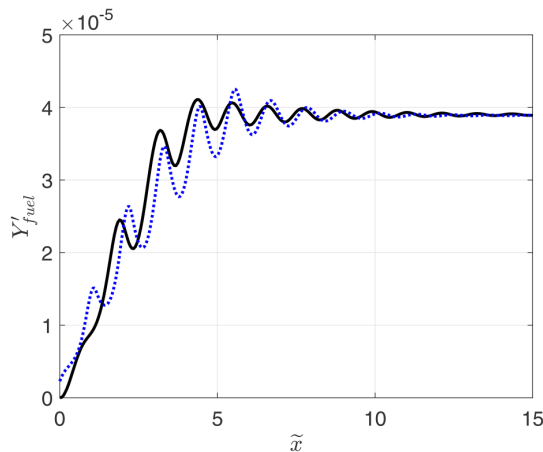


Figure 6. Comparison of analytical (—) and CFD (- - -) mass fraction profiles for given boundary conditions: $D_0 = 30 \mu\text{m}$, $f = 250 \text{ Hz}$, $\bar{u}_c = 5 \text{ m/s}$, $u' = 2.5 \text{ m/s}$, $T_{air} = 700 \text{ K}$, $T_{p0} = 300 \text{ K}$

which can exhibit different liquid evaporation time scales that will affect their frequency response. An estimate for the time delay of the transport process of vapour can be given by $\tilde{t} = \tilde{x} = 11.2$, which is almost equal to the value obtained by measuring the peak to peak signal from Figure 7. Furthermore, the evaporation process introduces an additional time delay due to the evaporation and transport processes, as seen in Figure 7, which can be a critical factor during combustion instability process. The time delay from only the convection process is plotted in Figure 8 phase plot as a solid red line. While the phase calculated from convection time delay agrees well for lower frequencies, there is a mismatch for higher frequencies. Therefore, an accurate characterisation of the evaporation response to acoustic excitation is necessary for robust thermoacoustic stability analysis of realistic spray flames.

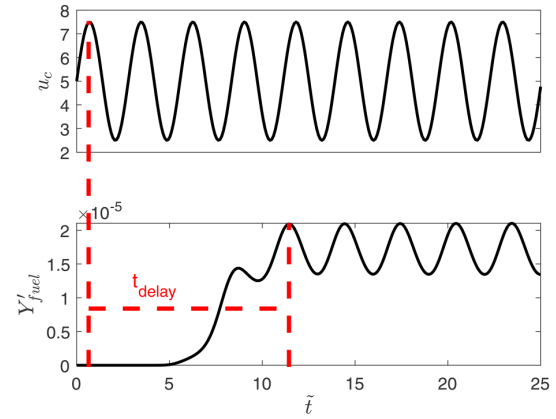


Figure 7. Time series of the air velocity (top) and fuel mass fraction measured at $\tilde{x} = 11.2$ for $D_0 = 30 \mu\text{m}$, $f = 100 \text{ Hz}$, $\bar{u}_c = 5 \text{ m/s}$, $u' = 2.5 \text{ m/s}$

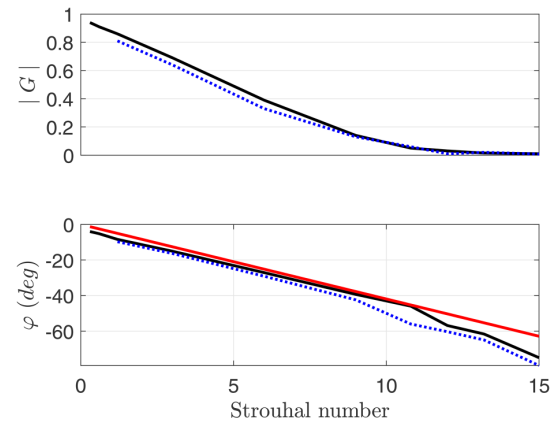


Figure 8. Calculated Analytical (—) and CFD (- - -) evaporation transfer function. The convective phase decay is shown in red.

Summary and Outlook

This work proposes an analytical solution of the response of a mono-disperse population of droplets to acoustic excitation in terms of the number density. Due to relative timing of the injection of droplets with gas velocity, a ND wave is formed. The analytical expression for a particle population response is extended by incorporating the evaporation of the droplets. The resulting analytical formulation describes the oscillatory evaporation rate for the linear drag regime. It is shown that the evaporation rate profile inherits the characteristics of the ND wave without any phase lag. The oscillatory evaporation rate gives rise to a fuel vapour wave, which convects downstream with the mean flow speed.


The propagation of vapour wave manifests itself in the form of equivalence ratio fluctuations. The latter are determined by solving a 1D convection-diffusion equation for gaseous phase using an appropriate Green's function. Results from the analytical approach are in good agreement with 1D Euler-Lagrange CFD simulations. The evaporation response of monodisperse evaporative spray to acoustic oscillations has been calculated. The resulting transfer function exhibits a low-pass behaviour. Additionally, the evaporation process introduces a characteristic time delay in the equivalence ratio fluctuation. An accurate determination of such a time delay is critical for thermoacoustic stability analysis.

Future work will explore the limits of the validity of the assumptions made in this work. Subsequent work will also consider the inclusion of transient droplet heating, which can be seamlessly integrated to the current formalism. Droplet heating may introduce a non-negligible time delay in the evaporation process. As such, a simple estimate of the global time delay associated with convection process ($t = x/V$ as done above) will not be accurate. Furthermore, the present work can be easily extended to account for poly-disperse flows. For that purpose, the current evaporation response has to be evaluated over the size distribution of the droplets. Finally, it will be important to perform the evaporation response study for turbulent flows, where increased mixing and turbulent diffusion might play a key role in determining the amplitude of equivalence ratio oscillations.

Acknowledgements

The present study is dedicated to the late *Javier Achury* who laid the foundation of the work. He derived the results for droplet position and number density wave of a population of droplets in the presence of an acoustic field. We also acknowledge the funding received from the European Union's Horizon 2020 research and innovation programme under Grant Agreement No 766264 Machine learning for Advanced Gas turbine Injection SysTems to Enhance combustoR performance (MAGISTER).

ORCID iD

Sagar Kulkarni  <https://orcid.org/0000-0002-1482-1921>

References

1. de la Cruz García M, Mastorakos E and Dowling AP. Investigations on the Self-excited Oscillations in a Kerosene Spray Flame. *Combust Flame* 2009; 156(2): 374–384. DOI: 10.1016/j.combustflame.2008.11.018.
2. Kitano T, Kaneko K, Kurose R et al. Large-eddy Simulations of Gas- and Liquid-fueled Combustion Instabilities in Back-step Flows. *Combust Flame* 2016; 170: 63–78. DOI: 10.1016/j.combustflame.2016.05.005.
3. Fratolocchi V and Kok JBW. Ethanol Turbulent Spray Flame Response to Gas Velocity Modulation. *Combustion Theory and Modelling* 2018; 22(1): 91–109. DOI: 10.1080/13647830.2017.1377848.
4. Yi T and Santavicca DA. Flame Transfer Functions for Liquid-Fueled Swirl-Stabilized Turbulent Lean Direct Fuel Injection Combustion. *J Eng Gas Turbine Power* 2010; 132(2): 021506-1-021506-6. DOI: 10.1115/1.3157101.
5. Pillai AL, Nagao J, Awane R et al. Influences of Liquid Fuel Atomization and Flow Rate Fluctuations on Spray Combustion Instabilities in a Backward-facing Step Combustor. *Combust Flame* 2020; 220: 337–356. DOI: 10.1016/j.combustflame.2020.06.031.
6. Zhu M, Dowling AP and Bray KNC. Transfer Function Calculations for Aeroengine Combustion Oscillations. *J Eng Gas Turbine Power* 2005; 127(1): 18–26. DOI: 10.1115/1.1806451.
7. Huber A and Polifke W. Dynamics of Practical Premix Flames, Part II: Identification and Interpretation of CFD Data. *Int J Spray Comb Dynamics* 2009; 1: 229–250. DOI: 10.1260/175682709788707440.
8. Lo Schiavo E, Laera D, Riber E et al. Effects of Liquid Fuel/wall Interaction on Thermoacoustic Instabilities in Swirling Spray Flames. *Combust Flame* 2020; 219: 86–101. DOI: 10.1016/j.combustflame.2020.04.015.
9. Pera C and Reveillon J. Direct Numerical Simulation of Spray Flame/acoustic Interactions. *Proc Combust Inst* 2007; 31(2): 2283–2290. DOI: 10.1016/j.proci.2006.07.153.
10. Tong AY and Sirignano WA. Oscillatory Vaporization of Fuel Droplets in An Unstable Combustor. *J Propuls Power* 1989; 5(3): 257–261. DOI: 10.2514/3.23146.
11. Duvvur A, Chiang CH and Sirignano WA. Oscillatory Fuel Droplet Vaporization - Driving Mechanism for Combustion Instability. *J Propuls Power* 1996; 12(2): 358–365. DOI: 10.2514/3.24036.
12. Sujith R, Waldherr G, Jagoda J et al. A Theoretical Investigation of the Behavior of Droplets in Axial Acoustic Fields. *J Vib Acoust* 1999; 121(3): 286–294.
13. Prud'homme R, Habiballah M, Matuszewski L et al. Theoretical Analysis of Dynamic Response of a Vaporizing Droplet to Acoustic Oscillations. *J Propuls Power* 2012; 26(1): 74–83. DOI: 10.2514/1.39379.
14. Dubey RK, Black DL, McQuay MQ et al. The Effect of Acoustics on An Ethanol Spray Flame in a Propane-fired Pulse Combustor. *Combust Flame* 1997; 110(1): 25–38. DOI: 10.1016/S0010-2180(97)00061-8.

15. Gurubaran RK and Sujith RI. An Experimental Investigation of Evaporative Sprays in Axial Acoustic Fields. In *44th AIAA - JPC Conference*. AIAA 2008–4769.
16. Gajan P, Strzelecki A, Platet B et al. Investigation of Spray Behavior Downstream of An Aeroengine Injector with Acoustic Excitation. *J Propuls Power* 2007; 23(2): 392–399.
17. Apeloig JM, d’Herbigny FX, Simon F et al. Liquid-Fuel Behavior in An Aeronautical Injector Submitted to Thermoacoustic Instabilities. *J Propuls Power* 2015; 31(1): 309–319. DOI: 10.2514/1.B35290.
18. Bodoc V, Desclaux A, Gajan P et al. Characterization of Confined Liquid Jet Injected Into Oscillating Air Crossflow. *Flow, Turbul Combust* 2020; 104(1): 1–18. DOI: 10.1007/s10494-019-00037-9.
19. Kaufmann J, Vogel M, Papenbrock J et al. Comparison of the flame dynamics of a premixed dual fuel burner for kerosene and natural gas. In *Symposium on Thermoacoustics in Combustion: Industry Meets Academia*. Online.
20. Gikadi J. *Prediction of Acoustic Modes in Combustors Using Linearized Navier-Stokes Equations in Frequency Space*. PhD Thesis, TU München, München, Germany, 2013.
21. Achury J and Polifke W. Modulation of Spray Droplet Number Density and Size Distribution by An Acoustic Field. *J of Computational Multiphase Flows* 2017; 9(1): 32–46. DOI: 10.1177/1757482X17690751.
22. Treleaven NCW, Garmory A and Page GJ. A Numerical Study on the Effects of Acoustic Forcing on Fuel Spray Dynamics in Gas Turbines. In *Volume 4A: Combustion, Fuels, and Emissions*. Virtual, Online: American Society of Mechanical Engineers. ISBN 978-0-7918-8412-6, p. V04AT04A009. DOI: 10.1115/GT2020-14238.
23. Giuliani F, Gajan P, Diers O et al. Influence of Pulsed Entries on a Spray Generated by An Air Blast Injection Device : An Experimental Analysis on Combustion Instability Processes in Aeroengines. *Proc Combust Inst* 2002; 29: 91–98.
24. Achury J and Polifke W. Theoretical Investigation of the Particle Response to An Acoustic Field. *Int J Spray Comb Dynamics* 2016; 8(4): 262–270. DOI: 10.1177/1756827716641118.
25. Hsiao GC, Meng H and Yang V. Pressure-coupled Vaporization Response of N-pentane Fuel Droplet At Subcritical and Supercritical Conditions. *Proc Combust Inst* 2011; 33(2): 1997–2003.
26. Katoshevski D, Shakked T, Sazhin SS et al. Grouping and Trapping of Evaporating Droplets in An Oscillating Gas Flow. *Int J Heat Fluid Flow* 2008; 29(2): 415–426. DOI: 10.1016/j.ijheatfluidflow.2007.10.003.
27. Emmert T, Meindl M, Jaensch S et al. Linear State Space Interconnect Modeling of Acoustic Systems. *Acta Acust United Acust* 2016; 102(5): 824–833. DOI: 10.3813/AAA.918997.
28. Sánchez AL, Urzay J and Liñán A. The Role of Separation of Scales in the Description of Spray Combustion. *Proc Combust Inst* 2015; 35(2): 1549–1577. DOI: 10.1016/j.proci.2014.08.018.
29. Elghobashi S. On Predicting Particle-laden Turbulent Flows. *Appl Sci Res* 1994; 52(4): 309–329. DOI: 10.1007/BF00936835.
30. Maxey MR and Riley JJ. Equation of Motion for a Small Rigid Sphere in a Nonuniform Flow. *Phys of Fluids* 1982; 26(4): 883–889. DOI: 10.1063/1.864230.
31. Clift R, Grace JR and Weber ME. *Bubbles, Drops, and Particles*. New York: Academic Press, 1978. ISBN 978-0-12-176950-5.
32. Jenny P, Roekaerts D and Beishuizen N. Modeling of Turbulent Dilute Spray Combustion. *Prog Energy Combust Sci* 2012; 38(6): 846–887. DOI: 10.1016/j.peccs.2012.07.001.
33. Flemmer R and Banks C. On the Drag Coefficient of a Sphere. *Powder Technol* 1986; 48(3): 217–221. DOI: 10.1016/0032-5910(86)80044-4.
34. Yuen MC and Chen LW. On Drag of Evaporating Liquid Droplets. *Combustion Science and Technology* 1976; 14(4-6): 147–154. DOI: 10.1080/00102207608547524.
35. Abramzon B and Sirignano W. Droplet Vaporization Model for Spray Combustion Calculations. *Int J Heat Mass Transf* 1989; 32(9): 1605–1618. DOI: 10.1016/0017-9310(89)90043-4.
36. Eckstein J, Freitag E, Hirsch C et al. Forced Low-Frequency Spray Characteristics of a Generic Airblast Swirl Diffusion Burner. *J Eng Gas Turbine Power* 2005; 127(2): 301–306. DOI: 10.1115/1.1789515.
37. Vignat G, Lo Schiavo E, Laera D et al. Dynamics of Spray and Swirling Flame Under Acoustic Oscillations : A Joint Experimental and LES Investigation. *Proc Combust Inst* 2020; 38(4): 6015-6024. S1540748920301024. DOI: 10.1016/j.proci.2020.05.054.
38. Xu Z, Travis J and Breitung W. Green’s function method and its application to verification of diffusion models of GASFLOW code. Technical Report FKZA 7293, Institute for Nuclear and Energy Technology, Karlsruhe, Germany, 2007.
39. Chaussonnet G, Müller A, Holz S et al. Time response of recent prefilming airblast atomization models in an oscillating air flow field. In *Proceedings of ASME Turbo Expo 2017: Turbomachinery Technical Conference and Exposition*. GT2017-63041, Charlotte, North Carolina, USA: ASME, pp. 1–12.

Confidence in Flame Impulse Response Estimation From Large Eddy Simulation With Uncertain Thermal Boundary Conditions

Sagar Kulkarni¹

Professur für Thermofluidynamik,
Technical University of Munich,
Garching D-85747, Germany
e-mail: kulkarni@td.mw.tum.de

Shuai Guo

Professur für Thermofluidynamik,
Technical University of Munich,
Garching D-85747, Germany
e-mail: guo@td.mw.tum.de

Camilo F. Silva

Professur für Thermofluidynamik,
Technical University of Munich,
Garching D-85747, Germany
e-mail: camilo.f.silva.g@gmail.com

Wolfgang Polifke

Professur für Thermofluidynamik,
Technical University of Munich,
Garching D-85747, Germany
e-mail: polifke@tum.de

Thermoacoustic stability analysis is an essential part of the engine development process. Typically, thermoacoustic stability is determined by hybrid approaches. These approaches require information on the flame dynamic response. The combined approach of advanced system identification (SI) and large eddy simulation (LES) is an efficient strategy to compute the flame dynamic response to flow perturbation in terms of the finite impulse response (FIR). The identified FIR is uncertain due in part to the aleatoric uncertainties caused by applying SI on systems with combustion noise and partly due to epistemic uncertainties caused by lack of knowledge of operating or boundary conditions. Carrying out traditional uncertainty quantification techniques, such as Monte Carlo, in the framework of LES/SI would be computationally prohibitive. As a result, the present paper proposes a methodology to build a surrogate model in the presence of both aleatoric and epistemic uncertainties. Specifically, we propose a univariate Gaussian Process (GP) surrogate model, where the final trained GP takes into account the uncertainty of SI and the uncertainty in the combustor back plate temperature, which is known to have a considerable impact on the flame dynamics. The GP model is trained on the FIRs obtained from the LES/SI of turbulent premixed swirled combustor at different combustor back plate temperatures. Due to the change in the combustor back plate temperature the flame topology changes, which in turn influences the FIR. The trained GP model is successful in interpolating the FIR with confidence intervals covering the “true” FIR from LES/SI. [DOI: 10.1115/1.4052022]

Introduction

To reduce NO_x emissions, lean premixed combustion systems have been developed. Lean premixed combustors, however, may exhibit thermoacoustic instabilities [1], which are detrimental to the engine operation. As a result, thermoacoustic stability analysis needs to be carried out at the design stage of the engine development. Generally, thermoacoustic stability is evaluated by a hybrid approach, where the calculation chain is divided into two steps. In the first step, acoustics and flame dynamics are calculated separately. On the one hand, acoustic models such as Helmholtz solver [2] or network models [3], which describe the propagation and scattering of acoustic waves within the system environment, are evaluated. On the other hand, flame response models characterize the influence of acoustic waves on the flame dynamics. Flame response model may be obtained experimentally [4] or numerically, i.e., by combining high fidelity simulations such as large eddy simulations (LES) and system identification techniques (LES/SI) [5,6]. In the second step of the hybrid approach, acoustics and flame response models are combined. The resulting eigenvalue problem delivers the growth rates and frequencies of the thermoacoustic modes of the system.

The flame response is highly sensitive to the burner geometry and operating conditions, i.e., incoming flow conditions (fuel composition, mean flow temperature) and burner thermal boundary conditions [7–11]. Most of the time operating and boundary conditions are uncertain. Such uncertainty is generally of

epistemic nature: a lack of knowledge in the flow or thermal boundary conditions at which the system operates. Modeling the flame response under uncertain boundary conditions leads to flame response models with epistemic uncertainties. The latter may alter the thermoacoustic stability prediction of the system [12].

The flame response model can be described in the time domain in terms of finite impulse response (FIR) coefficients. The FIR model is more general and realistic than an $n - \tau$ model, where only a constant time delay [13] is used. In the FIR model, the flame response to upstream flow perturbations is the result of distributed time delays [14], each one associated with a coefficient of the impulse response. The coefficients of the impulse response can be obtained by combining SI techniques with high-fidelity numerical simulation. Such evaluation of the impulse response can be challenging if the flame under evaluation is turbulent. Turbulent flames produce combustion noise, which is detrimental for an accurate evaluation of the FIR coefficients. Such a lack of accuracy leads to uncertainties in the FIR coefficients, which can be considered of aleatoric nature: combustion noise may be seen as a random process that cannot be set to zero by increasing the knowledge in the system. Summarizing, uncertainties in flame response models may be of epistemic (operating/boundary conditions) and aleatoric nature (applying SI on data corrupted by noise).

Previous works have concentrated on uncertainty quantification (UQ) in the second step of the hybrid approach by propagating the aleatoric uncertainties in the flame model to the growth rate of the eigenmodes of the system. In the majority of these studies, uncertainties in the flame model are assumed. Whether they are of epistemic or aleatoric nature is not of interest. For example, [15–18]

¹Corresponding author.

Manuscript received July 8, 2021; final manuscript received July 21, 2021; published online October 4, 2021. Editor: Jerzy T. Sawicki.

used the $n - \tau$ flame model to investigate the effect of uncertainties in n and τ on the thermoacoustic modes of different combustors. Guo et al. [19] considered the FIR model obtained by the LES/SI technique. Unlike previous studies, the aleatoric uncertainties in the flame model due to the application of SI were rigorously determined with residual analysis. They showed that irrespective of the nature of uncertainties present in the flame model, the thermoacoustic stability prediction is significantly impacted and that the aleatoric uncertainties in the flame model can be reduced by considering longer time series. However, these studies did not consider any epistemic uncertainty in the flame model. Therefore there is a need to quantify the uncertainties in the flame model reliably for robust thermoacoustic stability analysis.

To this day, the work of Avdonin and Polifke [20] is the only one that has focused on UQ in the first step of the hybrid approach. In that study, the uncertainty in the flame response obtained from high fidelity simulations was studied using the polynomial chaos expansion method. The work of Avdonin et al. [20] took into account only uncertainties of epistemic nature (operating and boundary conditions). As a laminar flame was investigated, no aleatoric uncertainties – associated with system identification on data corrupted by noise – were accounted for.

The present study focuses on UQ in the first step of the hybrid approach, where we aim at simultaneously quantifying both epistemic and aleatoric uncertainties in the FIR model coefficients characterizing the flame response of a turbulent, confined flame. A naive way to tackle the proposed UQ problem is by carrying out the Monte Carlo approach, which involves performing $\mathcal{O}(10^4)$ simulations, which is computationally prohibitive in the case of LES. Previous studies have shown that surrogate models can be used in Monte Carlo simulation to facilitate faster UQ analysis. However, in the presence of both aleatoric and epistemic uncertainties, the challenge lies in building the surrogate model itself, which constitutes the main goal of the current work. This challenge is twofold: first of all, since an FIR model usually contains 30–50 coefficients, this high output dimensionality would greatly impact the efficiency of any surrogate modeling approach. Secondly, for each wall temperature, the corresponding FIR coefficients are not unique due to the application of SI on data corrupted with noise. Building surrogate models for uncertain variables is not trivial.

To overcome the above-mentioned problems, we adopt the following strategy which represents the novelty of the current work: (1) to address the problem of high output dimensionality a univariate surrogate model is proposed, where the output FIR coefficients are described as a function of time delay and the uncertain boundary condition to deduce the mapping between the inputs (time delay and wall temperature) and the output (FIR coefficients). (2) To address the issue of variability of FIR coefficients, we propose a bootstrapping strategy. In this methodology we generate multiple realizations of training data based on the FIR coefficient uncertainty information given by the SI method; For each set of realization, we fit a surrogate model and record its corresponding uncertainty estimation. Finally, we aggregate the calculated ensemble of uncertainty estimates to derive the comprehensive uncertainty accounting for both aleatoric and epistemic uncertainty. Once the way of building a surrogate is finalized, any type of surrogate model can be chosen which can then be plugged into Monte Carlo simulation to facilitate subsequent UQ analysis. In this study we choose a univariate Gaussian Process as a surrogate model first, as it has been proven to accelerate UQ analysis in the framework of thermoacoustic problems [21]; Secondly, it not only outputs the prediction at unsampled points but also gives the associated prediction uncertainty courtesy of its Bayesian nature [22]. Later, the developed UQ methodology is applied to infer the FIR at any location in the investigated temperature range to search for a better agreement with the measured FIR highlighting the uncertainty of the boundary condition.

This paper is structured as follows: section “Thermoacoustic Framework” describes the computational setup of the thermoacoustic problem at hand along with the description of the flame

model identification procedure and the flame topology variation. Section “Gaussian Process Overview” provides the technical overview of the employed Gaussian Process followed by the description of the bootstrapping procedure to estimate the prediction uncertainty at a test temperature. Section “Results and Discussion” elucidate the application of the proposed univariate Gaussian Process on the thermoacoustic problem under investigation showing the performance of the Gaussian Process (GP) model and the effect of combined uncertainty on the FIR.

Thermoacoustic Framework

In this section, we discuss the computational test setup that is used to generate the time series data for the estimation of the flame dynamics response model. This is followed by the formal description of the flame model identification procedure and the comparison of the identified flame model against experimental measurements. Finally, the effect of variation of combustor back plate temperature on the flame topology is discussed.

Combustor Configuration. The system under investigation is the NOISEDyN combustor, which was conceived at the EM2C laboratory. Numerical validation of the flow field and flame of this combustor were carried out by Merk et al. [23] using AVBP [24]. Figure 1 shows the setup of the EM2C laboratory-scale test rig. The shaded area shows the computational domain, which fully resolves the radial swirler and the combustor geometry without geometric simplifications. Fully compressible LES-filtered Navier–Stokes equations are solved on an unstructured grid with approximately 19 million tetrahedral cells and 0.6 mm maximum cell size in flame region with a second-order accurate Lax–Wendroff scheme. The Dynamically thickened flame model is

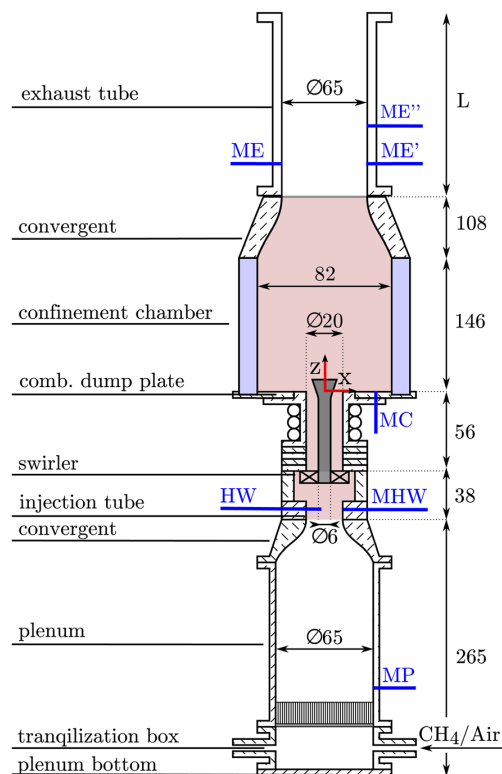


Fig. 1 Sketch of the NOISEDyN Turbulent Swirl Combustor. Dimensions are in mm [23].

used with an efficiency function adopted from Colin et al. [25], resolving the laminar flame thickness with seven cells. Classical Navier–Stokes characteristic boundary conditions [26] are used to treat inlet and outlet. According to Refs. [27,28], the inlet relaxation coefficient K controls the magnitude and phase of the inlet reflection coefficient. A value of $K = 6000 \text{ s}^{-1}$ is used to strike a balance between the drift of the mean velocity and acoustic reflection, which is aimed at low values. This relaxation factor corresponds to a cut-off frequency of $\sim 470 \text{ Hz}$ according to the theory [27]. For the outlet, the ambient pressure is imposed with outlet relaxation coefficient $K = 500 \text{ s}^{-1}$. Note that the time domain impedance boundary condition [28] used with success in the works of [23,29,30] are not implemented in version 7.0 of AVBP at the time of this work and, consequently, could not be adopted for the modeling of fully anechoic boundary conditions. The metallic combustor back (dump) plate is defined as a no-slip isothermal wall. In a first computation, the temperature is tuned to 823 K to match the LES outlet gas temperature with measurements [23]. Nevertheless, such a temperature is highly uncertain and constitutes a matter of investigation in the present study.

Flame Model. In this work, the flame response is characterized via the Finite Impulse Response model. This model can be transformed to the frequency domain through the z transform [31], resulting in the so-called flame transfer function (FTF), $\mathcal{F}(\omega)$

$$\mathcal{F}(\omega) \equiv \frac{\dot{Q}'(\omega)/\bar{Q}}{u'_{\text{ref}}(\omega)/\bar{u}_{\text{ref}}} \quad (1)$$

where \dot{Q}' is the integrated global heat release rate, u_{ref} is the velocity at reference location, overbar and prime indicate average and fluctuations. In the current study, the FTF is obtained by forcing the flame with a broadband signal and applying SI on the down-sampled time series data as has been successfully applied in previous studies [5,11,32,33]. Note that before excitation is applied, the cold flow and heat release characteristics are validated against experimental measurements. Further details on the LES validation procedure can be found in [23]. Once the simulation reaches a statistically stationary state after the initiation of combustion, the flame is acoustically forced with broadband excitation for $\sim 350 \text{ ms}$ to generate the time series of acoustic velocity and heat release rate fluctuations. This data is subsequently used to infer the FIR coefficients via advanced System Identification techniques [6]. The excitation signal applied at the inlet is the in-going characteristic wave external (wavelet type [34]). It is designed in such a way that it exhibits constant power spectral density up to a cut-off frequency of 1000 Hz . The excitation amplitude is equal to 10% of the mean flow velocity. This value of excitation amplitude is a compromise as low excitation amplitude leads to a low signal-to-noise ratio, while high excitation amplitude triggers a nonlinear response that cannot be studied by linear identification procedures used in this study. Time series length of $\sim 350 \text{ ms}$ has proven to be successful in describing the premixed flame dynamics [11,30]. Note that this time interval corresponds to roughly 35 times the length of the impulse response and such a temporal length is deemed appropriate in SI practice [31].

Compared to the Box-Jenkins model structure used for system identification in a previous study [30], a more simple structure – the FIR model [33,35] – is used in this work, as it converges to similar results as those provided by Box-Jenkins when short time series are considered [36]. Additionally, in this study, we focus exclusively on the flame response and do not aim at inferring source models of combustion noise. The FIR model structure is formally written as

$$\dot{Q}'_u(t) = \sum_{i=0}^{n_b} h_i u'(t - i\Delta t) \quad (2)$$

where n_b is the number of impulse response coefficients h_i , Δt is the model time-step and $\dot{Q}'_u(t)$ is the global heat release rate

fluctuation caused by the velocity fluctuation $u'(t)$ upstream of the flame. The detailed explanation on the FIR model structure can be found in [31]. The FIR identification procedure is applied on the time series generated by LES. A polynomial order $n_b = 25$ is considered. The identification procedure and data processing is realized in MATLAB 2018a.

Figure 2 shows the identified impulse response coefficients h_k 's and the associated FTF along with the confidence intervals. The confidence interval which shows the aleatoric uncertainty in the estimated FIR coefficients is represented by covariance matrix. A rigorous derivation of the covariance matrix which results from solving the least-squares approach is shown in the works of Sovardi et al. [37] and Guo et al. [19]. Explicitly, the diagonal elements of the covariance matrix shown in Fig. 2(c) represent the coefficient variances whereas the off-diagonal elements show the covariance among the pairs of parameters. The covariance matrix exhibits a diagonal dominant nature, which is expected in a typical flame response.

Flame Topology. First row in Fig. 3 shows the mean volumetric heat release rate calculated by LES in the mid-longitudinal plane at three different temperatures. Flow is from bottom to top. The depicted mean reaction zone is normalized by the maximum value found in the time series, which is averaged over 70ms worth of accumulated data. Numerous works have studied the flow and flame topology changes due to variation in the thermal state of the combustor walls [38,39] and have observed that the flame length changes, hence affecting the flame dynamic response.

The flame length at combustor back plate temperature of 720 K is longer than the flame at 926 K . Due to the cooler back plate temperature, the outer recirculation zone has higher heat loss and does not supply the flame root and the outer shear layer with burnt gases at adiabatic flame temperature resulting in reduced flame speed/longer flame length [9,11]. On the other hand, due to the hotter combustor back plate temperature, heat loss in the outer recirculation zone is reduced and the flame root is supplied by relatively hot burnt gases leading to increased flame speed/shorter flame length. This also leads to re-attachment of the flame outer branches to the outer rim of the injection tube and transition from V to M type flame [40]. The change in flame topology affects the flame dynamic response as shown in the FTF and FIRs of Fig. 3. The sensitivity of the flame response to thermal boundary conditions is indisputable in both gain and phase. The dependence of the flame response phase on the flame length is readily understood. The flame length affects the characteristic convection time of perturbations reaching the flame tip. This is evident when comparing the results of the case at 720 K with the other two cases: the slope of the identified FTF phase slightly changes, as shown in the phase plot in second row of Fig. 3.

The third row of Fig. 3 shows the estimated Finite Impulse Response at three corresponding temperatures which are obtained by LES/SI procedure. The FIR obtained from the LES/SI procedure is shown by solid lines and the uncertainty of the estimation is given by the shaded area. The confidence interval represents the aleatoric uncertainty caused by applying SI on a LES time series with combustion noise and finite length of time series for identification. The measured FIR is obtained by performing the inverse Fourier transform of the measured FTF. In order to facilitate the comparison of the FTFs, the number of coefficients n_b is held constant. As a result, the low frequency limit [41] for premixed flames at 720 K and 926 K do not start at the same point as 823 K indicating that the filter length is inadequate to describe flame response at these temperatures. Change in the filter length n_b leads to an appropriate low-frequency limit. For the sake of brevity, it is not shown here. The impulse response obtained from LES/SI is in good agreement with neither of the three temperatures highlighting the fact

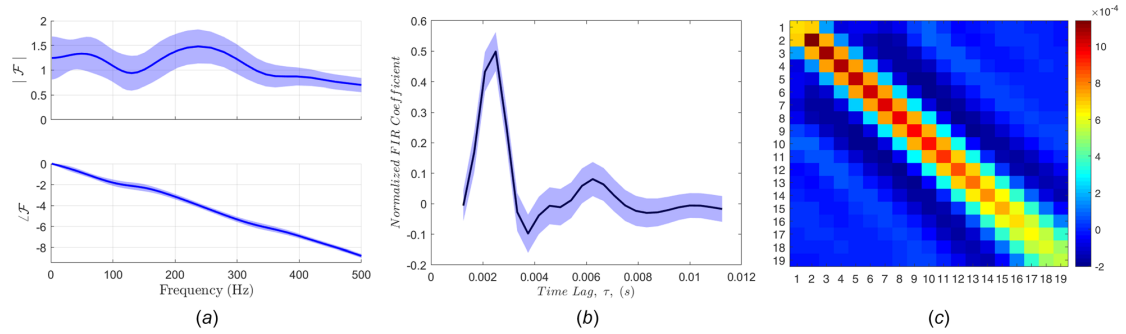


Fig. 2 FTF and FIR obtained from FIR identification along with covariance matrix

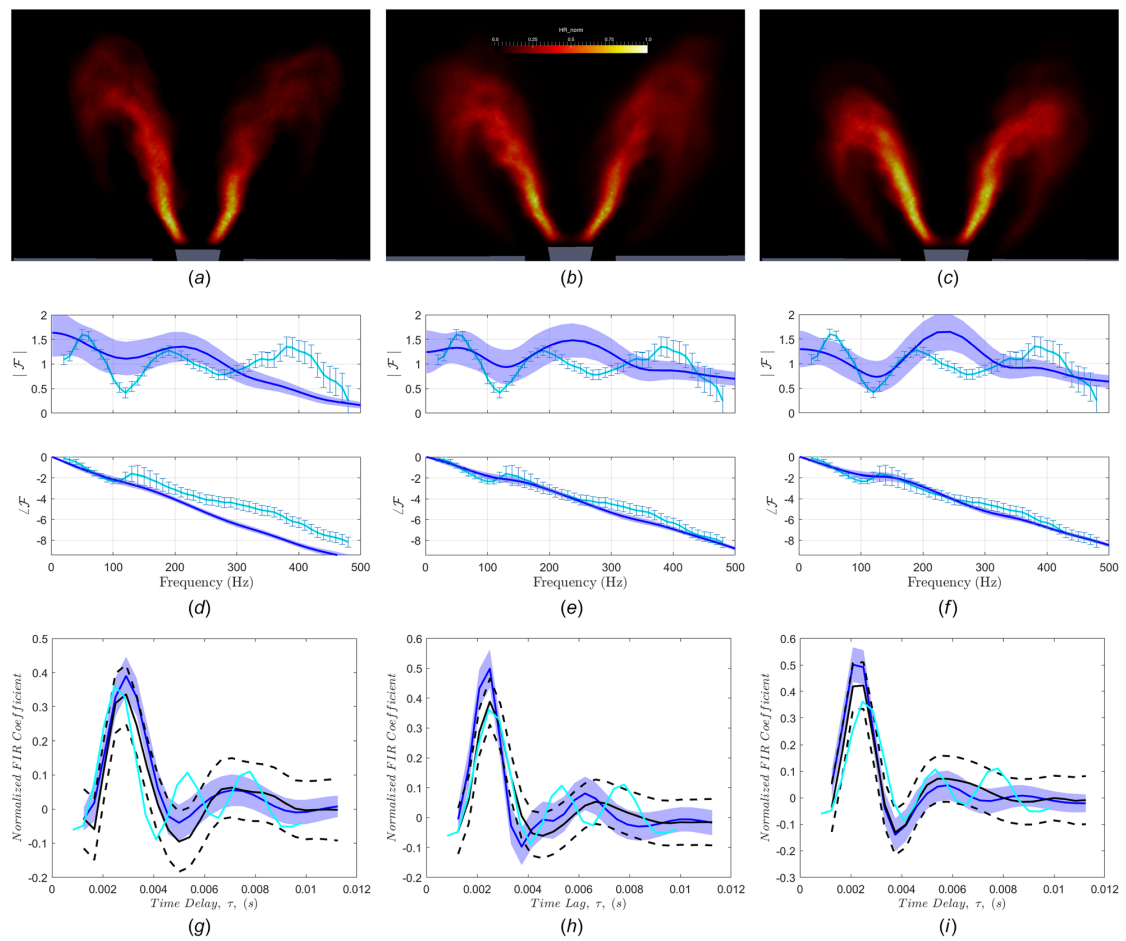


Fig. 3 Comparison of mean reaction zone calculated from LES, FTF inferred from FIR (—) and FIR's obtained from LES/SI (—), experimental measurement (—) and GP model prediction (—), at three different combustor back plate temperatures. Shaded and dashed lines represent the confidence interval of the estimated FIR from LES/SI and GP model, respectively. (Color version online.)

that the tuned combustor back plate temperature in the LES simulation of 823 K is only an educated guess. Later, the trained GP model is leveraged to predict the FIR at any temperature in the given range that is in better agreement with the measured FIR highlighting the effect of uncertain combustor back plate temperature.

Gaussian Process Overview

To efficiently address the impact of both aleatoric and epistemic uncertainties on the flame dynamics, a supervised machine learning algorithm called Gaussian Process surrogate model is employed in this UQ study. A Gaussian Process surrogate model has been applied

previously to UQ analysis in thermoacoustic problems, where only the impact of aleatoric uncertainties in the flame model on the growth rate of the thermoacoustic modes of the system has been studied [19]. Meanwhile, the impact of both aleatoric and epistemic uncertainties on flame dynamics has not been explored. In the following, we discuss various approaches to account for both uncertainties and their respective shortcomings. Afterwards, we briefly discuss the technical overview of the adopted bootstrapping univariate Gaussian Process followed by the bootstrapping methodology to obtain prediction uncertainty at any test temperature.

In this study, we aim at assessing the impact of uncertain combustor back plate temperatures T_w and combustion noise on the flame dynamics (FIR) estimation. A naive way to tackle this problem is by Monte Carlo simulation, which implies generating a large number of samples ($\mathcal{O}(10^4)$) of T_w according to a given predefined probability distribution, and obtaining the corresponding FIR from LES/SI for each T_w . However, carrying out $\mathcal{O}(10^4)$ realizations of LES is not a viable solution in reality. Therefore, surrogate modeling techniques (e.g., Gaussian Process) can be employed to learn the mapping between T_w and FIR coefficients based on a small number of carefully selected training samples, thus significantly improving the uncertainty propagation efficiency.

Mapping the input T_w to output FIR coefficients \mathbf{h} is not straight-forward due to the high output dimensionality of the FIR. Generally, the identified FIR has 20 – 60 FIR coefficients which exhibit a significant degree of correlation. Constructing a surrogate model for each coefficient would be cumbersome and computationally expensive, leading to a degraded UQ analysis. Furthermore, as previously mentioned, the FIR identified from LES/SI for each T_w is uncertain: the FIR coefficients are not deterministic but stochastic, and described by a given probability density function.

Ideally, for the current problem, a surrogate model which outputs the FIR coefficients h_i 's for a given input parameter (in this case, the combustor wall temperature T_w) is desired. Nevertheless, instead of building a surrogate model for all coefficients h_i given a value of T_w , we build a univariate GP model, where we treat the output FIR coefficients as a function of wall temperature T_w and time delay $\tau = n_b \Delta t$ (two inputs - one output). In the following section, we briefly introduce the fundamental overview of the univariate Gaussian Process and the bootstrapping procedure to obtain the prediction uncertainty.

Gaussian Process modeling is a supervised machine learning algorithm, that trains on carefully selected inputs and their corresponding responses to obtain a computationally efficient surrogate model that learns the underlying response surface. The trained model is then used in the desired UQ analysis. This avoids repetitive, computationally expensive, high fidelity solver calculations for predicting the distribution of the FIR coefficients at an untrained temperature. In the following, key formulas for the mean and the variance of the prediction are given. For a detailed derivation of the GP method please refer to [22,42].

GP model treats the output $f(\mathbf{x})$ of the high fidelity solver as the realization of the Gaussian process

$$f(\mathbf{x}) = \beta + Z(\mathbf{x}) \quad (3)$$

where β is a constant value and $Z(\mathbf{x})$ is the departure from β at x , which is modeled as a Gaussian distribution with zero mean, variance σ^2 , and covariance matrix defined as

$$\text{Cov}[Z(\mathbf{x}^i, \mathbf{x}^j)] = \sigma^2 R(\mathbf{x}^i, \mathbf{x}^j) \quad (4)$$

where $R(\mathbf{x}^i, \mathbf{x}^j)$ is the correlation between two sample locations \mathbf{x}^i and \mathbf{x}^j in the input space. In practice, generally a Gaussian kernel is used to describe the correlation function $R(\mathbf{x}^i, \mathbf{x}^j)$ which is represented as

$$R(\mathbf{x}^i, \mathbf{x}^j) = \exp \left[- \sum_{p=1}^M \theta_p (x_p^i - x_p^j)^2 \right] \quad (5)$$

where M denotes the number of input parameters, subscript p represents the p -th component of the input vector \mathbf{x} , and $\boldsymbol{\theta} = [\theta_1, \dots, \theta_M]$ controls the strength of correlation in the corresponding dimension p . A low value of $\boldsymbol{\theta}$ means there will be high level of correlation among input samples and vice versa.

For given samples $\mathbf{X} = [x^1, \dots, x^N]^T$ and their corresponding responses $\mathbf{Y} = [f(x^1), \dots, f(x^N)]^T$ we can train a GP model by finding the values for the hyperparameters $\beta, \sigma^2, \boldsymbol{\theta}$ such that the likelihood of matching the observations is maximized. Maximum likelihood estimate for the mean, β and variance, σ^2 is given by

$$\hat{\beta} = (\mathbf{1}^T \mathbf{R}_D^{-1} \mathbf{1})^{-1} \mathbf{1}^T \mathbf{R}_D^{-1} \mathbf{Y} \quad (6)$$

$$\hat{\sigma}^2 = \frac{1}{N} (\mathbf{Y} - \mathbf{1} \hat{\beta})^T \mathbf{R}_D^{-1} (\mathbf{Y} - \mathbf{1} \hat{\beta}) \quad (7)$$

where \mathbf{R}_D is N -by- N is correlation matrix between training samples and $\mathbf{1}$ is a vector of ones of size M . For estimating $\boldsymbol{\theta}$, the following auxiliary optimization problem has to be solved

$$\hat{\boldsymbol{\theta}} = \underset{\boldsymbol{\theta}}{\text{argmax}} \left[-\frac{N}{2} \ln(\hat{\sigma}^2) - \frac{1}{2} \ln(|\mathbf{R}_D|) \right] \quad (8)$$

Finally, the GP model prediction $\hat{f}(\mathbf{x})$ at multiple locations $\mathbf{X}_p = [x^1, \dots, x^L]^T$ is given by mean $\boldsymbol{\mu}(\hat{f}(\mathbf{x}))$ and covariance $\text{cov}(\hat{f}(\mathbf{x}))$ as

$$\boldsymbol{\mu}(\hat{f}(\mathbf{x})) = \mathbf{I} \hat{\beta} + \mathbf{R}_{pD}^T \mathbf{R}_D^{-1} (\mathbf{Y}_D - \mathbf{I} \hat{\beta}) \quad (9)$$

$$\text{cov}(\hat{f}(\mathbf{x})) = \hat{\sigma}^2 (\mathbf{R}_p - \mathbf{R}_{pD}^T \mathbf{R}_D^{-1} \mathbf{R}_{pD}) \quad (10)$$

where \mathbf{R}_{pD} represents the N -by- L correlation matrix between the prediction inputs \mathbf{X}_p and the training inputs \mathbf{X} . \mathbf{R}_p represents the L -by- L correlation matrix between the prediction inputs \mathbf{X}_p .

Gaussian Process Model Training. In this study, we train a single Gaussian Process surrogate model to predict the mean of the FIR distribution and then use the bootstrapping procedure to predict the variance, which accounts for the model approximation and FIR estimation uncertainty. To further quantify the uncertainty due to combustor wall temperature T_w , Monte Carlo is then performed on the configured surrogate model to obtain the comprehensive uncertainty estimate at any arbitrary temperature between the range considered. Detailed description of this procedure is given below:

Gaussian Process Interpolation

Step 1: Select N training samples $\mathbf{T}_w = T_w^1, \dots, T_w^N$. In the current study we assume that T_w follows a uniform distribution with $T_w \sim (T_{min}, T_{max})$. As a rule of thumb, N can be chosen as 10.

Step 2: For each $T_w^{(k)}, k = 1, \dots, N$ run LES and estimate FIR coefficients $\mathbf{h}^{(k)} \sim (\mathbf{m}^{(k)}, \mathbf{C}^{(k)})$. Here, \mathbf{m} denotes the mean value vector and \mathbf{C} denotes the covariance matrix. Note that the dimension of \mathbf{h} has to be kept the same for all identifications.

Step 3: Train a univariate GP model to determine the nominal FIR surface from the training set $(T_w, (\mathbf{m}^{(k)}))$ which fits a GP hypersurface $\mathbf{h} \sim \mathcal{GP}(\tau, T_w)$ as illustrated in Fig. 4.

Prediction Uncertainty. The procedure to determine the prediction uncertainty is described in Algorithm 1. First, to capture the uncertainty given by the SI procedure, multiple realizations (p) of the training data (N) are generated within the FIR coefficient uncertainty given by the SI procedure applied on the LES time series data. Further, for each prediction temperature i in S ,

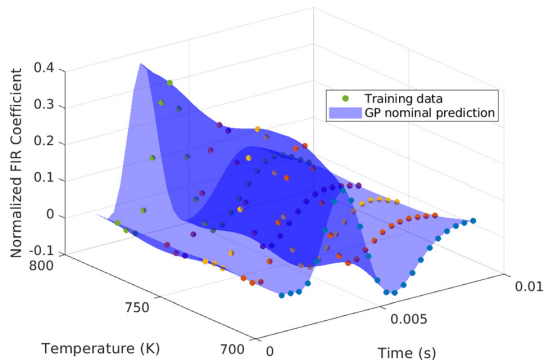


Fig. 4 Illustration of the interpolated GP hypersurface

the GP model hyperparameters for each r th realization in p are re-calculated. Then, the re-calculated GP model is leveraged to predict at i th temperature. At each prediction, q realizations are generated within the covariance matrix given by the GP model approximation (Eq. 10) and its corresponding uncertainty in the estimation of the FIR is recorded. Finally, we aggregate the ensemble of the uncertainty estimates to derive the total prediction uncertainty containing aleatoric and epistemic uncertainty. All the code and data to produce the results will be made open-source and can be found in the website.²

Algorithm 1 Total prediction uncertainty using bootstrapping GP model

```

1: Perform LES on  $N$   $T_w$  samples to create a training matrix  $(T_w, (\mathbf{m}^{(k)}))$ 
2: Train GP model  $\leftarrow \mathbf{h} \sim \mathcal{GP}(\tau, T_w)$ 
3: while  $j < \text{length}(N)$  do
4:   Obtain the uncertainty information for each of the  $N$  training data
    $(T_w^j, (\mathbf{m}^{(j)}, \mathbf{C}^{(j)}))$  given by SI.
5:   Generate  $p$  realizations within the covariance matrix to capture the
   uncertainty given by the SI procedure.
6: end while
7: Draw  $S$  samples from  $(T_{min}, T_{max})$  via Latin Hypercube Sampling
8: while  $i < \text{length}(S)$  do
9:    $i = i + 1$ .
10:  while  $r < \text{length}(p)$  do
11:    Re-calculate the GP model for each  $r$ th realization (surface) to
    obtain the updated hyperparameters.
12:    Predict FIR using the recalculated GP model at the  $i$ th temperature.
13:    Generate  $q$  realizations with the covariance of the GP model prediction
    given in (Eq. 10) to capture the model approximation uncertainty.
14:    Store the generated  $q$  realizations in a FIR holder.
15:  end while
16: end while
17: Aggregate all the calculated ensemble of uncertainties (SI, model
    approximation and  $T_w$ ) in a FIR container.
18: Determine the uncertainty statistics (mean and covariance) from the
    FIR container.

```

Results and Discussion

Section “Gaussian Process Overview” discussed the Gaussian Process training methodology to predict the FIR for any given combustor back plate temperature. In this section, the proposed methodology is applied to the data obtained from the identification procedure described in section “Thermoacoustic Framework”. The workflow of carrying out uncertainty quantification with the GP surrogate is discussed next. The comparison of the GP model prediction results against the LES/SI simulation follows.

²https://github.com/sagark9299/GaussianProcess_total_uncertainty.git

The overall workflow of quantifying the uncertainty in the FIR coefficients at a given temperature consists of two parts. The first part discusses the bootstrapping GP procedure to estimate \mathbf{h} given T_w . The second part leverages on the trained GP model to perform Monte Carlo simulation and to obtain uncertainty estimates at any arbitrary temperature, within the trained temperature space.

Sampling Plan: Following the training procedure elucidated in the section “Gaussian Model Training”, a uniform distribution on the combustor back plate temperature ranging from -15% to 15% is chosen with the expected value of this distribution equal to the base case, that is 823 K. A list of the temperature points used for training and testing is given in Table 1

Data Acquisition: Once the sample points are finalized, one LES for each temperature listed in Table 1 is executed. This generates the response matrix of the sample response pair (T_w, \mathbf{h}) .

GP model training: The GP model is trained using the Sample-Response pair (T_w, \mathbf{h}) . As explained in the section “Prediction Uncertainty”, from the training dataset (T_w, \mathbf{h}) , $p = 500$ realizations are generated from the FIR coefficient uncertainties of each training data. Further, $q = 500$ realizations are drawn from the covariance matrix given by the GP model prediction (Eq. 10) at the test location. The average of the ensembles ($500 \times 500, n_b$) gives the prediction uncertainty: FIR identification uncertainty and the GP model uncertainty. Finally, the total prediction uncertainty is obtained by using the trained GP model to predict at ~ 1000 T_w samples, which are drawn from the temperature range shown in Table 1. This gives the total prediction uncertainty due to FIR identification procedure and thermal boundary condition T_w .

Results of Gaussian Process Methodology. The third row of Fig. 3 shows the comparison of the prediction of the GP model (dashed lines) against the FIRs obtained from LES/SI (shaded area) for three selected temperatures except for the first and last index, as the only prediction based on GP interpolation is sought. For example, at prediction site of 823 K, all the temperatures except 823 K are used in the training dataset. The aggregated GP model interpolation fits closely the FIRs obtained from the LES/SI. The confidence intervals given by the aggregated GP model are wider than those obtained with LES/SI as it contains the aleatoric uncertainties from the noisy FIR obtained by system identification (low signal to noise ratio, shorter time series data) as well as the uncertainty due to the approximation caused by the GP model. The confidence interval of the GP model prediction increases for sparse sampling scheme as the approximating function may exhibit strong undulating behavior and the nearest training points then are not sufficient to infer the change in the FIR shape. Hence, a dense sampling scheme is used, as the main aim of this work is to demonstrate a methodology to account for joint aleatoric and epistemic uncertainties. Future work will focus on how to tackle the current UQ problem in more efficient way.

Figure 6 shows the GP model prediction within the temperature range investigated that is obtained by averaging the conditional distributions obtained for 1000 samples of T_w 's. The uncertainty marked by the confidence interval of the GP model is wider as it incorporates both the epistemic uncertainty from combustor back plate temperature T_w and the aleatoric uncertainty introduced by the noisy and limited training data. This can be validated by considering the PDF of any single FIR coefficient prediction (15th in this case) at given temperatures (no epistemic uncertainty) as seen in Fig. 5. Due to the absence of epistemic uncertainty, the obtained PDF is narrower than the total uncertainty resulting in narrower confidence interval as seen in the third row of Fig. 3. However, when the epistemic uncertainty is considered, the PDF of the single FIR coefficient prediction becomes wider due to the aggregation of all the aleatoric uncertainties. Wider PDF results in a wider confidence interval as seen in Fig. 6. This shows that the proposed way of building a surrogate model in the presence of both aleatoric and epistemic uncertainties is successful in

Table 1 List of combustor back plate temperatures used for GP surrogate model

Index	1	2	3	4	5	6	7	8	9	10	11	12	13
Temperature	700	720	740	760	786	800	823	842	860	885	905	926	946

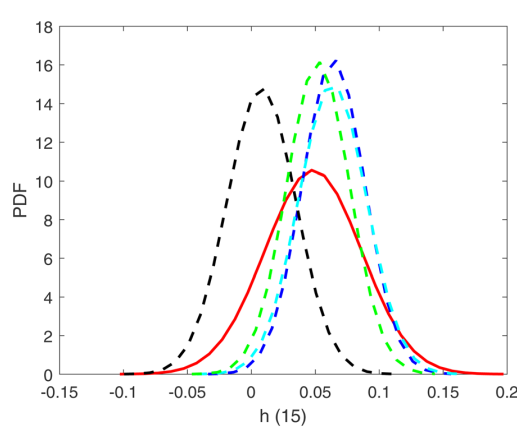


Fig. 5 Comparison of aleatoric uncertainty at three different temperatures (dashed) and total uncertainty (solid) PDF for a single FIR coefficient

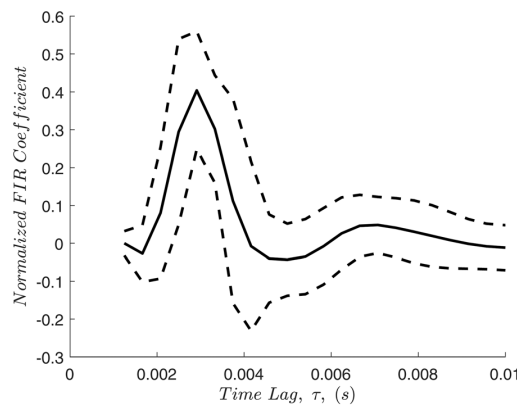


Fig. 6 GP model prediction uncertainty in the temperature range considered

accounting for both uncertainties. It also shows the suitability of the univariate GP model proposed.

In section “Flame Topology” we saw that the FIR obtained at three exemplary temperatures including the tuned combustor back plate temperature did not match well against the measured FIR, hence highlighting the uncertainty of the thermal boundary condition. We now leverage the trained GP model to predict the FIR within the temperature range of interest and to check for best fit against experimental measurements. By doing so, one may deduce a highly probable value of the combustor back plate temperature. Figure 7 shows the FIR and FTF obtained from GP prediction at 850 K, where the LES data at 850 K was *not* included in the training data. It can be seen that the 850 K results are in much better agreement with the measured FIR and FTF. Further, the GP model prediction is compared against the LES data. The GP model prediction is in good agreement with the LES data demonstrating the capability of the GP model to capture the underlying response

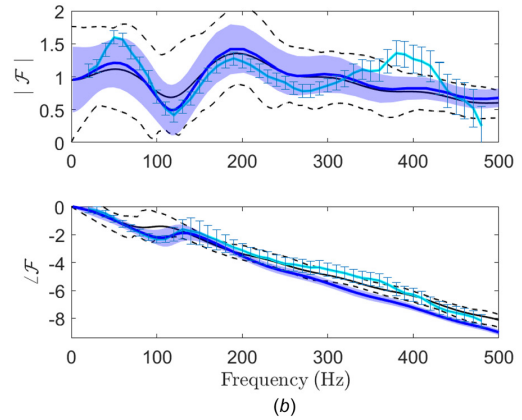
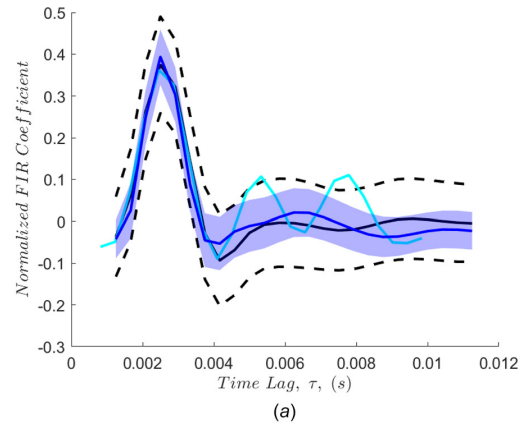


Fig. 7 Comparison of FIR and FTF of GP prediction (—) and LES (—) at 850 K temperature against measured (---) FIR and FTF. (Color version online.)

surface successfully. This serves as additional validation of the proposed UQ methodology.

Summary and Conclusion

Most UQ studies in thermoacoustics have focused on the propagation of uncertainties in the flame model to the growth rate of the thermoacoustic modes of the system. In this study, we made a step forward and focus on the first step of the hybrid approach, where we carry out UQ by combining high-fidelity numerical simulation (LES) with system identification and surrogate modeling. By means of the latter, we are able to propagate epistemic uncertainties – due to uncertainties in thermal boundary conditions in LES – and aleatoric uncertainties – due to system identification on LES data corrupted by noise – on the FIR coefficients that describe the flame response. One of the novelties of this work lies in the way the surrogate model is built. We employed a univariate bootstrapping Gaussian Process model because it fulfills the specifications required for our study: it is an affordable surrogate model with a simple structure that accounts for two inputs and one single output. As a result, the FIR coefficients were considered function of time delay and temperature.

To assess the uncertainty of the combustor back plate temperature, LES simulations were run at well-defined combustor wall temperatures. The FIR coefficients were identified for the corresponding wall temperatures using the LES/SI approach. Variations in the combustor wall thermal boundary condition showed to drive variations in the flame topology. In turn, changes in the flame topology resulted in changes in the flame dynamic response described by the FIR coefficients. The trained univariate Gaussian Process model was able to approximate the complex response surface of the FIRs, hence interpolating the FIR model with reasonable accuracy. The GP model was leveraged to evaluate the FIR coefficients at temperatures within the trained values, which it had not seen during the training. Such an exercise allowed to find a temperature, where the flame response model satisfactorily matches the experimental and LES results.

The present approach demonstrated a surrogate methodology to quantify uncertainties in the flame response model in the presence of both epistemic and aleatoric uncertainties by considering a uniform sampling space. Future works will focus on an active learning scheme, where fewer training points are used with longer simulation times to gain more quality information on the response surface. This enhances the efficiency of the surrogate model training and reduces the computational cost. Additionally, the present methodology of constructing a bootstrapping GP-based surrogate framework can be used in the case of forced spray flame response, where the liquid phase boundary conditions such as droplet diameter, velocity, and size distribution may be uncertain.

Acknowledgment

This project has received funding from the European Union's Horizon 2020 research and innovation programme under Grant Agreement No 766264 Machine learning for Advanced Gas turbine Injection SysTems to Enhance combustoR performance (MAGISTER). S. Guo is grateful for the financial support from doctoral scholarship of Chinese Scholarship Council (No. 201606830045). Computing time on the Supercomputer SuperMUC-NG was provided by Gauss Centre for Supercomputing e.V.

Funding Data

- European Union's Horizon 2020 Research and Innovation Programme (Grant No.: 766264; Funder ID: 10.13039/100010661).
- Chinese Scholarship Council (Grant No. 201606830045).

Nomenclature

FIR = finite impulse response
 FTF = flame transfer function
 GP = Gaussian process
 hi = FIR model coefficient
 LES = large eddy simulation
 N = number of FIR model coefficients
 SI = system identification
 Tw = combustor back plate temperature
 UQ = uncertainty quantification
 τ = mean of distributed time delay for axial velocity perturbation

References

- [1] Lieuwen, T. C., 2012, *Unsteady Combustor Physics*, Cambridge University Press, New York, NY.
- [2] Nicoud, F., Benoit, L., Sensiau, C., and Poinso, T., 2007, "Acoustic Modes in Combustors With Complex Impedances and Multidimensional Active Flames," *AIAA J.*, **45**(2), pp. 426–441.
- [3] Emmert, T., Meindl, M., Jaensch, S., and Polifke, W., 2016, "Linear State Space Interconnect Modeling of Acoustic Systems," *Acta Acust. United Acust.*, **102**(5), pp. 824–833.
- [4] Ducruix, S., Durox, D., and Candel, S., 2000, "Theoretical and Experimental Determinations of the Transfer Function of a Laminar Premixed Flame," *Proc. Combust. Inst.*, **28**(1), pp. 765–773.
- [5] Giauque, A., Poinso, T., and Nicoud, F., 2008, "Validation of a Flame Transfer Function Reconstruction Method for Complex Turbulent Configurations," *AIAA Paper No. 2008-2943*.
- [6] Polifke, W., 2014, "Black-Box System Identification for Reduced Order Model Construction," *Ann. Nucl. Energy*, **67**, pp. 109–128.
- [7] Duchaine, F., Boudry, F., Durox, D., and Poinso, T., 2011, "Sensitivity Analysis of Transfer Functions of Laminar Flames," *Combust. Flame*, **158**(12), pp. 2384–2394.
- [8] Mejia, D., Miguel-Brebion, M., Ghani, A., Kaiser, T., Duchaine, F., Selle, L., and Poinso, T., 2018, "Influence of Flame-Holder Temperature on the Acoustic Flame Transfer Functions of a Laminar Flame," *Combust. Flame*, **188**(2), pp. 5–12.
- [9] Kedia, K., Altay, H., and Ghoniem, A., 2011, "Impact of Flame-Wall Interaction on Premixed Flame Dynamics and Transfer Function Characteristics," *Proc. Combust. Inst.*, **33**(1), pp. 1113–1120.
- [10] Miguel-Brebion, M., Mejia, D., Xavier, P., Duchaine, F., Bedat, B., Selle, L., and Poinso, T., 2016, "Joint Experimental and Numerical Study of the Influence of Flame Holder Temperature on the Stabilization of a Laminar Methane Flame on a Cylinder," *Combust. Flame*, **172**, pp. 153–161.
- [11] Tay-Wo-Chong, L., and Polifke, W., 2013, "Large Eddy Simulation-Based Study of the Influence of Thermal Boundary Condition and Combustor Confinement on Premix Flame Transfer Functions," *ASME J. Eng. Gas Turbines Power*, **135**(2), p. 021502.
- [12] Juniper, M. P., and Sujith, R. I., 2018, "Sensitivity and Nonlinearity of Thermoacoustic Oscillations," *Annu. Rev. Fluid Mech.*, **50**(1), pp. 661–689.
- [13] McManus, K. R., Poinso, T., and Candel, S. M., 1993, "A Review of Active Control of Combustion Instabilities," *Prog. Energy Combust. Sci.*, **19**(1), pp. 1–29.
- [14] Polifke, W., 2020, "Modeling and Analysis of premixed flame Dynamics by Means of Distributed Time Delays," *Prog. Energy Combust. Sci.*, **79**, p. 100845.
- [15] Ndiaye, A., Bauerheim, M., and Nicoud, F., 2015, "Uncertainty Quantification of Thermoacoustic Instabilities on a Swirled Stabilized Combustor," *ASME Paper No. GT2015-44133*.
- [16] Magri, L., Bauerheim, M., Nicoud, F., and Juniper, M. P., 2016, "Stability Analysis of Thermo-Acoustic Nonlinear Eigenproblems in Annular Combustors. Part II. Uncertainty Quantification," *Comput. Phys.*, **325**, pp. 411–421.
- [17] Silva, C. F., Magri, L., Runte, T., and Polifke, W., 2017, "Uncertainty Quantification of Growth Rates of Thermoacoustic Instability by an Adjoint Helmholtz Solver," *ASME J. Eng. Gas Turbines Power*, **139**(1), p. 011901.
- [18] Avdonin, A., Jaensch, S., Silva, C. F., Česnovar, M., and Polifke, W., 2018, "Uncertainty Quantification and Sensitivity Analysis of Thermoacoustic Stability With Non-Intrusive Polynomial Chaos Expansion," *Combust. Flame*, **189**, pp. 300–310.
- [19] Guo, S., Silva, C. F., Ghani, A., and Polifke, W., 2019, "Quantification and Propagation of Uncertainties in Identification of Flame Impulse Response for Thermoacoustic Stability Analysis," *ASME J. Eng. Gas Turbines Power*, **141**(2), p. 021032–10.
- [20] Avdonin, A., and Polifke, W., 2019, "Quantification of the Impact of Uncertainties in Operating Conditions on the Flame Transfer Function With Non-Intrusive Polynomial Chaos Expansion," *ASME J. Eng. Gas Turbines Power*, **141**(1), p. 011020.
- [21] Guo, S., Silva, C. F., and Polifke, W., 2020, "Efficient Robust Design for Thermoacoustic Instability Analysis: A Gaussian Process Approach," *ASME J. Eng. Gas Turbines Power*, **142**(3), p. 031026.
- [22] Forrester, A., Sobester, A., and Keane, A., 2008, *Engineering Design Via Surrogate Modelling: A Practical Guide*, John Wiley & Sons, Ltd., UK.
- [23] Merk, M., Gaudron, R., Gatti, M., Mirat, C., Schuller, T., and Polifke, W., 2018, "Measurement and Simulation of Combustion Noise and Dynamics of a Confined Swirl Flame," *AIAA J.*, **56**(5), pp. 1930–1942.
- [24] CERFACS, and IMFT, 2008, *The AVBP Handbook*, accessed July 21, 2021, <http://www.cerfacs.fr/avbp7x/>
- [25] Colin, O., Ducros, F., Veynante, D., and Poinso, T., 2000, "A Thickened Flame Model for Large Eddy Simulation of Turbulent Premixed Combustion," *Phys. Fluids*, **12**(7), pp. 1843–1863.
- [26] Poinso, T., and Lele, S. K., 1992, "Boundary Conditions for Direct Simulation of Compressible Viscous Flows," *J. Comput. Phys.*, **101**(1), pp. 104–129.
- [27] Selle, L., Nicoud, F., and Poinso, T., 2004, "Actual Impedance of Nonreflecting Boundary Conditions: Implications for Computation of Resonators," *AIAA J.*, **42**(5), pp. 958–964.
- [28] Polifke, W., Wall, C., and Moin, P., 2006, "Partially Reflecting and Non-Reflecting Boundary Conditions for Simulation of Compressible Viscous Flow," *J. Comput. Phys.*, **213**(1), pp. 437–449.
- [29] Merk, M., Silva, C., Polifke, W., Gaudron, R., Gatti, M., Mirat, C., and Schuller, T., 2019, "Direct Assessment of the Acoustic Scattering Matrix of a Turbulent Swirl Combustor by Combining System Identification, Large Eddy Simulation and Analytical Approaches," *ASME J. Eng. Gas Turbines Power*, **141**(2), pp. 021035–021035-9.
- [30] Merk, M., Gaudron, R., Silva, C., Gatti, M., Mirat, C., Schuller, T., and Polifke, W., 2019, "Prediction of Combustion Noise of an Enclosed Flame by Simultaneous Identification of Noise Source and Flame Dynamics," *Proc. Combust. Inst.*, **37**(4), pp. 5263–5270.
- [31] Tangirala, A. K., 2014, *Principles of System Identification: Theory and Practice*, CRC Press, Boca Raton, FL.
- [32] Zhu, M., Dowling, A. P., and Bray, K. N. C., 2005, "Transfer Function Calculations for Aeroengine Combustion Oscillations," *ASME J. Eng. Gas Turbines Power*, **127**(1), pp. 18–26.
- [33] Schuurmans, B., Luebecke, H., Bajusz, D., and Flohr, P., 2005, "Thermoacoustic Analysis of Gas Turbine Combustion Systems Using Unsteady CFD," *ASME Paper No. GT2005-68393*.

- [34] Föller, S., and Polifke, W., 2011, "Advances in Identification Techniques for Aero-Acoustic Scattering Coefficients From Large Eddy Simulation," 18th International Congress on Sound and Vibration (ICSV18), Rio de Janeiro, Brazil, July 10–14, Vol. 4, pp. 3122–3129.
- [35] Blumenthal, R. S., Subramanian, P., Sujith, R., and Polifke, W., 2013, "Novel Perspectives on the Dynamics of Premixed Flames," *Combust. Flame*, **160**(7), pp. 1215–1224.
- [36] Jaensch, S., Merk, M., Emmert, T., and Polifke, W., 2018, "Identification of Flame Transfer Functions in the Presence of Intrinsic Thermoacoustic Feedback and Noise," *Combust. Theory Model.*, **22**(3), pp. 613–634.
- [37] Sovardi, C., Jaensch, S., and Polifke, W., 2016, "Concurrent Identification of Aero-Acoustic Scattering and Noise Sources at a Flow Duct Singularity in Low Mach Number Flow," *J. Sound Vib.*, **377**, pp. 90–105.
- [38] Tay-Wo-Chong, L., Zellhuber, M., Komarek, T., Im, H. G., and Polifke, W., 2016, "Combined Influence of Strain and Heat Loss on Turbulent Premixed Flame Stabilization," *Flow Turbul. Combust.*, **97**(1), pp. 263–294.
- [39] Chtere, I., Foley, C. W., Foti, D., Kostka, S., Caswell, A. W., Jiang, N., Lynch, A., Noble, D. R., Menon, S., Seitzman, J. M., and Lieuwen, T. C., and others, 2014, "Flame and Flow Topologies in an Annular Swirling Flow," *Combust. Sci. Technol.*, **186**(8), pp. 1041–1074.
- [40] Taamallah, S., Shanbhogue, S. J., Sanusi, Y. S., Mokheimer, E. M. A., and Ghoniem, A. F., 2015, "Transition From a Single to a Double Flame Structure in Swirling Reacting Flows: Mechanism, Dynamics, and Effect of Thermal Boundary Conditions," *ASME Paper No. GT2015-43998*.
- [41] Polifke, W., and Lawn, C. J., 2007, "On the Low-Frequency Limit of Flame Transfer Functions," *Combust. Flame*, **151**(3), pp. 437–451.
- [42] Guo, S., Silva, C. F., and Polifke, W., 2020, "Reliable Calculation of Thermoacoustic Instability Risk Using an Imperfect Surrogate Model," *ASME Paper No. GT2020-14434*.

List of Figures

1.1	Identification of FIR/FTF is impacted by different sources of uncertainties in the LES/SI procedure	3
2.1	Schematic of the feedback processes responsible for thermoacoustic instabilities	6
2.2	Illustration of different processes that can cause combustion instabilities. Courtesy Lieuwen et al. [25]	6
3.1	Schematic of the acoustic velocity coupling mechanism generating heat release rate oscillation for spray flames	7
4.1	Different turbulence modeling approaches visualized through turbulent energy spectrum against wave numbers	14
5.1	Effect of varying θ on correlation	21
5.2	Training dataset of FIR flame models obtained at different wall temperatures . .	23
5.3	Illustration of a GP hypersurface	24
5.4	Illustration of uncertainty aggregation in the bootstrapping procedure	24
5.5	Schematic of the identification process using input-output data. Courtesy of Tangirala [59]	25
5.6	Normalized broadband input-output time series generated by LES	26
7.1	Schematic of PERM injector	34
7.2	Sketch of the test rig at TU Munich	34
7.3	Computational domain of the test-rig	35
7.4	Polyhedral mesh visualized on the mid-longitudinal plane	35
7.5	Contour of LES quality index on the mid-longitudinal plane	36
7.6	Instantaneous and time averaged velocity field on the mid-longitudinal plane . .	37

7.7	Instantaneous and time averaged temperature field on the mid-longitudinal plane	38
7.8	Contour of droplet diameter distribution visualized on the mid-longitudinal plane	38
7.9	Time averaged mass source distribution visualized on the mid-longitudinal plane	39
7.10	Instantaneous temperature field superimposed with isocontours of mixture fraction	39
7.11	Time averaged field of heat release rate visualized on the mid-longitudinal plane	40
7.12	Comparison of FTF (blue) inferred from LES time series data against measured FTF (black) and FTF from URANS with isothermal wall boundary conditions (green, Figure 18 of [46])	41

List of Tables

7.1	Comparison of models between present study and Innocenti's URANS study . .	42
-----	--	----

Bibliography

- [1] Future of Aviation. Technical report, ICAO, 2022.
- [2] Martin Hepperle. Electric Flight - Potential and Limitations. In *Energy Efficient Technologies and Concepts of Operation*, Lisbon, Portugal, 2012. NATO Science and Technology Organization.
- [3] Alexander Bills, Shashank Sripad, William Leif Fredericks, Madalsa Singh, and Venkatasubramanian Viswanathan. Performance Metrics Required of Next-Generation Batteries to Electrify Commercial Aircraft. *ACS Energy Letters*, 5(2):663–668, February 2020.
- [4] David Kramer. Hydrogen-powered aircraft may be getting a lift. *Physics Today*, 73(12):27–29, December 2020.
- [5] Tim C. Lieuwen. *Unsteady Combustor Physics*. Cambridge University Press, New York, N.Y., USA, 2012.
- [6] Thierry Poinsot. Prediction and control of combustion instabilities in real engines. *Proceedings of the Combustion Institute*, 36(1):1–28, 2017.
- [7] S. Candel. Combustion Dynamics and Control: Progress and Challenges. *Proceedings of the Combustion Institute*, 29(1):1–28, 2002.
- [8] F. E. C. Culick. *Unsteady Motions in Combustion Chambers for Propulsion Systems*. Number AC/323(AVT-039)TP/103 in RTO AGARDograph AG-AVT-039. AGARD / NATO, 2006.
- [9] Ying Huang and Vigor Yang. Dynamics and Stability of Lean-Premixed Swirl-Stabilized Combustion. *Progress in Energy and Combustion Science*, 35(4):293–364, 2009.
- [10] Sébastien Ducruix, Daniel Durox, and Sébastien Candel. Theoretical and experimental determinations of the transfer function of a laminar premixed flame. *Proceedings of the Combustion Institute*, 28(1):765–773, January 2000.
- [11] P. Flohr, C. O. Paschereit, B. van Roon, and B. B. H. Schuermans. Using CFD for time-delay modeling of premix flames. In *Int'l Gas Turbine and Aeroengine Congress & Exposition*, GT-2001-0376, pages 10–10, New Orleans, LA, 2001. ASME.
- [12] T. Schuller, D. Durox, and S. Candel. A Unified Model for the Prediction of Laminar Flame Transfer Functions: Comparisons Between Conical and V-Flame Dynamics. *Combustion and Flame*, 134(1-2):21–34, July 2003.

BIBLIOGRAPHY

- [13] Guillaume Vignat, Ermanno Lo Schiavo, Davide Laera, Antoine Renaud, Laurent Gicquel, Daniel Durox, and Sébastien Candel. Dynamics of spray and swirling flame under acoustic oscillations : A joint experimental and LES investigation. *Proceedings of the Combustion Institute*, page S1540748920301024, August 2020.
- [14] Shigeru Tachibana, Kinya Saito, Takeshi Yamamoto, Mitsumasa Makida, Tomoaki Kitano, and Ryoichi Kurose. Experimental and numerical investigation of thermo-acoustic instability in a liquid-fuel aero-engine combustor at elevated pressure: Validity of large-eddy simulation of spray combustion. *Combustion and Flame*, 162(6):2621–2637, June 2015.
- [15] Tomoaki Kitano, Keisuke Kaneko, Ryoichi Kurose, and Satoru Komori. Large-eddy simulations of gas- and liquid-fueled combustion instabilities in back-step flows. *Combustion and Flame*, 170:63–78, August 2016.
- [16] Virginia Fratalocchi and Jim B. W. Kok. Ethanol turbulent spray flame response to gas velocity modulation. *Combustion Theory and Modelling*, 22(1):91–109, January 2018.
- [17] J. Eckstein, E. Freitag, C. Hirsch, T. Sattelmayer, R. von der Bank, and T. Schilling. Forced Low-Frequency Spray Characteristics of a Generic Airblast Swirl Diffusion Burner. *Journal of Engineering for Gas Turbines and Power*, 127(2):301–306, April 2005.
- [18] R. I. Sujith. An experimental investigation of interaction of sprays with acoustic fields. *Experiments in Fluids*, 38(5):576–587, May 2005.
- [19] Javier Achury and Wolfgang Polifke. Theoretical investigation of the particle response to an acoustic field. *Int. J. Spray Comb. Dynamics*, 8(4):262–270, 2016.
- [20] Wolfgang Polifke. Black-Box System Identification for Reduced Order Model Construction. *Annals of Nuclear Energy*, 67C:109–128, May 2014.
- [21] Alexander Avdonin and Wolfgang Polifke. Quantification of the Impact of Uncertainties in Operating Conditions on the Flame Transfer Function with Non-Intrusive Polynomial Chaos Expansion. *J. Eng. Gas Turbines and Power*, 141(1):011020, 2019.
- [22] Shuai Guo, Camilo F. Silva, Abdulla Ghani, and Wolfgang Polifke. Quantification and Propagation of Uncertainties in Identification of Flame Impulse Response for Thermoacoustic Stability Analysis. *J. Eng. Gas Turbines and Power*, 141(2):021032–10, February 2019.
- [23] L Crocco and S I Cheng. *Theory of Combustion Instability in Liquid Propellant Rocket Motors*. Number 8 in AGARDograph. Butterworths Science Publications, New York, 1956.
- [24] N. Noiray, D. Durox, T. Schuller, and S. Candel. A Unified Framework for Nonlinear Combustion Instability Analysis Based on the Flame Describing Function. *Journal of Fluid Mechanics*, 615:139–167, 2008.
- [25] Timothy Lieuwen and Vigor Yang, editors. *Combustion Instabilities in Gas Turbine Engines: Operational Experience, Fundamental Mechanisms and Modeling*, volume 210 of

- Progress in Astronautics and Aeronautics*. American Institute of Aeronautics and Astronautics, Reston, VA, USA, 2005.
- [26] Sebastien Ducruix, Thierry Schuller, D. Durox, and S Candel. Combustion Dynamics and Instabilities: Elementary Coupling and Driving Mechanisms. *Journal of Propulsion and Power*, Volume 19(Issue No. 5):pp. 722–734, September - Oktober 2003.
- [27] P Gajan, A Strzelecki, B Platet, R Lecourt, and F Giuliani. Investigation of spray behavior downstream of an aeroengine injector with acoustic excitation. *Journal of propulsion and power*, 23(2):392–399, 2007.
- [28] T. Komarek and W. Polifke. Impact of Swirl Fluctuations on the Flame Response of a Perfectly Premixed Swirl Burner. In *Int'l Gas Turbine and Aeroengine Congress & Exposition*, ASME GT2009-60100, Orlando, FL, U.S.A., June 2009.
- [29] P. Palies, T. Schuller, D. Durox, and S. Candel. Modeling of Premixed Swirling Flames Transfer Functions. *Proceedings of the Combustion Institute*, 33(2):2967–2974, 2011.
- [30] A. Duvvur, C. H. Chiang, and W. A. Sirignano. Oscillatory fuel droplet vaporization - Driving mechanism for combustion instability. *Journal of Propulsion and Power*, 12(2):358–365, 1996.
- [31] A. Y. Tong and W. A. Sirignano. Oscillatory vaporization of fuel droplets in an unstable combustor. *Journal of Propulsion and Power*, 5(3):257–261, 1989.
- [32] RI Sujith, GA Waldherr, JI Jagoda, and BT Zinn. A theoretical investigation of the behavior of droplets in axial acoustic fields. *Journal of vibration and acoustics*, 121(3):286–294, 1999.
- [33] Roger Prud'homme, Mohammed Habiballah, Lionel Matuszewski, Yves Mauriot, and Aurélie Nicole. Theoretical Analysis of Dynamic Response of a Vaporizing Droplet to Acoustic Oscillations. *Journal of Propulsion and Power*, May 2012.
- [34] Qiang Li, Gai Lei, and Wenjing Yang. Study on the clustering of dispersed particles in an oscillating flow field. *Powder Technology*, 311:167–174, April 2017.
- [35] David Katoshevski, Tal Shakked, Sergei S. Sazhin, Cyril Crua, and Morgan R. Heikal. Grouping and trapping of evaporating droplets in an oscillating gas flow. *International Journal of Heat and Fluid Flow*, 29(2):415–426, April 2008.
- [36] Titouan Moriniere. *Spray and Combustion Dynamics in an Aerojet Engine Gas Turbine Model Combustor*. PhD thesis, Université Toulouse 3 - Paul Sabatier, Toulouse, France, 2023.
- [37] Giandomenico Lupo and Christophe Duwig. *Advances in Droplet Evaporation*. KTH Royal Institute of Technology, 2019.
- [38] Sagar Kulkarni, Camilo F. Silva, and Wolfgang Polifke. Response of Spray Number Density and Evaporation Rate to Velocity Oscillations. *Int. J. Spray Comb. Dynamics*, 14(1-2):107–117, 2022.

BIBLIOGRAPHY

- [39] Abhishek L. Pillai, Jun Nagao, Ryo Awane, and Ryoichi Kurose. Influences of liquid fuel atomization and flow rate fluctuations on spray combustion instabilities in a backward-facing step combustor. *Combustion and Flame*, 220:337–356, October 2020.
- [40] E. Lo Schiavo, D. Laera, E. Riber, L. Gicquel, and T. Poinso. On the impact of fuel injection angle in Euler–Lagrange large eddy simulations of swirling spray flames exhibiting thermoacoustic instabilities. *Combustion and Flame*, 227:359–370, May 2021.
- [41] Johannes Eckstein and Thomas Sattelmayer. Low-order modeling of low-frequency combustion instabilities in aeroengines. *Journal of Propulsion and Power*, 22(2):425–432, 2006.
- [42] Antonio Andreini, Bruno Facchini, Andrea Giusti, and Fabio Turrini. Assessment of Flame Transfer Function Formulations for the Thermoacoustic Analysis of Lean Burn Aero-engine Combustors. *Energy Procedia*, 45(0):1422–1431, 2014.
- [43] Antonio Andreini, Bruno Facchini, Andrea Giusti, Ignazio Vitale, and Fabio Turrini. Thermoacoustic Analysis of a Full Annular Lean Burn Aero-Engine Combustor. In *Volume 1A: Combustion, Fuels and Emissions*, page V01AT04A069, San Antonio, Texas, USA, June 2013. American Society of Mechanical Engineers.
- [44] M. Zhu, A. P. Dowling, and K. N. C. Bray. Transfer Function Calculations for Aeroengine Combustion Oscillations. *Journal of Engineering for Gas Turbines and Power*, 127(1):18–26, 2005.
- [45] A Badhe, D Laera, and L Gicquel. High-fidelity Large Eddy Simulations of the Flame Transfer Function of a turbulent swirling spray flame. In *10th European Combustion Meeting*, page 6, Napoli, Italy, 2021.
- [46] Alessandro Innocenti, Antonio Andreini, Bruno Facchini, and Antonio Peschiulli. Numerical analysis of the dynamic flame response of a spray flame for aero-engine applications. *International Journal of Spray and Combustion Dynamics*, 9(4):310–329, May 2017.
- [47] J P Legier, T Poinso, and D Veynante. Dynamically thickened flame LES model for premixed and non-premixed turbulent combustion. page 12, 2000.
- [48] O. Colin, F. Ducros, D. Veynante, and T. Poinso. A Thickened Flame Model for Large Eddy Simulation of Turbulent Premixed Combustion. *Physics of Fluids*, 12(7):1843–1863, 2000.
- [49] B. Franzelli, E. Riber, M. Sanjosé, and T. Poinso. A two-step chemical scheme for kerosene–air premixed flames. *Combustion and Flame*, 157(7):1364–1373, July 2010.
- [50] S. A. Morsi and A. J. Alexander. An investigation of particle trajectories in two-phase flow systems. *Journal of Fluid Mechanics*, 55(02):193, September 1972.
- [51] *ANSYS Fluent User’s Guide, 2021R2*.
- [52] Noah Van Dam and Chris Rutland. Uncertainty Quantification of Large-Eddy Spray Simulations. *Journal of Verification, Validation and Uncertainty Quantification*, 1(2), June 2016.

-
- [53] Ralph Smith. *Uncertainty Quantification: Theory, Implementation, and Applications*. Society for Industrial and Applied Mathematics, Philadelphia, illustrated edition edition, March 2014.
- [54] Alexander Forrester, András Sóbester, and Andy Keane. *Engineering Design via Surrogate Modelling: A Practical Guide*. John Wiley & Sons Ltd., 2008.
- [55] C. E. Rasmussen and C. K. I. Williams. *Gaussian Processes for Machine Learning*. Adaptive Computation and Machine Learning Series. The MIT Press, Cambridge, Mass, 2006.
- [56] Sagar Kulkarni, Shuai Guo, Camilo F. Silva, and Wolfgang Polifke. Confidence in Flame Impulse Response Estimation From Large Eddy Simulation With Uncertain Thermal Boundary Conditions. *Journal of Engineering for Gas Turbines and Power*, 143(12):121002, December 2021.
- [57] Shuai Guo, Camilo F. Silva, and Wolfgang Polifke. Reliable calculation of thermoacoustic instability risk using an imperfect surrogate model. In *ASME Turbo Expo 2020: Turbo-machinery Technical Conference & Exposition*, ASME GT2020-14434, Virtual, Online, 2020.
- [58] Shuai Guo, Camilo F. Silva, Wolfgang Polifke, and Kah J. Yong. A Gaussian-Process-based framework for high-dimensional uncertainty quantification analysis in thermoacoustic instability prediction. *Proceedings of the Combustion Institute*, 38(4):6251–6259, January 2021.
- [59] A. K. Tangirala. *Principles of System Identification: Theory and Practice*. CRC Press, Boca Raton, FL, 2014.
- [60] Stephan Föllner and Wolfgang Polifke. Advances in Identification Techniques for Aero-Acoustic Scattering Coefficients from Large Eddy Simulation. In *18th International Congress on Sound and Vibration*, volume 4, pages 3122–3129, Rio de Janeiro, Brazil, 2011.
- [61] M. Merk, R. Gaudron, C. Silva, M. Gatti, C Mirat, T Schuller, and W. Polifke. Prediction of Combustion Noise of an Enclosed Flame by Simultaneous Identification of Noise Source and Flame Dynamics. *Proceedings of the Combustion Institute*, 37:5263–5270, 2019.
- [62] Luis Tay-Wo-Chong and Wolfgang Polifke. Large Eddy Simulation-Based Study of the Influence of Thermal Boundary Condition and Combustor Confinement on Premix Flame Transfer Functions. *Journal of Engineering for Gas Turbines and Power*, 135:021502, 2013.
- [63] S. Jaensch, M. Merk, T. Emmert, and W Polifke. Identification of Flame Transfer Functions in the Presence of Intrinsic Thermoacoustic Feedback and Noise. *Combustion Theory and Modelling*, 22(3):613–634, March 2018.
- [64] M. Merk, S. Jaensch, C. Silva, and W. Polifke. Simultaneous Identification of Transfer Functions and Combustion Noise of a Turbulent Flame. *J. Sound Vibration*, 422:432–452, May 2018.

BIBLIOGRAPHY

- [65] J.A. Carvalho, M.Q. McQuay, and P.R. Gotaç. The interaction of liquid reacting droplets with the pulsating flow in a Rijke-tube combustor. *Combustion and Flame*, 108(1-2):87–103, January 1997.
- [66] R. K. Dubey, D. L. Black, M. Q. McQuay, and J. A. Carvalho. The effect of acoustics on an ethanol spray flame in a propane-fired pulse combustor. *Combustion and Flame*, 110(1):25–38, July 1997.
- [67] J. Achury and W. Polifke. Modulation of Spray Droplet Number Density and Size Distribution by an Acoustic Field. *J. of Computational Multiphase Flows*, 9(1):32–46, 2017.
- [68] R. Kumara Gurubaran and R. I. Sujith. An Experimental Investigation of Evaporative Sprays in Axial Acoustic Fields. In *44th AIAA - JPC Conference*, AIAA 2008-4769, 2008.
- [69] F Giuliani, P Gajan, O Diers, and M Ledoux. Influence of pulsed entries on a spray generated by an air blast injection device : An experimental analysis on combustion instability processes in aeroengines. *Proceedings of the Combustion Institute*, 29:91–98, 2002.
- [70] Julien M. Apeloig, François-Xavier d’Herbigny, Frank Simon, Pierre Gajan, Mikael Orain, and Sébastien Roux. Liquid-Fuel Behavior in an Aeronautical Injector Submitted to Thermoacoustic Instabilities. *Journal of Propulsion and Power*, 31(1):309–319, 2015.
- [71] Virginel Bodoc, Anthony Desclaux, Pierre Gajan, Frank Simon, and Geoffroy Illac. Characterization of Confined Liquid Jet Injected into Oscillating Air Crossflow. *Flow, Turbulence and Combustion*, 104(1):1–18, January 2020.
- [72] Yogesh Aradhey, Chuchen Li, and Joseph Meadows. Coupled droplet dynamics: Investigation of acoustic-spray interactions in a reacting flow field. *Combustion and Flame*, 250:112645, April 2023.
- [73] M. R. Maxey and J. J. Riley. Equation of motion for a small rigid sphere in a nonuniform flow. *Phys. of Fluids*, 26(4):883–889, 1982.
- [74] A. Huber and W. Polifke. Dynamics of Practical Premix Flames, Part I: Model Structure and Identification. *International Journal of Spray and Combustion Dynamics*, 1(2):199–228, 2009.
- [75] Alexis Giauque, Thierry Poinso, and Franck Nicoud. Validation of a Flame Transfer Function Reconstruction Method for Complex Turbulent Configurations. In *14th AIAA/CEAS Aeroacoustics Conference (29th AIAA Aeroacoustics Conference)*, Vancouver, British Columbia, Canada, 2008. American Institute of Aeronautics and Astronautics.
- [76] F. Duchaine, F. Boudy, D. Durox, and T. Poinso. Sensitivity analysis of transfer functions of laminar flames. *Combustion and Flame*, 158(12):2384–2394, December 2011.
- [77] Benedict Enderle, Bastian Rauch, Felix Grimm, Georg Eckel, and Manfred Aigner. Non-intrusive uncertainty quantification in the simulation of turbulent spray combustion using Polynomial Chaos Expansion: A case study. *Combustion and Flame*, 213:26–38, March 2020.

-
- [78] Jannis Gikadi. *Prediction of Acoustic Modes in Combustors Using Linearized Navier-Stokes Equations in Frequency Space*. PhD thesis, TU München, München, Germany, 2013.
- [79] Manohar L. Munjal and Allan G. Doige. Theory of a Two Source-Location Method for Direct Experimental Evaluation of the Four-Pole Parameters of an Aeroacoustic Element. *Journal of Sound and Vibration*, 141(2):323–333, 1990.
- [80] Alexander J. Eder, Camilo F. Silva, Matthias Haeringer, Johannes Kuhlmann, and Wolfgang Polifke. Incompressible versus compressible large eddy simulation for the identification of premixed flame dynamics. *International Journal of Spray and Combustion Dynamics*, 15(1):16–32, 2023.
- [81] I. B. Celik, Z. N. Cehreli, and I. Yavuz. Index of Resolution Quality for Large Eddy Simulations. *Journal of Fluids Engineering*, 127(5):949–958, September 2005.
- [82] Franck Nicoud and Frédéric Ducros. Subgrid-Scale Stress Modelling Based on the Square of the Velocity Gradient Tensor. *Flow Turbulence and Combustion*, 62(3):183–200, 1999.
- [83] D.D. Joseph, J. Belanger, and G.S. Beavers. Breakup of a liquid drop suddenly exposed to a high-speed airstream. *International Journal of Multiphase Flow*, 25(6-7):1263–1303, September 1999.
- [84] A. D. Gosman and E. Ioannides. Aspects of Computer Simulation of Liquid-Fueled Combustors. *Journal of Energy*, 7(6):482–490, November 1983.
- [85] B Abramzon and WA Sirignano. Droplet vaporization model for spray combustion calculations. *International Journal of Heat and Mass Transfer*, 32(9):1605–1618, September 1989.
- [86] Sergei S Sazhin. Advanced models of fuel droplet heating and evaporation. *Prog. Energy Combust. Sci.*, 32(2):162–214, 2006.
- [87] Robert W. Bilger, Sten H. Starnner, and Robert J. Kee. On reduced mechanisms for methane-air combustion in nonpremixed flames. *Combustion and Flame*, 80:135–149, 1990.
- [88] Jannis Gikadi. *Prediction of Acoustic Modes in Combustors Using Linearized Navier-Stokes Equations in Frequency Space*. PhD thesis, TU München, München, Germany, 2013.
- [89] Kevin Prieur. *Dynamique de La Combustion Dans Un Foyer Annulaire Multi-Injecteurs Diphasique*. These de doctorat, Université Paris-Saclay (ComUE), December 2017.
- [90] C. Mirat, D. Durox, and T. Schuller. Stability analysis of a swirl spray combustor based on flame describing function. *Proceedings of the Combustion Institute*, 35(3):3291–3298, 2015.
- [91] Audrey Blondé, Bruno Schuermans, Khushboo Pandey, and Nicolas Noiray. Effect of Hydrogen Enrichment on Transfer Matrices of Fully and Technically Premixed Swirled Flames. *Journal of Engineering for Gas Turbines and Power*, 145(12):121009, December 2023.

BIBLIOGRAPHY

- [92] Alexander J. Eder, André Fischer, Claus Lahiri, Moritz Merk, Max Stauffer, Ruud Eggels, Camilo F. Silva, and Wolfgang Polifke. Identification of the dynamics of a turbulent spray flame at high pressure. In *Symposium on Thermoacoustics in Combustion*, Zurich, Switzerland, 2023.
- [93] Johannes Kuhlmann, S. Marragou, Isaac Boxx, Thierry Schuller, and Wolfgang Polifke. LES based prediction of technically premixed flame dynamics and comparison with perfectly premixed mode. *Physics of Fluids*, 34(8):085125, 2022.
- [94] A. M. Garcia, S. Le Bras, J. Prager, I. Boxx, and W. Polifke. Impact of H₂-enrichment on the response of a partially premixed CH₄-air flame to velocity and equivalence ratio fluctuations. *Combustion and Flame*, 2024.
- [95] C. Pera and J. Reveillon. Direct numerical simulation of spray flame/acoustic interactions. *Proceedings of the Combustion Institute*, 31(2):2283–2290, January 2007.